School of Medicine and Surgery

Dottorato di Ricerca in / PhD program
Medicina Molecolare e Traslazionale – DIMET
Ciclo / Cycle XXXII

Advanced proteomics MALDI-MSI imaging in chronic glomerulonephrites: from diagnostics to precision medicine

Mariia Ivanova

Matricola / Registration number: 799493

Tutore / Tutor: Prof. Fulvio Magni, Prof. Olena Dyayk

Cotutore / Co-tutor: Dr. Andrew Smith

Coordinator: Prof. Andrea Biondi

2016-2019

To whom it may concern

CONTENTS:

CHAPTER I: Introduction

1.1 Chronic kidney disease

Chronic kidney disease (CKD) is a worldwide health problem with a rapidly increasing incidence worldwide representing an important health and socioeconomic burden for a word healthcare system which is hard to overlook. It includes a heterogeneous group of disorders, affecting normal kidney structure and function, followed by multiple renal and non-renal symptoms having a various impact on health.

CKD is defined as abnormalities of kidney function or structure with and implication on individual's health, which can have an abrupt occurrence, following by resolution or chronisation.

This includes all people with markers of kidney damage and those with a glomerular filtration rate (GFR) of less than 60 ml/min/1.73 m^2 on at least 2 occasions separated by a period of at least 90 days (with or without markers of kidney damage). [1,2]

Although CKD in primary healthcare system is often asymptomatic, isolated CKD is rather an exception than rule, and is usually diagnosed in presence of other co-morbidities (like hypertension, cardiovascular disease, diabetes, obesity). Effective and on-time identification of CKD is important to prevent its progression to acute kidney injury (AKI), end-stage renal disease (ESRD), cardiovascular events and other complications, improving patients' safety and quality of life. [1,3]

It was considered historically, that the management of CKD patients is a responsibility of nephrologists, but with the evolution of disease

understanding it is clear that primary care clinicians may play the pivotal role in the early stage diagnosis. [3, 4]

Given the known asymptomatic nature of early-stage CKD and available strategies to delay or even prevent the CKD progression, public health usually uses simple laboratory tests to detect CKD, and tests for CKD are simple and freely available. There is an evidence that treatment can prevent or delay the progression of CKD, reduce or prevent the development of complications, and reduce the risk of cardiovascular disease. [1-3]

However, the effectiveness of detection and monitoring and its recognition CKD is still debatable among physicians, including concerns about tests' accuracy and their results' estimation. Furthermore, the cost-effectiveness data in general population is questionable and conflicting [5-7]

So far, CKD is often unrecognised because there are no specific symptoms, and it is often not diagnosed or diagnosed at an advanced stage. [1,2]

The development of the dialysis and kidney transplantation has given a vast life-saving opportunity to CKD and ESRD patients, permitting also to improve lifestyle quality, irrespective of the cause of the disease, but these options still remain too expensive for a great part of the world. [8]

Taking into account the existing issues, we should be aware of the prevalence of CKD undiagnosed in the general population and of the kidney failure with poor outcomes and high financial and social costs. [5-8]

1.1.1 Problem and epidemiology

Chronic kidney disease (CKD) is a global health issue, affecting approximately 11%–13% of the population across countries, having serious consequences on the quality of life, as well as on social cost in case of ESRD. The number of patients with CKD is projected to further increase due to the ageing population and increased prevalence of non-communicable diseases, such as hypertension, cardiovascular disease as diabetes [2,5,7]

One of the biggest recent studies, "The Global Burden of Disease" [5], described the change in burden of CKD from 1990 to 2016 involving incidence, prevalence, death, and disability-adjusted-life-years (DALYs). The data has shown, that the incidence of CKD globally increased by 89% by estimated number of 21,328,972 (uncertainty interval 19,100,079– 23,599,380), prevalence increased by 87% to 275,929,799 (uncertainty interval 252,442,316–300,414,224), death due to CKD increased by 98% to 1,186,561 (uncertainty interval 1,150,743–1,236,564), and DALYs increased by 62% to 35,032,384 (uncertainty interval 32,622,073–37,954,350). The measures were subjective to geography and level of the country development, thus variated substantially (Fig. 1).

Main reasons driving the increase of CKD DALYs were called population growth and aging. More of CKD strain on the healthcare system was shown in low and lower-middle income countries (63%) and there has been a reverse relationship between age standardized CKD DALY rate and the quality/accessibility of health care facilities. The prevalence rate of CKD per 100,000 population by age group

analysis was also highlighting an earlier disease onset (60-64 years) in countries with low Sociodemographic Index (SDI), while high SDI countries had a much steep dynamics with prevalence in elderly patients group (>90). [5]

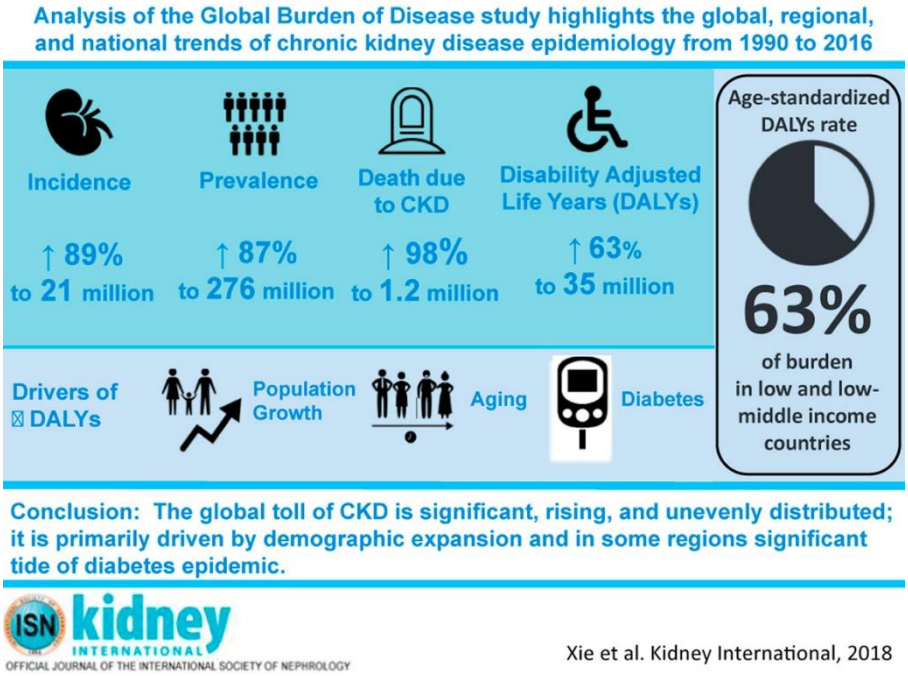

Figure 1. Global burden of Disease study data analysis (By Xie et al. Kidney Int. 2018 [Reference 5]).

Another study provided by International Society of Nephrology (ISN) conducted similar research including 10 countries of in Eastern and Central European region to uncover their demographic and socioeconomic characteristics, having impact on CKD progression started in 2017. [9]

The authors provided the aetiology analysis from these countries, of which the main were: diabetes mellitus (24%), hypertension and vascular disease (23%), and glomerulonephritis (14%), which are relatively the same worldwide. However, the alerting emphasize was brought up to renal replacement therapy (RRT) possibilities – the mean incidence of RRT was 198.3 (range 97.4–654) per million population, though mean prevalence of end-stage kidney disease (ESKD) requiring RRT was 934.1 (range 358–1052) per million population. The data has been compared to the statistics in United Kingdom reporting that despite the general growth of RRT in Eastern and Central European region, it still, unfortunately, falls far behind from United Kingdom and other European countries (Fig. 2).

Authors point out that despite of peritoneal dialysis (PD) is seen less profitable comparing to haemodialysis (HD), HD often remains unreachable to small cities, where the distance to the closest HD unit may be as 20-30 km, as well as financial factor of mean HD session cost remains challenging comparing to PD. [9]

Nevertheless, HD remains a dominant dialysis modality for these countries with the lagging numbers of kidney transplantation due to lack of organization of deceased and living donor programs, insufficient medical training, little number of skilled transplantation teams and social awareness about donation, that prevent a widespread use of this type of RRT. [9]

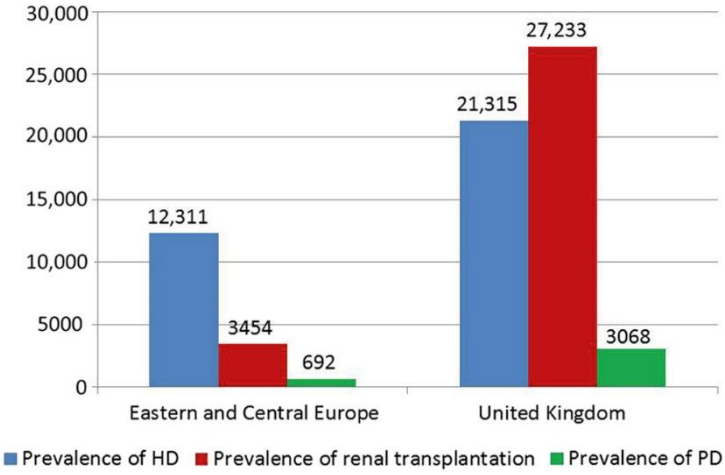

Figure 2. Prevalence of renal replacement therapy modalities per million patients in 2016: comparison between Eastern and Central European region and United Kingdom (UK); HD – haemodialysis, PD – peritoneal dialysis) (By Spasovski et al. Kidney Int. 2019 [Reference 9]).

On the contrary, the study of Rondeau et al. (2019) [10] stresses out the "privileged position" of Western Europe where nephrology units can provide a comprehensive care to patients with all forms of kidney disease and the main challenges are related to the aging of population (around 30% on chronic dialysis are aged ≥ 75) and shortage of organs available for transplantation with growing numbers on a waiting list. Authors also express the professional issue, where nephrology is no longer as attractive as a specialization due to working challenges and lack of innovations comparing to other disciplines. To overcome, international training is required with possibility of worldwide collaboration. [10]

The important objection is present in current situation of the Russian Federation (RF) and the Newly Independent States (NIS) region, which emerged after the dissolution of the Union of 15 Soviet Socialist Republics (USSR). The authors describe the economic and political problems following the collapse of the former USSR, despite the serious decline in healthcare had been noticed even earlier, in the periods of perestroika and glasnost. [11]

While nowadays RF and NIS regions encompass 11 countries and population of 270 million, they have a high variability in cultural, economic and environmental structures. Major part of them is middle or upper-middle income, thus economic and financial barriers are often an obstacle for a qualified nephrological help. The other problems of the area include low CKD awareness, suboptimal CKD screening, poor follow-up, undiagnosed and untreated CKD, lack of optimized resources for early detection and prevention, poorly developed renal pathology, PD and HD services, insufficient and controversial legal base for transplantation. [11]

Similar trend has been described in North and East Asia (2018), where the population of 1.6 billion is also very diverse in terms of their income, economy, culture and environment. [12]

The region holds the highest ESRD prevalence in the elderly population (≥65 years) and the reason for this was the aging of population overall.

Thus the number is still growing, large number of patients with ESRD potentially imposes a huge economic burden on the society as they inevitably incur high medical expenses through RRT.
The authors expect that worldwide prevalence of RRT will double in 2030 worldwide with fastest growth in Asia, demanding comprehensive treatment facilities access in retarding countries. [12]

In conclusion, the global CKD incidence has shown a dramatic rise over the past thirty years, followed by increase of disability and death. The main problems world healthcare system is facing are dissimilarity in demographic, epidemiologic, economic and educational levels of the countries and regions; population growth and aging; increase of co-morbidities with diabetes and hypertension leading.
CKD typically evolves over a long time, usually having a long latent period so there is a high risk of CKD being undetected and the rate of CKD progression varies in individuals. [8]
Complications of CKD affect all organ systems and leads to pathological state of uremia. CKD has been recognized as an independent risk factor for cardiovascular disease and other common conditions affecting the elderly, such as infection and impairments in cognitive function. Alteration of gut microbiota has been reported too. In addition, CKD is associated with increased risk from adverse effects of drugs, intravascular radiocontrast administration, surgery and other invasive procedures. [1,2, 8, 13]
Though most of the CKD causes are irreversible demanding life-long treatment, aiming to slow down the progress, it is also possible to

decline the idea of CKD irreversibility itself – in some cases, CKD is entirely reversible, either spontaneously or with treatment, and in other cases, treatment can cause partial regression of kidney damage and improvement in function (e.g., immunosuppressive therapies).
Undiagnosed and complicated CKD is associated with higher morbidity, mortality and cost. If CKD is detected early, the associated complications and the progression to kidney failure can be delayed or even prevented through appropriate interventions. [1, 9]

The rising burden of CKD should be reflected in the global and national healthcare systems. [3-12]

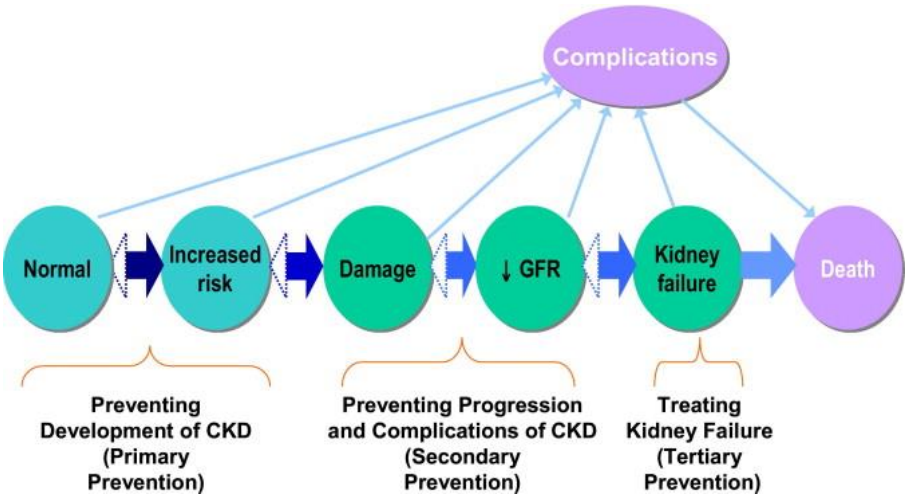

Figure 3. Conceptual model of chronic kidney disease (CKD) (by Levey AS, Stevens LA, Coresh J (2009) [Reference 8])

1.1.2 Diagnosis and classification

Chronic kidney disease (CKD) is defined as abnormalities of kidney function or structure present for more than 3 months, with implications for health of an individual. This includes all people with markers of kidney damage and those with a glomerular filtration rate (GFR) of less than 60 ml/min/1.73 m^2 on at least 2 occasions separated by a period of at least 90 days (with or without markers of kidney damage). [1,2]

The group includes a vast group of heterogeneous disorders, which may have sudden onset and relapse, or progress and become chronic with potential progress to the end-stage renal disease (ESRD).

It is usually diagnosed in presence of other comorbidities, in which top rates belong to hypertension, diabetes and cardiovascular disesase.

Effective early identification and management is extremely important to prevent CKD progression and its complications, as well as reduce the risks of acute kidney injury (AKI). Rapidly progressive diseases may lead to kidney failure within months but most diseases evolve over decades, and some patients do not progress during many years of follow-up. [1-3]

According to the last KDIGO (Kidney Disease: Improving Global Outcomes) and NICE (English National Institute for Health and Care Excellence) guidelines, a patient is diagnosed CKD if abnormalities of kidney structure function are present for 3 months or more.

The glomerular filtration rate (GFR) is generally accepted as the best overall index of kidney function. According to KDIGO and NICE

guidelines, a GFR <60 ml/min/ 1.73 m2 is referred as decreased and a GFR <15 ml/min/ 1.73 m2 as kidney failure. [1-3]
The criteria of CKD diagnosis are present in Tab. 1. [1]

Markers of kidney damage (one or more)	- Albuminuria (AER≥30 mg/24 hours; ACR≥30 mg/g [≥3 mg/mmol]) - Urine sediment abnormalities - Electrolyte and other abnormalities due to tubular disorders - Abnormalities detected by histology - Structural abnormalities detected by imaging - History of kidney transplantation
Decreased GFR	GFR<60 ml/min/1.73 m2 (GFR categories G3a-G5)

Table 1. Criteria for CKD (either of the following present for >3 months) (Data from reference [1]). CKD – chronic kidney disease; GFR – glomerular filtration rate)

KDIGO recommends to classify CKD based on cause, GFR category, and albuminuria category (CGA staging) (Fig. 4) [1]

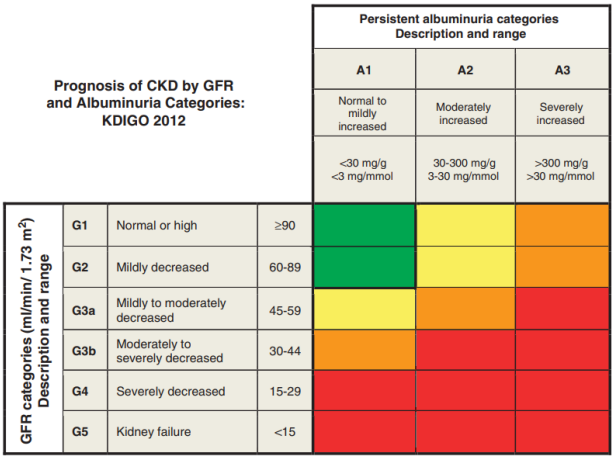

Figure 4. Prognosis of CKD based GFR and CGA category. [1]

The rationale for this recommendation comes as forth the severity of CKD, as expressed by the level of GFR and the level of albuminuria, links to risks of adverse outcomes including mortality and kidney outcomes. These basic factors will therefore guide management of CKD and this recommended classification is consistent with other classification systems of disease which are based on the general domains of cause, duration and severity, helping to define the progression and prognosis. [1,2]

It is important to bear in mind that staging and definition of prognosis is important, as most kidney diseases do not have symptoms or findings until later in their course and are detected only when they are chronic. Thus the main aim is CKD management, allowing to slow down or even stop it. Even kidney failure may be reversed with transplantation. [1,2,9]

1.1.3 Chronic glomerulonephritis

Chronic glomerulonephritis (GN) is a group of immunocomplex mediated diseases affecting glomeruli of both kidneys and one of the main reasons of ESRD.

Some of the most common GN worldwide are: membranous nephropathy, mesangioproliferative GN, IgA nephropathy, Lupus nephritis, focal segmental glomerulosclerosis, diabetic nephropathy, mesangioproliferative nephropathy and many others. [14]

The kidney biopsy is now the cornerstone and the golden standard for glomerular disease evaluation. Once done, it is important to assess the adequacy of tissue sample, addressing the size and number of cores to assess the confident histopathological report. [14,15]

The main questions to be answered are the patterns of damage and if they are acute or chronic.

In some cases, diagnosis may be possible even by examination of a single glomerulus (like in membranous nephropathy), but generally a substantially larger specimen is required to represent all kidney compartments (glomeruli, tubules, vessels, interstitium) for a reliable report. [14-16]

One also has to keep in mind, that sufficient tissue is needed to perform immunohistochemical staining, where the classic panel includes IgG, IgA, IgM, C3, C1q, but additional light chains markers, connective tissue markers, or others may be stained on demand. [17]

The need of electron microscopy remains controversial, but it may play critical role in some cases, nevertheless its worldwide availability and application is difficult. [14,15]

Renal biopsy reports should use widely accepted descriptive terminology in describing glomerular, tubular, vascular and interstitial lesions, as well as their widespread and distribution, reflecting the level of disease activity or chronicity. [16]

Notwithstanding, the kidney biopsy report is an important document, that reflects only the actual state of the disease and individual approach should be applied in every patient's case evaluation.

1.1.4 IgA nephropathy

IgA nephropathy (IgAN) is one of the most common primary glomerulonephritis in the world, firstly described by Berger and Hinglais in 1968. It is a type of chronic GN with predominant IgA deposits in mesangium in the absence of systemic disease. [16-18]

The etiology is not yet well known, where the key player nowadays declared is galactose-deficient IgA1 and immune complexes formation to it.

Basically the process starts with increased level of poorly O-galactosylated IgA1 glycoforms, that invoke production of specific antibodies and IgA1-containing immune complexes formation, that are deposited in glomerular mesangium. As a chain reaction, we observe mesangial cells proliferation, extracellular matrix augmentation, cytokines and chemokines activation, which results in glomerular injury. [17-19]

It is known elevated serum IgA level in about half of patients and male to female incidence ratio is 2:1 with peak age of 20-30 years.

The disease usually presents with microhematuria in majority of the cases (macrohematuria is less common), proteinuria, hypertension and nephrotic syndrome. [16-17]

The microscopic pathology is characterized by high variation of glomerular lesions. Usually, increase of mesangial cells number with increased matrix production is observed (which refers to a

mesangioproliferative pattern), focal inflammation and/or sclerosis is not uncommon, with possible passage to global glomerulosclerosis. Other possible findings include endocapillary hypercellularity, necrotizing and crescentic lesions, tubulointerstitial inflammation, red cell casts in tubules. Vessels rarely may represent vasculitis.

Immunofluorescent/immunohistochemical assay has predominant IgA staining of glomeruli in mesangial and/or segmental glomerular basement membrane (GBM) deposits. IgG and IgM deposits are usually also present, but less prominent, than IgA. C3 deposits are present in majority of cases and C1q is relatively a rare finding and is associated with a poor outcome. [20]

Electron microscopy may uncover electron-dense mesangial deposits and hypercellularity and abnormalities of GBM – like lamination or thinning. In presence of proteinuria extensive foot process effacement is visualised. [14-17, 21]

Differential diagnosis should be with Henoch-Schoenlein purpura, lupus-nephritis (especially if IgA, IgG, IgM, C3, C1q "full house" staining is present), postinfectious glomerulonephritis, focal segmental glomerulosclrosis and HIV should be excluded. [16, 17, 20, 21]

In spite of the abundance of IgA in IgAN kidney biopsies, as a unique hallmark, the disease has a striking heterogeneity in presentation, clinical course and outcome. This suggests more complex underlying mechanisms of pathogenesis that need comprehension and reliable prognostic biomarkers should be established. [18-19, 22]

In case of IgAN, kidney biopsy may establish diagnosis, exclude co-existent renal pathology and define the advancement of the lesions. However, unfortunately, by now there are no reliable clinical or histological markers to predict outcome and response to the therapy with a high level of certainty. The most precise prognostic classification for now is a MEST-score of the Oxford classification, but it is reported a need in new biomarkers to improve prediction of renal prognosis in IgAN. [15, 18-21, 23]

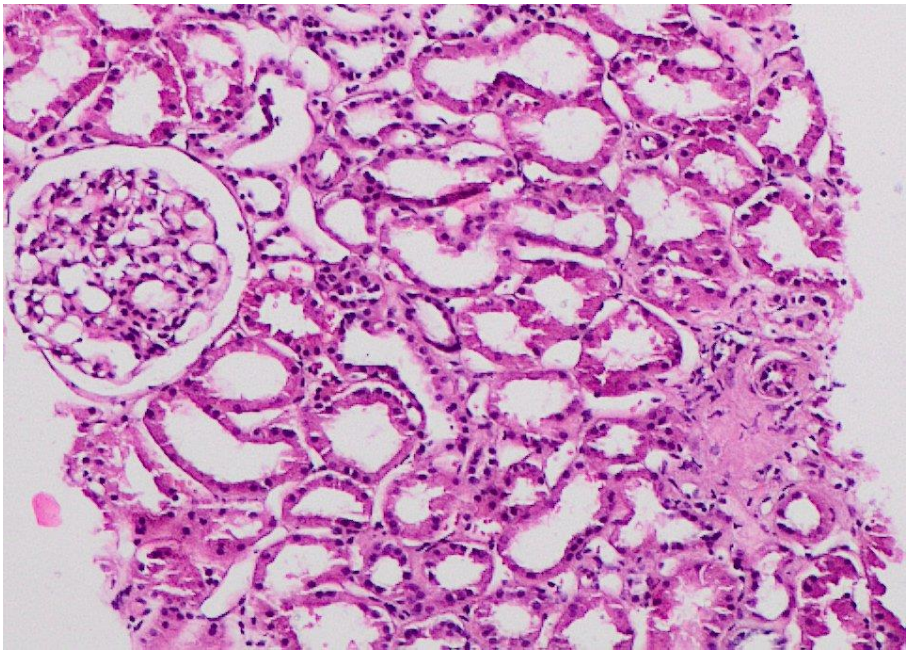

Figure 5. IgA nephropathy. Haematoxylin & Eosin staining, x100

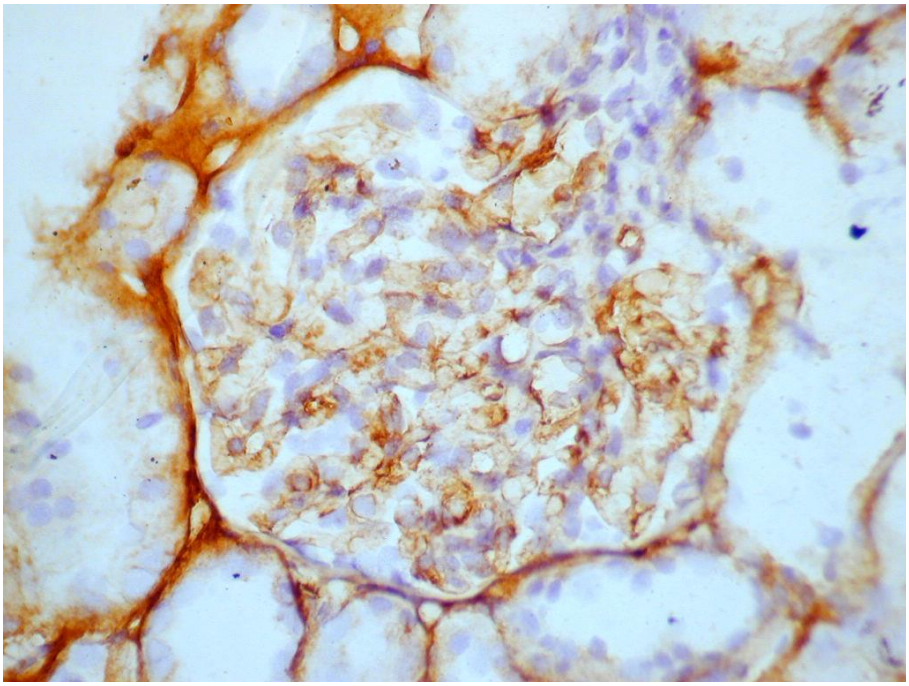

Figure 6. Glomerular mesangial deposits of IgA in IgA nephropathy. IgA immunohistochemical staining, x400

(Courtesy of Prof. Dyadyk, National Medical Academy of Post-Graduate Education Named After P.L. Shupik, Kyiv, Ukraine)

1.1.5 Diabetic Nephropathy

Diabetic nephropathy (DN) is a disease affecting kidney in presence of diabetes mellitus (DM) types 1 and 2.

Diabetes around the world has reached epidemic proportions with more than 8% of global population affected mentioned by now. [17, 24]

It is estimated that more than 40% of patients with diabetes will develop CKD with significant number developing ESRD, requiring dialysis and transplantation. As for now, type 2 diabetes mellitus represents 30-50% cases of ESRD worldwide. [25-27]

Diabetes mellitus incorporates a large group of multi-targeting organ damage – besides CKD those patiens are prone to high risk for cardiovascular disease through both atherosclerotic and nonatherosclerotic mechanisms, mineral bone disorder, anemia, infections and excessive fluid retention. [26]

The etiology of DM type 1 is the destruction of pancreatic islets due to the autoimmune process and the etiology of DM type 2 is insulin resistance, but both types result in insulin deficiency and hyperglycemia and the removal of hyperglycemic state can cause regression of DN lesions. Both types of diabetes should consider the CKD treatment options with a high level of safety awareness due to glycmeic control and concurrent diseases. [17, 26-28]

Histological changes in DN are similar for type one and two.

The earliest change is usually observed in glomeruli, as thickening of GBM. Glomeruli increase in size up to 50%, presenting mesangial expansion and nodular sclerosis with a specific aspect (Kimmelstiel-Wilson nodules, Fig. 7). Further mesangiolisys may contribute to capillary lumen confluence and micronaneurisms. Hyaline deposition in glomerular capillary walls creates “fibrin caps”. Glomerulosclerosis may be both segmental and global.

Tubules may have protein resorption and lipid droplets, interstitium may meet occasional inflammation. Advanced stages lead to tubulointestitial sclerosis. [16, 17]

Another important target of DM is arteries and arterioles: larger arteries show intimal fibrosis, medium-sized artheries develop atherosclerosis in andvanced DM, small arterioles typically present hyalinosis (plasma proteins insudation) which leads to aretrioles’ wall thickening and luminal occlusion. [17]

Immunofluorescent/immunohistochemical staining will show diffuse linear staining of GBM for IgG, segmental sclerotic lesions may contain nonspecific IgM and C3.

Electron microscopy brings up the diffuse thickening of GBM and increased amount of mesangial matrix. [16, 17]

Differential diagnosis with membranoprolifrative glomerulonephritis, amyloidosis, monoclonal immunoglobulin deposition disease, idiopathic nodular glomerulosclerosis, fibrillary immunotactoid glomerulonephritis should be performed. [16, 17]

It is also important to stress out the comorbidity of DM and hypertension, while both of them lead to progressive glomerulosclerosis and ESRD. Blood pressure levels along with glycemia and dyslipidemia are important prognostic factors in predicting DM patients to ESRD progression. However, in advanced stage patients it is sometimes difficult to distinguish primary origin of the glomerular lesions and overload contributes to cardiovascular morbidity and mortality is not well described. [16, 17, 25, 26]

The complicated course of the disease and its growing epidemiology make a prevention of CKD in diabetic patients a matter of a high priority, taking ito account growing numbers of ESRD worldwide.

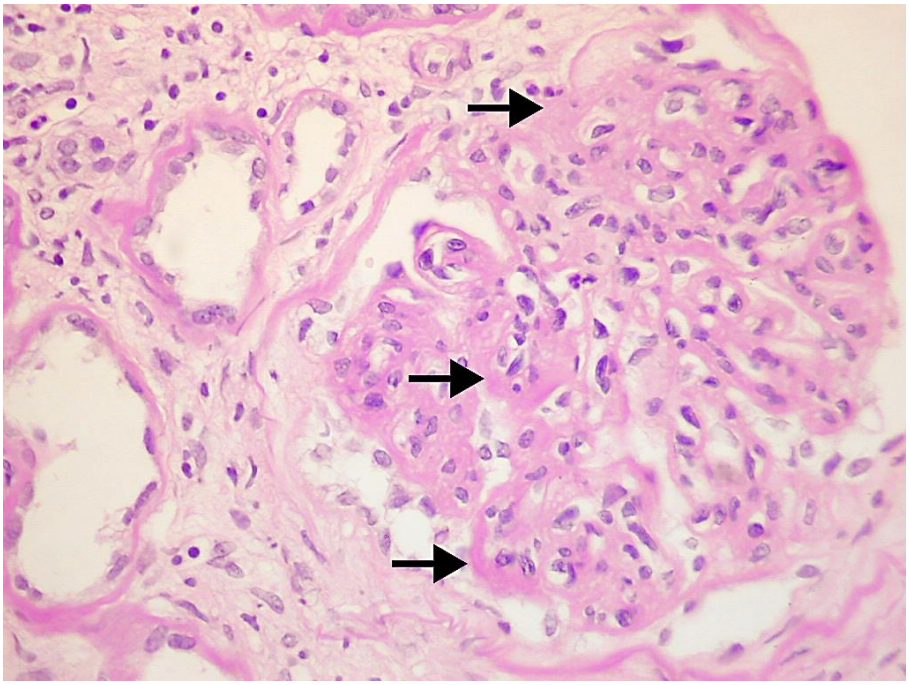

Figure 7. Diffuse and nodular glomerulosclerosis in patient with diabetes (Kimmelstiel-Wilson nodules). Haematoxylin & Eosin staining, x400

(Courtesy of Prof. Dyadyk, National Medical Academy of Post-Graduate Education Named After P.L. Shupik, Kyiv, Ukraine)

1.1.6 Membranous nephropathy

Membranous nephropathy (MN), or membranous glomerulonephritis is an idiopathic chronic glomerular disease characterized by diffuse subepithelial immune complex deposition followed by matrix formation (so-called subepithelial "spikes") and nephrotic range proteinuria. [16, 17]

The etiology of the disease is still not very clear, however the antigen is believed to be attached on the podocyte surface and the predominant autoantibodies identified have been to IgG4 subclass and M-type phospholipase A2 receptor (PLA2R), which is expressed on podocytes and proximal collecting tubules of the kidney. Oftenly, PLA2R autoantigen is co-localized with IgG4 in glomerulus. Another autoantigents for the moment identified are: aldose reductase (AR), manganese superoxide dismutase 2 (SOD2) and membrane metalloendopeptidase (MME) also known as CD10, which are also co-localized to subepithelial deposits and expressed on podocytes.

Another recently discovered podocyte antigen is thrombospondin-like domain 7A (THSD7A) established that membranous nephropathy is an autoimmune disease.

The genetic factors known by now include 2 strongly linked loci in genome-wide association studies (PLA2R allele and HLA-DQA1 allele). [1, 15-17, 29]

The disease may have primary or secondary origin.
Clinically, as many types of GN, MN may have an insidious onset, with typical presentation of nephrotic syndrome, asymptomatic proteinuria, hematuria (usually microscopic) and rarely – renal vein thrombosis. The peak age of the onset is 30-50 years, twice as frequent in males than females. [1, 16, 17, 29]

Microscopically MN is characterized by diffuse thickening of glomerular capillary wall subepithelial deposits described as "spikes" formation (Fig. 8, Fig. 9). Segmental or global sclerosis may be present depending on the advancement of the disease, however mesangial hypercellularity and inflammatory infiltrates are not typical of this disease. Interstitium and tubules may represent foam cells and protein resorption droplets, in latter stages we may observe tubulointerstitial fibrosis, tubular atrophy and arteriosclerosis.
Typical immunofluorescent/immunohistochemical finding is diffuse fine staining for IgG along glomerular basement membrane (GBM) and kappa and lambda light chains, while IgG4 is a dominant subclass and IgA and IgM are not prominent. The staining is usually global with respect to glomerulus, rather than segmental. Mesangial deposits are not typical for MN.
Electron microscopy presents subepithelial electron-dense deposits with incident "spikes". [15- 17]

Differential diagnosis should be made up with lupus nephritis, which may have similar histology at Class V, postinfectious glomerulonephritis and secondary membranous glomerulonephritis.

Being one of the most frequent causes of nephrotic suyndrome in adults, discrimination of primary origin og MN is a matter of a great importance. Its natural course is characterized by the "Rule of third", where only one third of patient's experiences a spontaneous remission, one third has persistent proteinuria but stable renal function and one third has a rapid progress to ESRD. This approach highlights the unpredictability of these patients when administering therapeutic treatment. [29]

Secondary membranous glomerulonephritis presents itself as MN in association with underlying disease or result of therapeutic administration.

There is a variety of infectious agents, associated with secondary MN (HIV, Hepatitis B, Hepatitis C, Epstein-Barr virus, syphilis), as well as autoimmune disorders (Systemic lupus erythematosus, rheumathoid arthritis and other mixed connective tissue disease).

It may also arise as a result of neoplastic diseases of various origin and pharmacologic agents administration (Gold, Penicillamine, Lithium, Mercury, NSAIDs and others).

Clinical presentation does not differ from the one in primary MN, including proteinuria and nephrotic syndrome and the same goes for microscopic pathology with an exception of that GBM thickening and

“spikes” are accompanied by possible mesangial hypercellularity and increased number of leucocytes within glomerular capillaries.

The immunofluorescent/immunohistochemical assay does not differ from primary MN, however electron microscopy data research should be addressed to the underlying disease or condition.

There are also rare cases of combined MN with IgA nephropathy described in the literature, as well as other MN subtypes (MN with anti-tubular basement membrane antibodies, graft glomerulopathies) which we don’t highlight in this capital. [15- 17, 29]

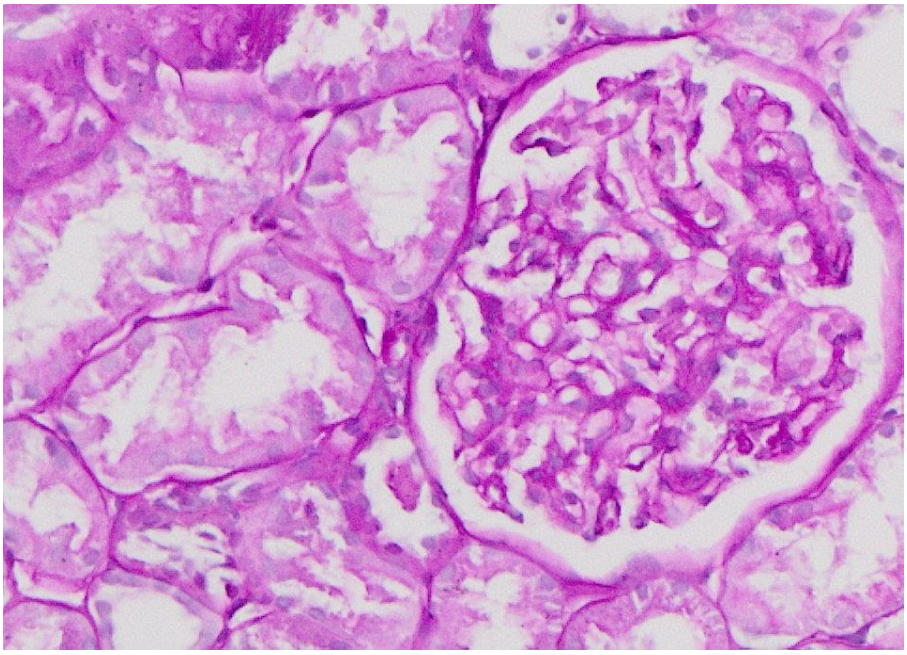

Figure 8. Diffuse glomerular capillary wall thickening in membranous nephropathy. PAS staining, x200
(Courtesy of Prof. Dyadyk, National Medical Academy of Post-Graduate Education Named After P.L. Shupik, Kyiv, Ukraine)

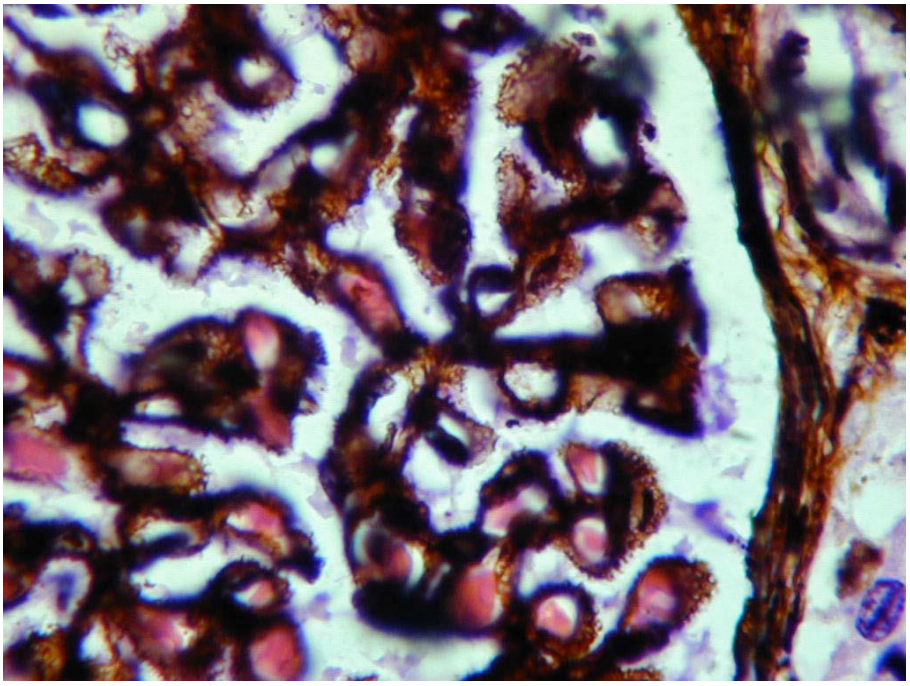

Figure 9. Subepithelial immune deposits (“spikes”) in membranous nephropathy. Jones methenamine silver staining, x1000
(Courtesy of Prof. Dyadyk, National Medical Academy of Post-Graduate Education Named After P.L. Shupik, Kyiv, Ukraine)

1.2 MALDI-MS imaging

1.2.1 A Brief introduction to MALDI-MS imaging

Mass spectrometry (MS) based techniques have become some of the most prevalently employed analytical strategies for the detection and identification of endogenous biomolecules in tissue, including metabolites, lipids and proteins. The application of these techniques is now commonplace in clinical research given that it can be used to analyse a wide range of sample types, from cells to tissue sections. [30-32] Using this technique, analytes are desorbed and ionised from the surface of the sample after being incident with a pulsed laser beam. This process is aided by the presence of an organic matrix that is designed to absorb some of the energy from this laser pulse. These ions are then separated in a mass analyser in base of their physical properties and their electrical signals recorded by a detector. As a result, signals are correlated with a mass-to-charge ratio (*m/z*) and the output come displayed in the form of mass spectrum with corresponding relative intensity of each signal in m/z function. [30]

One of the primary advantages of the technique is associated with its ability combine the chemical specificity of MS with the imaging capabilities offered by optical microscopy in order to simultaneously detect the distribution and relative intensity of hundreds, if not thousands, of biomolecules directly *in situ*. Furthermore, images deriving from direct molecular measurements do not rely on reagents or antibodies. Together, these aspects make MALDI-MSI an ideal discovery method for new potential biomarkers [31].

In terms of its conception, the terms “Matrix-assisted laser desorption/ionization” (MALDI) and “mass spectrometry imaging” (MSI) appeared when, in 1985 F. Hillenkamp and M. Karas first used this technology to analyse small molecules like proteins, peptides, sugars, and polymers ionizing them to create single-charged ions. In the late 1990s MSI was introduced into clinical setting, employing MALDI to analyze a wide range of biomolecules, including proteins, directly on an intact tissue, leading to a new era of clinical and pharmacological research. [30, 32].

Taking into account the ability of MALDI to analyse a wide range of endogenous biomolecules and its’ widespread availability, it remains the most commonly applied MSI technique. In particular relevance to clinical research, given that proteins play a significant role in the wide array of pathways involved in cellular signaling cascades, the ability to resolve their spatial localization concurrently within the same section of tissue can significantly facilitate the detection of pathological processes and hence determine the risk-groups. It’s also becoming more readily used for the detection of lipids and metabolites, meaning that multiple disease mechanisms can be described and integrated with proteomic findings. Since the development of MALDI-MSI, it has employed in a large number of clinically orientated studies, focusing on fields such as oncology, pathology, and even forensics [33]. It also proved to be a valuable tool for the detection of xenobiotics and their metabolites directly *in situ* [34].

1.2.2 Experimental procedures in MALDI-MSI

As briefly touched upon previousoly, MALDI-MSI is performed by acquiring a mass spectrum at specific spatial co-ordinates within a defined measurement region, which is usually related to an entire section or particular regions of interest present within a tissue section. Using the acquired mass spectra, the spatial distribution of the analytes can be visualised and a molecular image of the tissue reconstructed. These molecular images can then be correlated with tissue images obtained by traditional histology.

Specific steps of specimen preparation include tissue washing in order to remove potential contaminants (eg. salt and polymers), on-tissue digestion with protease enzymes (commonly trypsin), and finally matrix application itself [35, 36].

Fresh samples are considered to be the primary source of tissue for MALDI-MSI experiments and are commonly collected for this type of analysis. However, fresh samples also need to be frozen immediately following collection in order to stabilise the proteome through inhibition of the enzymatic processes. The significant advantage offered by fresh-frozen (FF) tissue is that it closely mimics the native state of the tissue, with the tissue morphology and integrity being preserved. The freezing process here must be performed in a gradual and homogenous manner in order to avoid the formation of ice crystals, which can lead to tissue cracking. The most common approach involves loosely wrapping the tissue in aluminium foil and freezing in liquid nitrogen or cooled alcohol (to approximately -70^{o}C) for approximately one minute. Alternatively, the tissue can also be cooled

in isopentane dry ice. A further approach that can be employed in order to avoid protein degradation is conductive heat transfer. However, it is important to verify the compatibility of each tissue with this treatment, given that the tissue morphology can be altered during the process. Once stabilisation has been performed, the tissue is stored at -80^{o}C prior to MALDI-MSI analysis.

In recent years, which is also arguably of greater significance to clinical MALDI-MSI studies, protocols have been developed in order to enable formalin-fixed paraffin-embedded (FFPE) tissue to be analysed [35]. FFPE tissue represents the major proportion of the patient samples collected and stored in hospitals and other medical centres, meaning that they are becoming invaluable to histopathological studies involving MALDI-MSI and can unearth a plethora of new information. Ultimately, the analysis of FFPE tissue enables retrospective studies with much larger cohorts of patients. This is especially important when attempting to collect samples of particularly rare diseases, which would take a considerably longer period of time if attempting to obtain an equivalent number of FF specimens. In terms of sample storage, FFPE tissue can also be stocked at room temperature for up to 10 years, far greater than would be possible with FF tissue, even at -80^{o}C.

Matrix application is an important part in the sample preparation for MALDI-MSI given that it is a major factor in the spatial resolution that can be achieved. The general aim of this step is to achieve an optimal balance between crystal shape/dimension (should be small and homogenous) and maximal analyte extraction, all whilst avoiding any

lateral diffusion of the analaytes, whiche makes this step one of the most crucial for an effective analysis [30].

Depending upon the target analyte of choice, a number of different matrices can be used. For example, sinapinic acid (SA; 3, 5-dimethoxy-4-hydroxycinnamic acid) and α-CHCA (α-cyano-4-hydroxycinnamic acid) are most commonly the matrices of choice for the extraction of proteins, peptides and lipids (1-20kDa). Alternatively, DHB (2, 5-Dihydroxybenzoic acid) is also commonly used for the extraction of low molecular weight proteins. These matrices are dissolved in a solution containing organic solvents, water and trifluoroacetic acid (TFA). TFA is added to the matrix solution is order to assist in the MALDI ionisation process while the organic solvents facilitate optimal crystal formation.

Finally, there are a number of methods, both manual and automated, that can be employed for the deposition of MALDI matrices. However, and most commonly, in order to achieve a homogenous coating of matrix, automated spraying of the matrix solution onto the surface of the sample is performed. In these instances, the spraying devices produce very small droplets which, after drying, produce a very homogenous and thin layer of solid matrix crystals which are less than 20μm in diameter.

Once MSI analisys has been performed, the MALDI matrix can be removed using alcohol-based solvents and the tissue section treated with histological stains, such as Hematoxylin and Eosin or Periodic acid–Schiff (PAS). This allows the direct overlap of molecular and histological information and can enable us to visualise the spatial

distribution and relative intensity of signals within the histologically relevant regions of tissue [29, 30].

1.2.3 MALDI-MSI in clinical research

In general, MALDI-MSI has vast applicability in the study of various diseases, including CKD.

Of particular note, Baluff et al. decided to employ MALDI-MSI in order to study different tumor microenvironments in gastric cancer and breast carcinoma. Using this approach, they were able to identify different tumour microenvironments within tumour tissue that appeared homogenous when evaluated using traditional histological techniques. Employing a novel combination of segmentation and multivariate analysis methods, they detected a number of tumour sub-populations, within histologically homogenous regions, that were associated with changes in the levels of DEFA-1 and Histone H2A. This molecular information was then combined with clinical data taken from patients in order to predict the survival rate of patients based upon the number of observed molecular tumour sub-populations. This is a prime example of not only how MALDI-MSI can provide information that is confirmatory, or complimentary to histological information, but also how it can provide further information that was not previously possible [37, 38].

Y. Ucal, et al. also provided an extensive summary of the role MALDI-MSI in various other cancer types and neurodegenerative diseases. Using MALDI-MSI, proteomic signatures of different grades of glial tumors, specific peptides in multiple myeloma, the distribution of pharmacological agents in ovarian cancer, changes in glycosylation patterns in prostate cancer, and the screening of renal cell carcinoma

have all been performed. Furthermore, specific proteins implicated in Alzheimer's, Parkinson's, and Huntington's disease have also been obtaineded and represent highly promising studies [39, 40].

CKD, being one of the major health and socioeconomic burdens expresses a strong need for new reliable diagnostic biomarkers and markers indicative of treatment efficacy that can be used alongside the classical clinical and pathological tools. The world nephrology and pathology community still continues to struggle in detecting the disease onset, predicting the individual's risk of disease development and/or progression, prediction to therapy response, and classification. It is already known that proteomics could be a reliable diagnostic method itself given that the large proportion of urinary proteins are generated by the kidney and are thus carrying the substantial information about renal state. There is a great number of existing studies that focus on primary and secondary glomerulonephritis, focusing on focal segmental glomerulosclerosis (FSGS), IgA-nephropathy, membranous glomeroulonephritis (MGN) and minimal change disease (MCD) and others. [41, 42]

Initially, to study renal deseases, several studies have employed animal models. Xu et al. employed laser capture microdissection (LCM) to specifically isolate glomeruli from rats with FSGS, with the glomerular proteome then being analysed by MALDI-MS. Proteomic patterns of sclerotic and nonsclerotic glomeruli within FSGS were generated. However, they also noted that non-sclerotic

glomeruli within FSGS were in fact more similar to sclerotic glomeruli than completely normal glomeruli from a proteomic standpoint, hypothesizing that the early onset of sclerotic processes can be detected by molecular analyses at an earlier stage [43]. Employing a mouse model, Kaneko et al. studied the pathogenesis of IgA nephropathy (IgAN). The authors investigated the molecular distribution of a variety of lipids in IgAN murine kidneys using MALDI-MSI and noted that there were a number that were over-expressed in cortical regions of kidneys affected by the disease, with respect to healthy controls [44].

Mainini et al. first investigated the potential of employing MALDI-MSI directly on human renal bioptic material. It was noted that the glomeruli and tubules of healthy kidney tissue present similar proteomic profiles. However, in cases of primary glomerulonephritis (GN), including MGN and MCD, proteomic differences were observed between glomeruli and tubules. Furthermore, proteomic alterations were observed in GN tubules, even in regions without morphological indications of the disease. This finding indicated that it is possible to detect pathological alterations at the molecular level prior before being able to note changes with traditional histology [45].

Building upon this, Smith et al. applied MALDI-MSI to bioptic renal tissue taken from patients with the most frequent glomerular kidney diseases: FSGS, IgAN and membranous nephropathy (MN). They succeeded in generating molecular signatures capable of discriminating normal from GN tissue, as well as detecting a

number of potential molecular markers of CKD progression. More specifically, they also detected a number of signals specific for each form of GN. One particular protein, identified as alpha-1-antitrypsin (A1AT) by MS/MS, was shown to be localised to the podocytes of sclerotic glomeruli following antibody validation. Given the localization of this protein, they hypothesized that its presence may be associated with podocyte stress that occurs during the development of sclerosis. Furthermore, the same peptide fragment of A1AT was detected in the urine of GN patients who were shown to progress to the latter stages of renal disease. This body of work highlighted how findings generated by MALDI-MSI could also be also translated into less-invasive proteomic analysis employing urine. [42]

MALDI-MSI has also been recently employed in the study of membranous nephropathy (MN), aiming to distinguish primary and secondary form. The work of Beck et al. presented a large step forward in the diagnosis of MN, detecting the circulating antigens phospholipase A2 receptor (PLA2R), IgG4, and thrombospondin type-1 domain-containing 7A (THSD7A) in the sera of primary MN patients [46]. Continuously, Smith et al. employed MALDI-MSI to FFPE tissue of 20 patients to evaluate the capability of this technology to detect alterations in the tissue proteome of primary and secondary MN patients and represented the first example of MALDI-MSI being applied to FFPE renal biopsies for this purpose. The positive results obtained with this proteomic approach facilitated the detection of a number of signals that could differentiate the different forms of iMN

that were positive to PLA2R or IgG4 as well as distinguish primary from secondary MN. [29]

All these studies show vast potential and represent the value of employing modern proteomic techniques for diagnostic purposes, particularly in CKD. It is hoped that this already strong platform will encourage further, more in-depth, studies that could eventually reveal new specific and sensitive biomarkers that could be used for the diagnosis, prognosis, and management of renal disease. Renal diseases, as a very specific entity, have been more widely investigated and understood than ever before during recent decades. However, given the ever increasing worldwide incidence of CKD, in addition to advancements in analytical instrumentation, it is both important, and possible, to obtain much more molecular information than was ever possible. Understanding the molecular nature of this disease will open new horizons in its diagnosis management strategies.

1.3 Scope of the thesis

The aim of our work was to study several of the most diffuse forms of chronic glomerulonephritis by means of MALDI-MSI in order to enlighten molecular alterations that were associated with the diagnosis, prognosis or response to therapy of these diseases.

CHAPTER II: Pilot study in which the MALDI-MSI of renal biopsies with various forms of mesangioproliferative glomerulonephritis were performed in order to enlighten proteomic alterations that may be associated with the progression of IgA nephropathy.

CHAPTER III: Integrating high spatial resolution MALDI-MSI with high mass accuracy MALDI-FTICR-MS and nLC-ESI-MS/MS analysis to detect tissue proteins to discriminate cases of diabetic nephropathy from those of hypertensive nephrosclerosis.

CHAPTER IV: Exemplify the advantage of using high spatial resolution MALDI-MSI for the study of membranous nephropathy by highlighting the possibility to generate protomic profiles of the individual cell types within the kidney as well as visualize the distribution of proteins that may be implicated in the differential response to immunosuppressive treatment.

References

1. KDIGO Clinical Practice Guidelines for Glomerulonephritis. Chapter 1: Introduction, Kidney International Supplements, Volume 2, Issue 2, 2012, 156-162, http://www.kdigo.org/clinical_practice_guidelines/pdf/KDIGO-GN-Guideline.pdf
2. NICE Chronic kidney disease in adults: assessment and management. Clinical guideline, 2015, https://www.nice.org.uk/guidance/cg182#
3. Fraser SD, Blakeman T. (2016). Chronic kidney disease: identification and management in primary care. Pragmatic and observational research, 7, 21–32. doi:10.2147/POR.S97310
4. Fraser SD, Roderick PJ, May C, et al. (2015) The burden of comorbidity in people with chronic kidney disease stage 3: a cohort study. BMC Nephrol. 16:193.
5. Xie Y et al. (2018) Analysis of the Global burden of Disease study highlights the global, regional, and national trends of chronic kidney disease epidemiology from 1990 to 2016. Kidney Int 94:567-581
6. Komeda et al (2016) Cost-effectiveness of Primary Screening for CKD: A Systematic Review. American Journal of Kidney Diseases 63:789-797
7. Yamada Y, Ikenoue T, Saito Y, et al (2019) Undiagnosed and untreated chronic kidney disease and its impact on renal outcomes in the Japanese middle-aged general population. J

Epidemiol Community Health Published Online First: 28 September 2019. doi: 10.1136/jech-2019-212858

8. Levey AS, Stevens LA, Coresh J (2009) Conceptual Model of CKD: Applications and Implications.
   American Journal of Kidney Diseases 53:S4-S16
9. Spasovski G et al. (2019) Nephrology in Eastern and Central European region: challenges and opportunities. Kidney Int 96:287-290
10. Rondeau E et al. (2019) Challenges and opportunities for nephrology in Western Europe. Kidney Int 95: 1037-1010
11. Tchokhonelidze I et al. (2019) Current status, challenges and the role of ISN in advancement of Nephrology in Newly Independent States and Russia region. Kidney Int 96: 48-51
12. Wang, Jinwei et al. (2018) Disease burden and challenges of chronic kidney disease in North and East Asia. Kidney Int 94:22-25
13. Sumida K, Kovesdy CP (2019) The gut-kidney-heart axis in chronic kidney disease. Ahead of print https://doi.org/10.1556/2060.106.2019.19
14. KDIGO Clinical Practice Guidelines for Glomerulonephritis. Chapter 2: General principles in the management of glomerular disease, Kidney International Supplements,Volume 2, Issue 2, 2012, 156-162, http://www.kdigo.org/clinical_practice_guidelines/pdf/KDIGO-GN-Guideline.pdf

15. Floege J, Sharon G et al. (2019) Management and treatment of glomerular diseases (part 1): conclusions from a Kidney Disease: Improving Global Outcomes (KDIGO). Kidney Int 95:268-280
16. Jennette JC, Olson JL, Silva FG, D'Agati, VD. (2015). Heptinstall's Pathology of the Kidney Philadelphia: Wolters Kluwer Health.
17. Colvin R (2011) Diagnostic pathology. Kidney diseases. Amyrsys, Manitoba
18. Yeo SC, Cheung CK., Barratt J (2018) New insights into the pathogenesis of IgA nephropathy. Pediatr Nephrol 33:763-777.
19. Coppo R (2016) Biomarkers and targeted new therapies for IgA nephropathy. Pediatr Nephrol 32:725-731.
20. Lee HJ et al. (2013) Association of C1q deposition with renal outcomes in IgA nephropathy. Clin. Nephrol 80:98-104.
21. Cook TH (2007) Interpretation of Renal Biopsies in IgA Nephropathy. In: Tomino Y (ed): IgA Nephropathy Today. Contrib Nephrol. Karger, Basel. Vol. 157, pp 44-49.
22. Tomino Y. (2016) Pathogenesis And Treatment in IgA Nephropathy. Springer, Tokyo
23. Trimarchi H, Barrat J, Cattran DC, Cook HT, Coppo R, Haas M, Liu ZH, Roberts IS, Yuzawa Y, Zhang H, Feehaly J (2017) IgA nephropathy Oxford Classification update. Kidney Int 91:1014-1021.

24. IDF Atlas 2017. http://www.diabetesatlas.org/IDF_Diabetes_Atlas_8e_interactive_EN/ (Accessed March 12, 2018)
25. American Diabetes A. 10. Microvascular Complications and Foot Care: Standards of Medical Care in Diabetes-2018. Diabetes Care 2018; 41:S105-S18.
26. Perkovic V et al. (2016) Management of patients with diabetes and CKD: conclusions from a “Kidney Disease: Improving Global Outcomes” (KDIGO) Controversies conference. Kidney Int 90:1175-1183
27. Luis-Lima S et al. (2019) The error of estimated GFR in Type 2 diabetes mellitus. J Clin Med 8. doi: 10.3390/jcm8101543.
28. Mann JFE, Orsted DD, Brown-Frandsen K, et al. (2017) Liraglutide and Renal Outcomes in Type 2 Diabetes. N Engl J Med 377:839-48.
29. Smith A, L'Imperio V, Ajello E, Ferrario F, Mosele N, Stella M, Galli M, Chinello C, Pieruzzi F, Spasovski G, Pagni F, Magni F (2017) The putative role of MALDI-MSI in the study of Membranous Nephropathy. Biochim Biophys Acta Proteins Proteom 1865:865-874.
30. Vlahou A, Mischak H, Zoidakis J, Magni F (2018) Integration Of Omics Approaches And System Biology For Clinical Applications. Wiley, Hoboken
31. Rubakhin SS, Sweedler JW (2010) Mass Spectrometry Imaging. Springer, New York.

32. Karas M, Bachmann D, Hillenkampf F. Influence of the Wavelight in High-Irradiance Ultraviolet Laser Desorption Mass Spectrometry of Organic Molecules". Anal. Chem. 1985;57 (14): 2935-9.
33. Chughtai K, Heeren RMA. (2010) Mass spectrometric imaging for biomedical tissue analysis. Chem Rev 110:3237-77. doi: 10.1021/cr100012c.
34. Cornett DS, Frappier SL, Caprioli RM. (2008) MALDI-FTICR imaging mass spectrometry of drugs and metabolites in tissue. Anal Chem 80:5648-5653.doi:10.1021/ac800617s.
35. De Sio G et al. (2015) A MALDI-Mass Spectrometry Imaging method applicable to different formalin-fixed paraffin-embedded human tissues. Mol Biosyst 11:1507-14. doi: 10.1039/c4mb00716f.
36. Addie RD et al. (2015) Current State and Future Challenges of Mass Spectrometry Imaging for Clinical Research.Anal Chem 87:6426-33
37. Baluff B et al. (2014) De novo discovery of phenotypic intratumor heterogeneity using imaging mass spectrometry. J Pathol 235:3-13
38. Deininger SO et al. (2008) MALDI imaging combined with hierarchical clustering as a new tool for the interpretation of complex human cancers. J Proteome Res 7:5230-5236
39. Ucal Y et al. (2017) Clinical applications of MALDI imaging technologies in cancer and neurodegenerative diseases.

Biochim Biophys Acta. pii: S1570-9639(17)30005-5. doi: 10.1016/j.bbapap.2017.01.005. [Epub ahead of print]

40. Kasap M, Akpinar G, Kanali A (2017) Proteomic studies associated with Parkinson's disease. Expert Rev Proteomics 14:193-209
41. Sun L, Zou LZ, Chen MJ (2016) Make precision medicine work for chronic kidney disease. Free supplementary material doi: 10.1159/000455101.
42. Smith A, L'Imperio V, De Sio G, et al. (2016) Alpha-1-Antitrypsin detected by MALDI imaging in the study of glomerulonephritis: Its relevance in chronic kidney disease progression. Proteomics 16:1759- 66.
43. Xu BJ, Shyr Y, Liang X, et al. (2005) Proteomic patterns and prediction of glomerulosclerosis and its mechanisms. J Am Soc Nephrol 16:2967-2975.
44. Kaneko Y, Obata Y, Nishino T, et al. (2011) Imaging mass spectrometry analysis reveals an altered lipid distribution pattern in the tubular areas of hyper-IgA murine kidneys. Exp Mol Pathol 91:614-621.
45. Mainini V et al. (2014) MALDI imaging mass spectrometry in glomerulonephritis: feasibility study. Histopathology 64:901–906.
46. Beck LH, Bonegio RGB, Lambeau G, et al. (2009) M-type phospholipase A2 receptor as target antigen in idiopathic membranous nephropathy. N Engl J Med 361:11-21.

CHAPTER II

Matrix assisted laser desorption/ionization mass spectrometry to uncover protein alterations associated with the progression of IgA nephropathy

Mariia Ivanova[a,c*], Olena Dyadyk[b], Dmytro Ivanov[b,] Francesca Clerici[a], Andrew Smith[a] and Fulvio Magni[a]

a) Department of Medicine and Surgery, Clinical Proteomics and Metabolomics Unit,
University of Milano-Bicocca, Vedano al Lambro, Italy
b) P.L. Shupyk National Medical Academy of Postgraduate Education (NMAPE), Kiev, Ukraine
c) Bogomolets National Medical University, Kiev, Ukraine

Accepted to Virchow's Archiv

Abstract: IgA nephropathy (IgAN) is one of the most diffuse glomerulonephrites worldwide and many issues still remain regarding our understanding of its pathogenesis. The disease is diagnosed by renal biopsy examination, but potential pitfalls still persist with regards to discriminating its primary origin and, as a result, determining patient outcome remains challenging.

In this pilot study, matrix-assisted laser desorption/ionization (MALDI) mass spectrometry imaging (MSI) was performed on renal biopsies obtained from patients with IgAN (n=11) and other mesangioproliferative glomerulonephrites (MesPGN, n=6) in order to enlighten proteomic alterations that may be associated with the progression of IgAN.

Differences in the proteomic profiles of IgAN and MesPGN tissue could clearly be detected using this approach and, furthermore, fourteen signals ($AUC \geq 0.8$) were observed to have an altered intensity among the different CKD stages within the IgAN group. In particular, large increases in the intensity of these signals could be observed at CKD stages II and above. These signals primarily corresponded to proteins involved in either inflammatory and healing pathways and their increased intensity was localised within regions of tissue with large amounts of inflammatory cells or sclerosis.

Despite much work in recent years, our molecular understanding of IgAN progression remains incomplete. This pilot study represents a promising starting point in the search for novel protein markers that can assist clinicians in better understanding the pathogenesis of IgAN and

highlighting those patients who may progress to end-stage renal disease.

Keywords: IgA nephropathy, mesangioproliferative glomerulonephritis, chronic kidney disease, MALDI-MSI, mass spectrometry, proteomics.

Ethical Responsibilities of Authors Section: all authors contributed equally.

1 INTRODUCTION

Mesangioproliferative glomerulonephritis (MesPGN) is a group of kidney diseases of little or unknown etiology, that mostly affect glomeruli, with a pattern of mesangial proliferation upon light microscopy [1]. MesPGN is divided into subtypes depending upon the prevalence of immune deposits (IgM, IgA, IgG, C3, C1q) either singularly or in combination. There is also a rare no immunoglobulin deposit pattern. [1] In cases where the prevalent immune deposition of IgA occurs, in the absence of systemic diseases, the established diagnosis is IgA nephropathy (IgAN). [1, 2] It is one of the most common primary glomerulonephrites (GN) worldwide but the incidence varies among different populations. [3] The diagnosis can be confirmed only by renal biopsy that provides evidence of possible co-existent renal pathology, however the impact on predicting disease outcome is still unclear. [2, 4]

There have been many attempts to uncover important prognostic factors for IgAN. [5, 6] Among them, several studies have been undertaken to establish progression and loss of kidney function, which was defined by the loss of glomerular filtration rate (GFR), stating that the loss of kidney function had a strong positive correlation with proteinuria and blood pressure, but the pathological findings did not add any significant information to the prognostic model. [5] Overall, the prognostic data for the therapy is still quite subtle and, in a major proportion of cases, the strategy remains generic and not specific. As a result, the treatment options remain the same as used in many other glomerular and kidney diseases, focusing on the downregulation of

immune response. [6, 7] Besides the absence of a specific therapy, known clinical problems also include marked heterogeneity in disease manifestation, great variability in terms of morphological changes, [8-10] and a limited understanding of the complex pathogenesis that underpins the disease. [9-11]

Nowadays, the modern understanding of IgAN pathogenesis represents a complex of multiple pathways. The abnormal synthesis of poorly glycosylated IgA1 (galactose-deficient IgA1) is considered to play a primary role, followed by the formation of circulating immune complexes and their glomerular (mainly mesangial) deposition evocating the inflammatory response, podocyte damage, increased permeability of glomerular filtration membrane, urinary abnormalities, decrease of GFR and loss of kidney function. [10, 11] In light of this, there are many ongoing researches and trials, aiming at defining the immunological and molecular basis of the disease and attempting to find the reasons of unfavourable prognosis. [10-12]

Recently, proteomics studies are also being used to discover specific molecular disease patterns in glomerular diseases and have already show promising results. [10, 12] Among them, matrix-assisted laser desorption/ionization (MALDI) mass spectrometry imaging (MSI) has developed into a highly powerful analytical tool for the visualization of biomolecules directly in situ, thus avoiding their extractions from the tissue. The detection of tissue proteins represents one of the most stimulating aspects of MSI providing the information of the proteins with an altered expression and their localization within the tissue section. Therefore, the ability to resolve the spatial

localization of multiple proteins within a single section of pathological tissue can enable the detection of disease candidates and improve our understanding of disease pathogenesis. Given the high degree of tissue heterogeneity associated with glomerular diseases, such as IgAN, MALDI-MSI therefore could represent an ideal tool in this branch of renal histopathology, offering a complementary molecular dimension. This technique has already been demonstrated to be capable of detecting in-situ molecular alterations and is being currently used in a variety of studies driving forward clinical application [12-17] Nowadays, the high spatial resolution permits us to spatially resolve specific kidney structures (glomeruli, tubuli, vessels and interstitium) within a bioptic tissue, giving possibility to assess precisely the structural alterations in tissue structures and accurately detect potential biomarkers [18].

In this pilot study, we employed MALDI-MSI in order to determine proteome alterations associated with different stages of progression of IgAN. This resulted in the detection of nine protein signals whose intensity was associated with the different CKD stages in IgAN. In particular, these proteins were associated with inflammatory and healing pathways and may provide complementary insights into the progression of IgAN. To confirm the validity of our findings, we performed immunochemical staining of the same IgAN cases with Vimentin and Collagen IV, highlighting a correspondence between MALDI-MSI and those obtained using routine diagnostic tools.

2 MATERIALS AND METHODS

2.1 Patient Selection

Renal biopsies with a histological diagnosis of IgA nephropathy (IgAN, n=11) or mesangioproliferative glomerulonephritis (MesPGN, n=6), obtained during the period between 2015 and 2018, were selected at random from the archive of Pathology Department of P. L. Shupyk National Medical Academy of Postgraduate Education, Kiev, Ukraine. The appropriate Ethical Committee approved the collection of these specimens and informed consent was obtained from all participants. Each biopsy contained at least 8 glomeruli and a full immunohistochemical panel (IgG, IgA, IgM, C3, C1q, CD20) had been previously performed, along with routine histological evaluation, in order to establish diagnosis. De-identified patient data was requested at the time of biopsy and included age, sex, pathologic diagnosis, date of biopsy and eGFR. There were 10 males and 7 females included in the study and were aged between 5 and 36 years. The clinical parameters of renal function were used to match the cases in terms of their CKD stage (Table 1). The histological grading of IgAN patients were performed according to Oxford classification [19] and MesPGN patients were histologically graded according to Sethi et al. [20] and is given in Supplementary Table 1.

Tab 1. CKD stages of the patient cohort included in this study

Chronic Kidney Disease (CKD) stage	IgA (11)	MesPGN (6)
Mild (CKD I, GFR >90mL/min/1.73 m2)	2	4
Moderate (CKD II, GFR >60-89 mL/min/1.73 m2)	6	2
Advanced (CKD III or more, GFR <59mL/min/1.73 m2)	3	0

Supplementary table 1.

Immunohistochemical assay of the analysed cases

			IgG	IgA	IgM	C3	C1q *	MESTscore (IgAN)/ MesPGN type with chronicity index
Mild (CKD I)	IgAN	Patient 1	+- ++	++	+	++	-	M0 E0 S0 T0 C0
		Patient 2	+	++- +++	++	++	-	M1 E0 S0 T1 C0
	MesPGN	Patient 3	++	+	++	++- +++	-	MesPGN, CG 0 (GS 0, IF 0, TA 0, CV 0) Minimal chronic changes
		Patient 4	++	+	+++	++	+	MesPGN, CG 0 (GS 0, IF 0, TA 0, CV 0) Minimal chronic changes

		Patient 5	+	+- ++	++	++	++	MesPGN, CG 1 (GS 0, IF 1, TA 0, CV 0) Minimal chronic changes
		Patient 6	+	+- ++	++- +++	+++	++	MesPGN, CG 0 (GS 0, IF 0, TA 0, CV 0) Minimal chronic changes
Moderate (CKD II)	IgAN	Patient 7	++	+++	++	++	-	M1 E0 S1 T1 C0
		Patient 8	++	++- +++	+- ++	+	+	M1 E1 S1 T1 C0
		Patient 9	++	++- +++	+- ++	+	+	M1 E1 S1 T1 C1
		Patient 10	+- ++	+++	++	+	-	M1 E1 S1 T1 C1
		Patient 11	+- ++	++- +++	++	++	-	M1 E1 S1 T0 C0
		Patient 12	++	+++	++	+- ++	-	M1 E0 S1 T1 C0

	MesPGN	Patient 13	+- ++	+- ++	+++	++- +++	+	MesPGN, CG 3 (GS 1, IF 1, TA 1, CV 0) Mild chronic changes
		Patient 14	++	++	++	+++	++	MesPGN, CG 2 (GS 1, IF 1, TA 0, CV 0) Mild chronic changes
Advanced (CKD III)	IgAN	Patient 15	++	+++	++	+	-	M1 E1 S1 T1 C1
		Patient 16	++	++- ++	++	+	+	M1 E1 S1 T1 C0
		Patient 17	++- +++	++- +++	++- +++	+	-	M1 E1 S1 T2 C2

* - patients with “full house” pattern did not meet criteria of diagnosis of lupus nephritis.

2.2 Sample preparation for MALDI -MSI

For this analysis, fixation time was set at 12 hours following the biopsy procedure, as previously described [12]. Four-micron-thick sections were cut and mounted onto conductive indium tin oxide glasses. Paraffin removal and antigen retrieval was performed as previously described [17, 18]. Then, trypsin deposition (Sigma-Aldrich, 20 ng/µl) was performed using the iMatrixSpray (Tardo Gmbh, Subingen, Switzerland) automated spraying system and then

left in a humid chamber overnight at 40oC. Finally, matrix deposition for MALDI-MSI analysis was performed by spraying six layers of α-cyano-4-hydroxycinnamic acid (10 mg/ml in 50:50 acetonitrile:water w/0.4% trifluoroacetic acid) using the iMatrixSpray (Tardo Gmbh, Subingen, Switzerland) with an optimised method and an incorporated heat bed set at 40^{o}C [18].

2.3 MALDI-MSI analysis

For fourteen of the cases, mass spectra were acquired in reflectron positive mode, within the *m/z* 700 to 3000, using an ultrafleXtreme (Bruker Daltonik GmbH, Bremen, Germany) MALDI-TOF/TOF MS equipped with a Smartbeam laser operating at 2kHz frequency. A mixture of standard peptides within the mass range of m/z 750 to 3150 (PepMix I, Bruker Daltonik) was used for external calibration directly applied on the glass slide. MALDI-MS images were acquired with a laser diameter of approximately 40 µm and a raster sampling of 50 µm in both *x* and *y* dimensions.

The analysis of three additional tissue sections was performed using a rapifleX MALDI Tissuetyper™ (Bruker Daltonik GmbH, Bremen, Germany) MALDI-TOF/TOF MS equipped with a Smartbeam 3D laser operating at 5kHz frequency. MALDI-MS images were acquired with a single spot laser setting of 18 µm and a raster sampling of 20 µm in both *x* and *y* dimensions.

Following MALDI-MSI analysis, the matrix was removed with increasing concentrations of ethanol (70%, 90% and 100%) and the slides were stained using Hematoxylin and Eosin (H&E) stain. The

slides were converted to digital format using a ScanScope CS digital scanner (Aperio, Park Center Dr., Vista, CA, USA), thus allowing for the direct overlap of images and the integration of proteomic and morphological data.

2.4 MALDI-MSI data analysis

Data files containing the individual spectra of each entire measurement region (40,256 for IgAN and 17,143 for MPGN, respectively) were then imported into SCiLS Lab 2019c Pro software (Bruker Daltonik GmbH) to perform pre-processing: baseline subtraction (Convolution algorithm), normalisation (Total Ion Current algorithm) and spatial denoising (Weak). Average (Avg) spectra, representative of the whole measurement regions, were generated to display differences in the protein profiles. Peak picking and alignment were performed as feature extraction for statistical analysis and this resulted in the detection of 116 *m/z* features within the dataset. Receiver Operative Characteristic (ROC) analysis was performed using random subsets of spectra (containing equivalent numbers), with an AUC (Area Under the Curve) of ≥ 0.80 being required for a peak to be considered as statistically significant. These signals were curated to only include *m/z* values representative of the monoisotopic mass of a tryptic peptide.

2.5 Putative identification of discriminatory m/z features

Signals of interest present within the MALDI-MSI dataset were correlated with our in-house library of identified peptide sequences obtained from bioptic renal tissue using nLC-ESI-MS/MS [16] or using

information available via MSIMass list (www.maldi-msi.org/mass) [21]. A protein identification was putatively assigned to a signal if an error of less than ±150 ppm was noted between the *m/z* value measured by MALDI-MSI and the theoretical *m/z* value of the amino acid sequence.

2.6 Immunohistochemical validation of putatively identified proteins

After putatively identifying discriminatory signals of interest, we performed a validation immunochemistry step on the same IgAN cases that were used for MALDI-MSI analysis (n=8). Vimentin (Vimentin monoclonal antibody, clone N9, Thermo Fisher Scientific, Waltham, USA) and Collagen IV (Collagen IV monoclonal antibody, clone CIV22, Master Diagnostica S. L., Granada, Spain) immunohistochemical stain with UltraVision Quanto Detection System (Thermo Fisher Scientific, Waltham, USA) were used.

Microscopic investigation and photoarchivation was conducted with «ZEISS» (Oberkochen, Germany) light microscope with data elaboration system «AxioImager. A2», on 5x, 10x, 20x and 40x magnifications, binocular capping 1,5 and oculars 10 with ERc5s «ZEISS» (Oberkochen, Germany) camera with “Primo star” data elaboration system on 4x, 10x, 40x magnifications with camera AxioCam 105color.

3 RESULTS

The aim of this pilot study was to generate proteomic signatures of IgAN and highlight *in situ* alterations that may be associated with the progression of the disease. This scope is particularly relevant to the field of nephrology given that the clinical course of IgAN is less favourable with respect to other forms of MesPGN and there remains the need for complementary molecular information that can support the prognostic assessment of these patients.

3.1 Histological characteristics

Within our series, the cases of IgAN were characterised by the presence of glomerular inflammation, mesangial hypercellularity, segmental sclerotic lesions, and tubulointerstitial inflammation. Whilst these histological features were also present in MesPGN, the grade of mesangial hypercellularity, inflammatory and sclerotic lesions were less pronounced than IgAN cases at the same CKD stage. The most noticeable difference between the two disease groups were represented by the prominence of inflammatory cells and sclerotic patterns in IgAN, in particular at the moderate and advanced stages. These histological patterns are exemplified in Fig. 1. The complete immunohistochemical panel of the cases series are also provided in Supplementary Tab 1.

Fig 1. Representative Hematoxylin & Eosin stained (x200) images highlighting the histological characteristics of the IgAN and MesPGN cases included in our series at different CKD stages

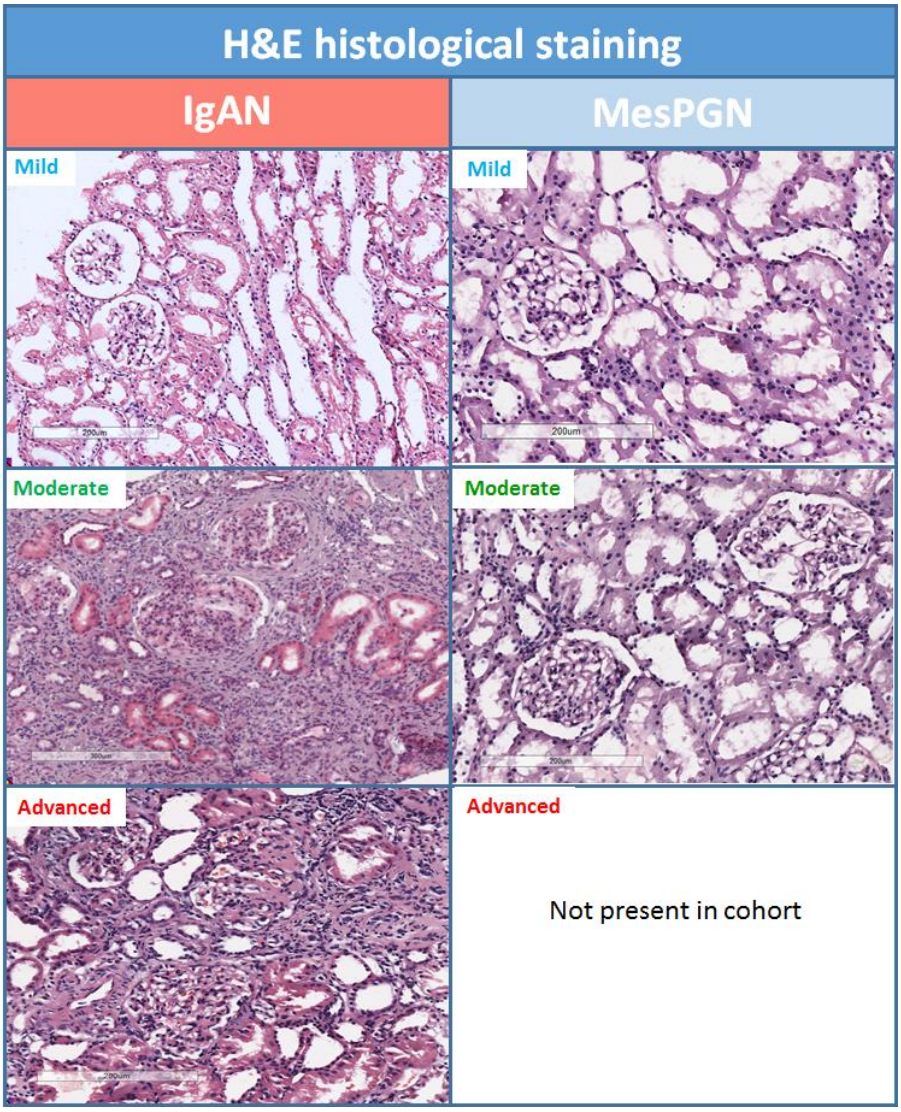

3.2 Proteomic signatures of IgA nephropathy and mesangioproliferative glomerulonephritis

In order to assess the feasibility to detect specific protein signatures of IgAN, average tryptic peptide profiles were generated for IgAN (n=8) and MesPGN (n=6) within the *m/z* 1000 to 2500 range. Clear differences could be observed in the profiles of the two disease groups and, following ROC analysis, a total of eight *m/z* signals, from among the 116 detected, were detected with an AUC ≥ 0.8 (Fig 2).

Fig 2. (Left) The eight m/z signals detected with an AUC ≥ 0.8 when comparing the two disease groups

(Right) The average tryptic peptide profiles of IgAN (red) and MesPGN (green) in the m/z 1000 to 2500 range. Absolute intensity is expressed in arbitrary units. Signals highlighted by ROC analysis are denoted by asterisks (*)

ROC Analysis	
m/z interval	AUC Value
1325.5	0.82
1459.5	0.86
1465.5	0.80
1562. 7	0.8
1585.8	0.89
1626.6	0.83
1655.6	0.84
1706.7	0.81

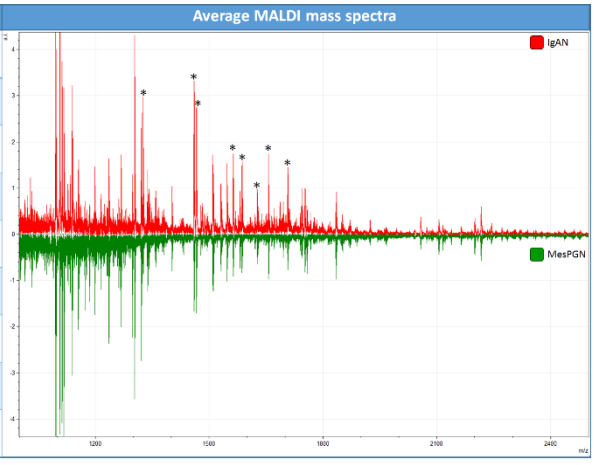

3.3 Proteomic signatures associated with the progression of IgA nephropathy

Given the evidence that this technique may be able to generate specific protein signatures of IgAN, the cases were then separated in base of their CKD stage (Tab 1) in order to evaluate the capability to highlight *in situ* protein alterations associated with the progression of the disease. Focusing on the IgAN group, significant differences were noted and fourteen *m/z* signals were detected with an AUC $\geq$ 0.8 when comparing between the mild, moderate, and advanced stages (Tab 2). Conversely, only one *m/z* signal with an AUC $\geq$ 0.8 was detected (1095.2) when comparing the mild and moderate stages of MesPGN and this was not one of the fourteen signals detected among the IgAN groups (data not shown).

These fourteen *m/z* signals were then correlated with our in-house library of identified peptide sequences obtained from bioptic renal tissue using nLC-ESI-MS/MS [16] or using information available via MSIMass list (www.maldi-msi.org/mass) [21]. This led to the putative identification of eleven of the signals and are highlighted in Tab 3.

Tab 2. The fourteen signals (AUC ≥ 0.8) detected by ROC analysis when comparing the different stages of IgAN

***m/z* interval**	**AUC Value (Mild Vs Moderate)**	**AUC Value (Moderate Vs Advanced)**
1028.5	0.86 (↑ in moderate)	0.87 (↑ in moderate)
1116.6	0.86 (↑ in mild)	0.92 (↑ in advanced)
1127.7	<0.80	0.86 (↑ in advanced)
1143.7	0.86 (↑ in mild)	0.96 (↑ in advanced)
1235.7	0.97 (↑ in mild)	0.93 (↑ in advanced)
1267.7	<0.80	0.80 (↑ in moderate)
1303.6	0.81 (↑ in moderate)	0.81 (↑ in moderate)
1325.5	0.92 (↑ in moderate)	0.90 (↑ in moderate)
1459.5	0.89 (↑ in moderate)	<0.80
1508.5	<0.80	0.83 (↑ in advanced)
1546.8	0.80 (↑ in mild)	0.98 (↑ in advanced)
1580.7	<0.80	0.98 (↑ in advanced)
1655.6	0.91 (↑ in moderate)	<0.80
1707.8	<0.8	0.91 (↑ in advanced)

Tab 3. Putative identifications of the fourteen signals (AUC ≥ 0.8) detected when comparing the different stages of IgAN.
Mass errors (ppm) are provided in the right column

***m/z* interval**	**Putative identification (peptide sequence)**	**Mass error (ppm)**
1028.5	Vimentin (SVSSSSYRR), VIM	2 ppm
1116.6	--	--
1127.7	Collagen alpha-1(XIV) chain (SQDDIIPPSR), COL14A1	130 ppm
1143.7	Tubulin beta-2C chain (LAVNMVPFPR), TB2C	33 ppm
1235.7	Histone H1.4 (KALAAAGYDVEK), HIST1H1A	72 ppm
1267.7	Na(+)/H(+) exchange regulatory cofactor NHE-RF2 (VEPGSPAEAAALR), SLC9A3R2	7 ppm
1303.6	Macrophage migration inhibitory factor (PMFIVNTNVPR + Oxidation), MIF	55 ppm
1325.8	Histone H4 (DNIQGITKPAIR), H4	72 ppm
1459.8	Collagen alpha-1(I) chain precursor (GSAGPPGATGFPGAAGR + Hydroxylation), COL1A1	71 ppm
1508.5	Hypoxia up-regulated protein 1 (AEAGPEGVAPAPEGEK), HYOU1	123 ppm
1546.8	--	--
1580.7	--	--
1655.7	Collagen alpha-2(I) chain precursor (GLHGEFGLPGPAGPR + Hydroxylation), COL1A2	103 ppm

1707.8	Keratin, type I cytoskeletal 10 (GSLGGGFSSGGFSGGSFSR + Phosphorylation), KRT10	23 ppm

When evaluating the change in intensity of these protein signals, two predominant trends were highlighted. Firstly, four of these signals had a gradual increase between the mild, moderate, and advanced stages, respectively (Fig 3a). Of the putatively identified proteins signals, all of them are associated with the presence of fibrotic and sclerotic tissue and this was also supported by the histological characteristics observed within our case series (Fig 1). Secondly, six of the signals had a marked increase in the moderate stage (Fig 3b) and, in particular, are all proteins implicated in inflammatory processes and the excess formation of connective tissue. This was again supported by the histological characteristics present in our case series, where a marked increase of inflammatory cells was observed at the moderate stage (Fig 1). Finally, there was a further group of signals which did not show a clear trend (Fig A1) and did not correlate with the histological characteristics of the case series.

Fig 3a. Box plot charts highlighting the gradual increase in signal intensity of m/z 1127 (COL14A1), 1508 (HYOU1), 1580, and 1707 (KRT10) among the mild (blue), moderate (green) and advanced (red) IgAN stages. Error bars representative of the standard deviation are provided.

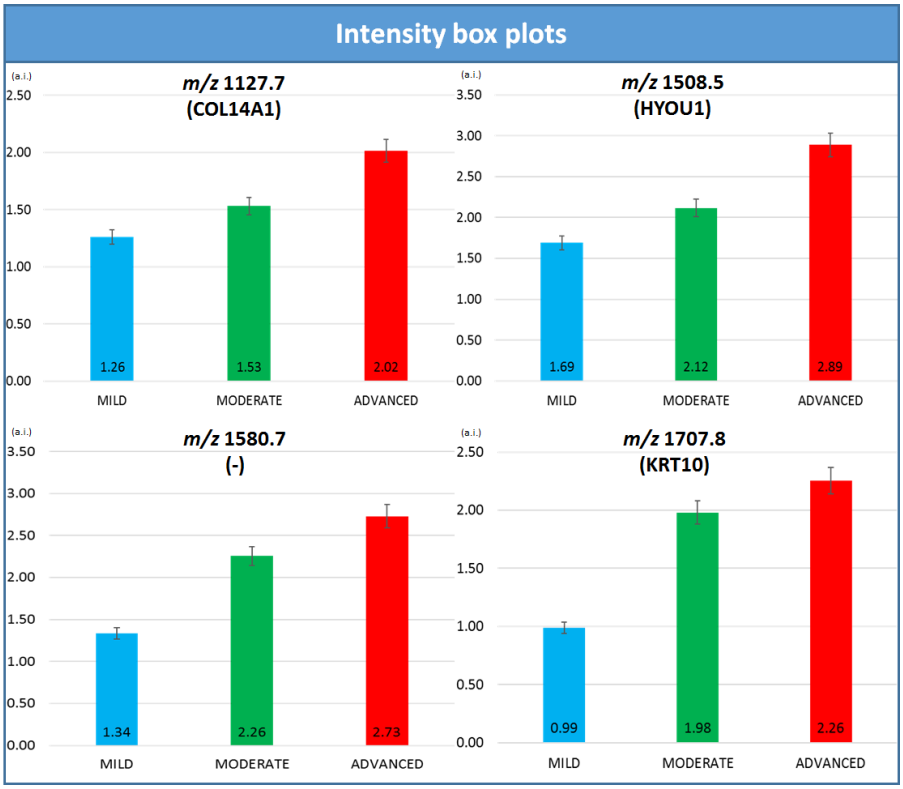

Fig 3b. Box plot charts highlighting the marked increase in signal intensity of m/z 1028 (VIM), 1267 (SLC9A3R2), 1303 (MIF), 1235 (H4), 1459 (COL1A1) and 1655 (COL1A2) at the moderate (green) stage of IgAN. Error bars representative of the standard deviation are provided

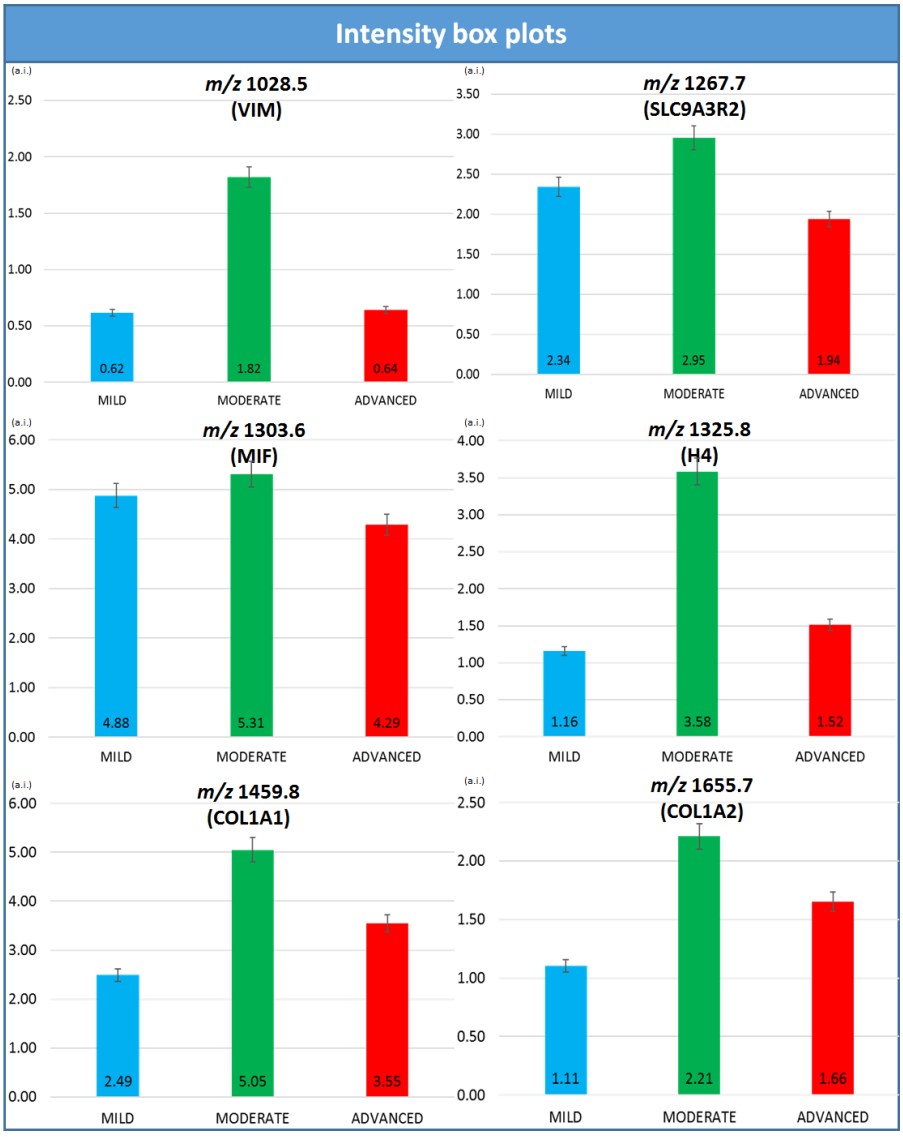
Intensity box plots
(a.i.)
m/z 1028.5
(VIM)
0.62
1.82
0.64
MILD
MODERATE
ADVANCED
m/z 1267.7
(SLC9A3R2)
2.34
2.95
1.94
m/z 1303.6
(MIF)
4.88
5.31
4.29
m/z 1325.8
(H4)
1.16
3.58
1.52
m/z 1459.8
(COL1A1)
2.49
5.05
3.55
m/z 1655.7
(COL1A2)
1.11
2.21
1.66

Fig A1. Box plot charts highlighting the change in signal intensity of m/z 1116, 1143 (TB2C), 1235 (HIST1H1A), and 1546 among the mild (blue), moderate (green) and advanced (red) IgAN stages. Error bars representative of the standard deviation are provided

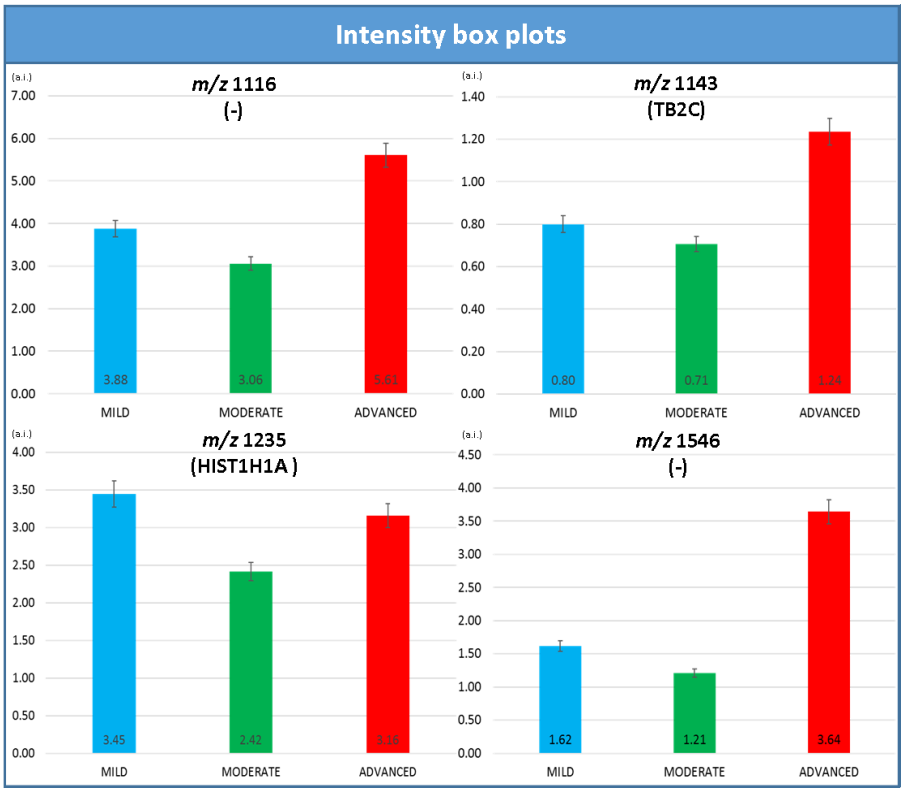

3.4 Correlation of MALDI-MS imaging with histological features

Three additional cases of IgAN were analysed by high spatial resolution MALDI-MSI in order to better visualise the distribution of these proteins within the different tissue compartments (Fig 4). Focusing on those putatively identified signals which had a correlation with the histological characteristics of the IgAN cases, VIM and MIF, in particular, were localised to tubulointersitial and glomerular regions with the notable presence of infiltrating inflammatory cells. Furthermore, SLC9A3R2, H4, COL1A1 and COL1A2 were localised to regions with the early formation of fibrosis within an inflammatory context. On the other hand, COL14A1, HYOU1, and KRT10 were localised to regions of tissue with extensive fibrosis and sclerosis and presenting minimal cellularity.

Fig 4. Exemplary MALDI-TOF-MS images, overlaid with the Hematoxylin & Eosin stained counterpart, highlighting the spatial distribution of m/z 1028.5 (VIM), 1127.7 (COL14A1), 1267.7 (SLC9A3R2), 1303.6 (MIF), 1325.8 (H4), 1459.8 (COL1A1), 1508.5 (HYOU1), 1655.7 (COL1A2) and 1707.8 (KRT10) in IgAN renal tissue. Intensity scale bars are provided.

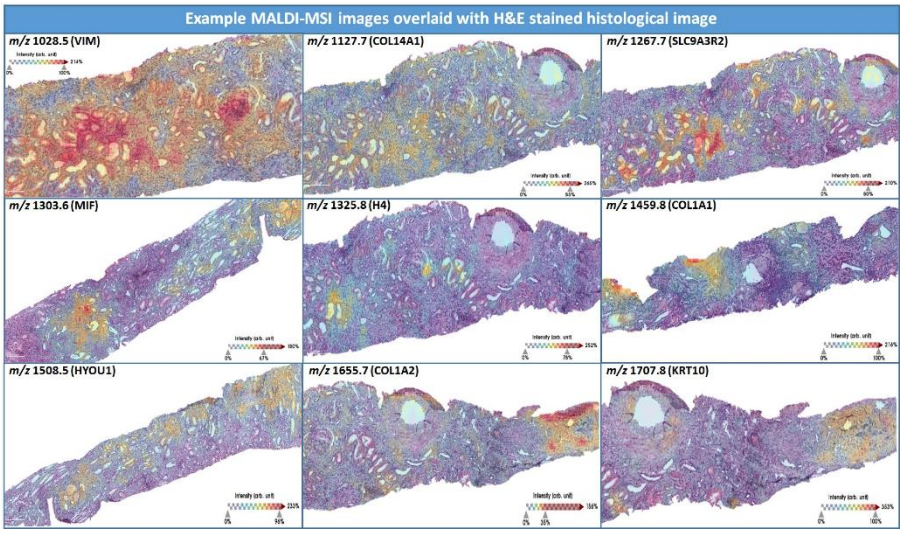

3.5 Immunohistochemical validation of Vimentin and Collagen IV

In order to confirm the data obtained using MALDI-MSI, we performed immunochemical staining on the same IgAN cases (n=8) with two antibodies that are routinely employed in renal pathology: Vimentin and Collagen IV (Fig 5). The data obtained shows that intensity of the staining at the different disease stages corresponded with the findings observed with MALDI-MSI.

Fig5. Immunohistochemical staining of IgAN patients with Vimentin and Collagen IV at different CKD stages (x100, x400). The signal intensities of the relevant signals (m/z 1028.5 (VIM), 1127.7 (COL14A1)), observed in MALDI-MSI are provided in the far right of the figure.

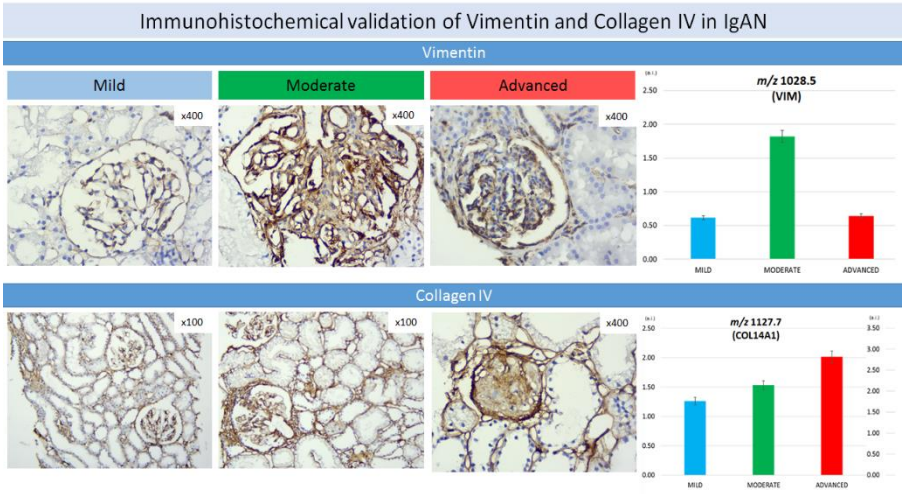

4 DISCUSSION

MesPGN is an important histological pattern in renal diseases, uniting a wide array of GN. IgAN, representing one of the diseases in this group, is one of the most common diseases worldwide and a leading cause of chronic kidney disease (CKD) and end-stage renal disease (ESRD). [1, 2, 22] The disease is characterised by a highly heterogenous and complex clinical presentation, sudden onset, rapid progression, aggressive clinical course and unpredictable response to therapy. [2, 6-8, 11]. Being diagnosed exclusively by performing kidney biopsy with ongoing immunofluorescence/immunochemistry scoring, it is stated that distribution of IgA deposits in kidney tissue is

not always predictive of prognosis and the consequences of the disease. Furthermore, the obtained histological data may be controversial due to the multiform nature of the disease as well as the relatively subjective definition of the lesions obtained by the pathologist [8].

Until now, our knowledge is restricted to the facts that advanced stage of IgAN, has an increase presence of fibrosis/sclerosis, less prominent immune deposition and this, altogether, predicts a poorer outcome of the patient, even after the administration of therapy [23, 24]. From this point, control of the disease progression becomes quite unpredictable. This problem could be partially resolved by repeat biopsies, which, however, are rarely indicated and available. The abundance of IgA deposits itself, as a marker of activity in the earlier stages, all the same does not accurately predict the therapy response [19] and the VALIGA cohort raised many concerns with regards to the Oxford Classification system raised and the impact of discrepancies in biopsy scoring [19, 23, 24]. Considering these aspects, there is a clear requirement for further research that aims to find a sensitive and specific biomarker for the prognosis of IgAN [10, 11, 25].

The reported use of additional immunohistochemical markers of connective tissue (alpha-smooth muscle actin, vimentin, desmin, myosin), which are the hallmark of epithelial-to-mesenchymal transition (EMT), and indicate a response to progressive damage due to the formation of fibrosis and subsequent loss of kidney function, have somewhat additional value but as markers themselves are relatively unspecific [27, 28]. Despite the outbreak of omics research in nephrology, there are currently very little data published on IgAN

and the major proportion of them focus on urinary proteomics, and as such do not analyse issue at the origin of the disease and may have greater difficult in detecting those proteins which play a key role in the pathogenesis of the disease. [14, 28-30].

The capability of MALDI-MSI to provide spatially resolved proteomics analysis of complex renal tissue makes it a highly promising tool in the search for prognostic or predictive markers in glomerular diseases. In fact, MALDI-MSI has already been shown to be capable of playing a key role in the identification of diagnostic and prognostic markers in kidney disease. [31, 32] Furthermore, recent advancements in MALDI-MSI instrumentation have made the concept of resolving the spatial localization of proteins within single glomeruli feasible and has already been employed to detect more specific protein profiles of mesangial cells and podoctyes. [18] In this direction, we aimed to employ this technique in order to detect protein signatures that may provide further insights into the progression of IgAN.

As presented in Fig 1, the protein profile of IgAN was vastly different from that of MesPGN, highlighting the capacity to detect a specific protein signature for this disease. When the two diseases were grouped in base of their CKD stage (Tab 1), these proteomic differences become even more apparent. Performing ROC analysis, fourteen *m/z* signals were observed to have an altered intensity (AUC≥0.8) between the mild and moderate, or moderate and advances, stages of IgAN. On the contrary, only one *m/z* signal ((AUC≥0.8) was noted between mild and moderate MesPGN, indicating that little change in the tissue proteome of MesPGN is noted at these stages. This

data was supported by the histological characteristics observed in our case series, where a large increase in inflammatory cells and the presence of fibrosis/sclerosis was observed in the latter stages of IgAN, whilst little differences were observed between the histological pattern of mild and moderate MesPGN (Fig 1).

Focusing on IgAN, the immunohistochemical confirmation strengthens the objective value of the data obtained by MALDI-MSI. The Vimentin and Collagen IV immunohistochemical staining not only confirmed the presence and spatial distribution of the latter signals, but also reflected the same trend in signal intensity among the different disease stages. As such, this suggests the reliability of the findings obtained using this technique and indicates how they can be translated into complementary immunohistochemical tools that can be employed within the routine clinical workflow in nephropathology.

Those signals whose trend gradually grows within the mild, moderate and advanced stage of the disease (*m/z* 1127, 1508, 1580 and 1707) may play key roles in the development of CKD. In particular, to Collagen alpha-1 chain (COL14A1) and Keratin type 1 (KRT10), have been already observed to increase in expression during progressive kidney damage and the development of fibrosis in multiple studies, which is also in coherence with the tissue localisation observed in our study [14, 33-35] Hypoxia up-regulated protein (HYOU1), co-localised in tubular epithelium cells and is mentioned as an important factor in the development of proteinuria and has a negative prognostic effect in IgAN as a cause of the endoplasmic reticulum stress that leads to cell apoptosis. [25, 36]

Both fibrosis and apoptosis are closely related with phenomena of EMT, where the epithelial tubular cells of the kidney are losing their initial differentiation and start to express mesenchymal (connective tissue) markers leading to loss of kidney function. The detected signals of *m/z* 1459 and 1655 (Collagen chains COL1A1, COL1A2)), which we observed in areas of tubulointerstitial sclerosis, are known for their unfavourable prognostic role in tubulointerstitial fibrosis, podocyte damage, growth of proteinuria and CKD progression and the data is supported in literature. [33-35, 37]

Histone H1.4 (*m/z* 1235) and Histone H4 (*m/z* 1325) are known to promote the increase of IgA antibodies [38] and widely investigated in inflammatory and natriuretic peptide system (NPS) pathways, being shown to promote acute kidney injury (AKI), [39-41]. In our study, these histones were co-localised to regions with the presence inflammatory infiltrates in tubulointerstitial area, so these molecules could be used as potential biomarkers and therapy targets by inhibiting histone deacytilisation and thus avoiding the spread of inflammatory process and progressive damage. [40-42] A similar effect on endoplasmatic reticulum stress, with following proteinuria and autophagy activation, is associated with the downregulation of Na(+)/H(+) exchanger-1 (NHE-1) [43]. This is suggestive that these family of proteins may have an effect on podocyte injury and targeting its activation could provide a positive influence on the preservation of kidney function. Curiously, we observed an increased signal intensity in the moderate IgAN stage, distributed mainly in in tubulointerstitial

area with following decrease in advanced IgAN, which suggests the presence of certain mechanisms of self-protection.

Finally, Vimentin,(*m/z* 1028) and Macrophage migration inhibitory factor (*m/z* 1303), which we observed to have a significantly increased intensity at the moderate stage of IgAN in areas of tubulointerstitial inflammation and glomeruli, are known to play a key role in immunity and inflammatory processes. In fact, Vimentin has recently been shown to be secreted by activated macrophages in glomerular diseases in response to pro-inflammatory signalling, as well as been excreted heavily during the formation of sclerosis, and proposed as a therapeutic target in other forms of GN. [44] Furthermore, Macrophage migration inhibitory factor has been reported to increase its level of urine expression in proliferative glomerulonephritis following the progressive worsening of kidney function [16, 45-47] and its targeting might be an effective treatment for GN and CKD with further investigations needed.

Whilst many of these proteins have already been reported singularly in literature, this is the first time they have been reported collectively in this context. This represents one of the primary advantages of MALDI-MSI with respect to immunohistochemistry based techniques given that the multiple proteins can be monitored within a single analysis, all within an objective manner. [48] Furthermore, being able to consider multiple proteins as a collective panel may also help us to better differentiate complex diseases, [49] such as IgAN, and stratify those patients who may progress to ESRD. One of the biggest limitations of this study, however, is the modest size

of the sample cohort and this should be addressed in future studies in order to confirm these findings. Notwithstanding this limitation, this study represents a promising starting point in the search for protein signatures associated with the progression of IgAN and, if the aforementioned limitation is overcome, provide relevant clinical findings that may assist clinicians in the prognostic assessment of these patients. According to the positive results we obtained, following cohort expansion, with sufficient cases from each disease stage, and immunohistochemical confirmation, these findings could provide an important contribution to routine clinical practice.

ACKNOWLEDGEMENTS

The research leading to these results has received funding from the MIUR: FIRB 2007 (RBRN07BMCT_11), FAR 2014–2018; and in part by Fondazione Gigi & Pupa Ferrari Onlus.

All authors contributed equally

There are no conflicts of interests to disclose

Supplementary table 2. Patient demographics.

			Age (y.o.)	Sex	Ethnicity
Mild (CKD I)	IgAN	Patient 1	5	M	Caucasian
		Patient 2	7	M	Caucasian
	MesPGN	Patient 3	24	F	Caucasian
		Patient 4	36	M	Caucasian
		Patient 5	15	F	Caucasian
		Patient 6	35	F	Caucasian
Moderate (CKD II)	IgAN	Patient 7	11	F	Caucasian
		Patient 8	8	M	Caucasian
		Patient 9	34	M	Caucasian
		Patient 10	32	F	Caucasian
		Patient 11	25	M	Caucasian
		Patient 12	22	F	Caucasian
	MesPGN	Patient 13	29	M	Caucasian
		Patient 14	23	M	Caucasian
Advanced (CKD III)	IgAN	Patient 15	26	M	Caucasian
		Patient 16	33	F	Caucasian
		Patient 17	31	M	Caucasian

5 REFERENCES

1. Glassock RJ (2010) IgA Nephropathy and Henoch-Schonlein Nephritis. In: Floege J, Johnson RJ, Feehaly J. Comprehensive Clinical Nephrology, 4th edn. Elsevier, Amsterdam, pp 270-281
2. Tomino Y. (2016) Pathogenesis And Treatment in IgA Nephropathy. Springer, Tokyo
3. KDIGO Clinical Practice Guidelines for Glomerulonephritis. Chapter 1: Introduction, Kidney International Supplements,Volume 2, Issue 2, 2012, 156-162, http://www.kdigo.org/clinical_practice_guidelines/pdf/KDIGO-GN-Guideline.pdf
4. KDIGO Clinical Practice Guidelines for Glomerulonephritis. Chapter 2: General principles in the management of glomerular disease, Kidney International Supplements,Volume 2, Issue 2, 2012, 156-162, http://www.kdigo.org/clinical_practice_guidelines/pdf/KDIGO-GN-Guideline.pdf
5. Bartosik LP, Lajoie G, Sugar L, Cattran, DC (2001) Predicting progression in IgA nephropathy. Am J Kidney Dis 38:728-735.
6. Feehally J (2001) Predicting prognosis in IgA nephropathy. Am J Kidney Dis 38(4):728-735.
7. Floege J, Boor P, Moeller M J (2018) Was ist gesichert in der Therapie der Glomerulonephritis? Internist (Berl) 59:1268-1278.

8. Cook TH (2007) Interpretation of Renal Biopsies in IgA Nephropathy. In: Tomino Y (ed): IgA Nephropathy Today. Contrib Nephrol. Karger, Basel. Vol. 157, pp 44-49.
9. Yeo SC, Cheung CK., Barratt J (2018) New insights into the pathogenesis of IgA nephropathy. Pediatr Nephrol 33:763-777.
10. Schena FP, Cox SN (2018) Biomarkers and Precision Medicine in IgA Nephropathy. Semin Nephrol 38:521-530.
11. Coppo R (2016) Biomarkers and targeted new therapies for IgA nephropathy. Pediatr Nephrol 32:725-731.
12. Smith A, L'Imperio V, Ajello E, Ferrario F, Mosele N, Stella M, Galli M, Chinello C, Pieruzzi F, Spasovski G, Pagni F, Magni F (2017) The putative role of MALDI-MSI in the study of Membranous Nephropathy. Biochim Biophys Acta Proteins Proteom 1865:865-874.
13. Vlahou A, Mischak H, Zoidakis J, Magni F (2018) Integration Of Omics Approaches And System Biology For Clinical Applications. Wiley, Hoboken
14. Krochmal M, Cisek K, Filip S, Markoska K, Orange C, Zoidakis J, Gakiopoulou C, Mischak H, Delles C, Vlahou A, Jankowski J (2017) Identification of novel molecular signatures of IgA nephropathy through an integrative -omics analysis. Sci Rep 7:9091.
15. Mainini V, Pagni F, Ferrario F, Pieruzzi F, Grasso M, Stella A., Cattoretti, G., Magni, F (2014) MALDI imaging mass spectrometry in glomerulonephritis: Feasibility study, Histopathology 64:901–906.

16. L'Imperio V, Smith A, Ajello E, Piga I, Stella M, Denti V, Tettamanti S, Sinico RA., Pieruzzi F, Garozzo M, Vischini G, Nebuloni M, Pagni F, Magni M (2018) MALDI-MSI pilot study highlights glomerular deposits of macrophage migration inhibitory factor as a possible indicator of response to therapy in membranous nephropathy. Proteomics Clin Appl. https://onlinelibrary.wiley.com/doi/full/10.1002/prca.201800019
17. De Sio G, Smith A, Galli M, Grancini M, Chinello C, Bono F, Pagni F, Magni F (2015) A MALDI-Mass Spectrometry Imaging method applicable to different formalin-fixed paraffin-embedded human tissues, Mol Byosyst 11:1507-14.
18. Smith A, L'imperio V, Denti V, Mazza M, Ivanova M, Stella M, Piga I, Chinello C, Ajello E, Pieruzzi F, Pagni F, Magni F (2018) High Spatial Resolution MALDI-MS Imaging in the Study of Membranous Nephropathy. Proteomics Clin Appl. https://onlinelibrary.wiley.com/doi/full/10.1002/prca.201800016
19. Trimarchi H, Barrat J, Cattran DC, Cook HT, Coppo R, Haas M, Liu ZH, Roberts IS, Yuzawa Y, Zhang H, Feehaly J (2017) IgA nephropathy Oxford Classification update. Kidney Int 91:1014-1021.
20. Sethi S, D'Agati VD, Nast CC, Fogo AB, De Vriese AS, Markowitz GS, Glassock RJ, Fervenza FC, Seshan SV, Rule A, Racusen LC, Radhakrishan J, Winearls CG, Appel GB, Bajema IM, Chang A, Colvin RB, Cook TH, Hariharan S, Herrera

Hernandez LP, Kambham N, Mengel M, Nath KA, Rennke HG, Ronco P, Rovin BH, Haas M (2017) A proposal for standardized grading of chronic changes in native kidney specimen. Kidney International 91:787-789.

21. McDonnel LA, Walch A, Stoeckli M, Corthals GL (2014) MsiMass list: a public database of identifications for protein MALDI MS imaging, J Proteome Res 13:1138-42.
22. Colvin R (2011) Diagnostic pathology. Kidney diseases. Amyrsys, Manitoba
23. Barbour SJ, Espino-Hernandez G, Reich HN, Coppo R, Roberts IS, Feehally J, Herzenberg AM, Cattran DC (2016) VALIGA; Oxford Derivation and North American Validation The MEST score provides earlier risk prediction in IgA nephropathy. Kidney Int 89:167–175.
24. Levey AS, De Jong PE, Coresh J, El Nahas M, Astor BC, Matsushita K, Gansevoort RT, Kasiske BL, Eckardt KU (2011) The definition, classification, and prognosis of chronic kidney disease: a KDIGO Controversies Conference report. Kidney International 80:17-28.
25. Gutierrez E (2019) IgA Nephropathy: is a new approach beyond proteinuria necessary? Pediatr Nephrol 34:921-924.
26. Dyadyk A, Dyadyk E (2011) Guidelines in nephrology. Chetverta hvilya, Donetsk
27. Ivanova M. (2012) Immunohistochemical markers of interstitial fibrosis in primary proliferative glomerulonephritis. Abstracts of the international scientific & practical conference,

dedicated to the World Health Day, Ukrainian Scintific Medical Youth Journal 1:228.

28. Li H, Han J, Pan J, Liu T, Parker CE, Borchers CH (2017) Current trends in quantitative proteomics – an update. J Mass Spectrom 52:319-341.
29. Schena FP, Serino G, Sallustio F, Falchi M, Cox SN (2018) Omics studies for comprehensive understanding of immunoglobulin A nephropathy: state-of-the-art and future directions. Nephrol Dial Transplant 33:2101-2112.
30. Prikryl P, Vojtova L, Maixnerova D, Vokurka M, Neprasova M, Zima T, Tesar V (2017) Proteomic Approach for Identification of IgA Nephropathy-Related Biomarkers in Urine. Physiol Res 66:621-632.
31. Smith A, L'Imperio V, De Sio G, Ferrario F, Scalia C, Dell'Antonio G, Pieruzzi F, Pontillo C, Filip S, Markoska K, Granata A, Spasovski G, Jankowski J, Capasso G, Pagni F, Magni F (2016) α-1-Antitrypsin detected by MALDI imaging in the study of glomerulonephritis: Its relevance in chronic kidney disease progression. Proteomics 16:1759-66
32. Ivanova M, Dyadyk O, Smith A, Santorelli L, Stella M, Galli M, Chinello C, Magni F (2017) Proteomics and Matrix-Assisted Laser Desorption/ Ionization Mass Spectrometry Imaging as a Modern Diagnostic Tool in Kidney Diseases. Pochki 6:25-30.
33. Minz RW, Bakshi A, Chhabra S, Joshi K, Sakhuja V (2010) Role of myofibroblasts and collagen type IV in patients of IgA

nephropathy as markers of renal dysfunction. Indian J Nephrol 20:34-39.

34. Stribos EGD, Nielsen SH, Brix S, Karsdal MA, Seelen MA, van Goor H, et al. (2017) Non-invasive quantification of collagen turnover in renal transplant recipients. PLoS ONE 12(4): e0175898. https://doi.org/10.1371/journal.pone.0175898
35. Djudjaj S, Papasotiriou M, Bu¨low RD , Wagnerova A, Lindenmeyer MT, Cohen CD, Strnad P, Goumenos DS, Floege J, Boor P (2018) Keratins are novel markers of renal epithelial cell injury. Kidney International 89: 792–808 .
36. Lindemeyer MT, Rastaldi MP, Ikehata M, et al. (2008) Proteinuria and Hyperglycemia Induce Endoplasmic Reticulum Stress. J Am Soc Neph 11:2225-36.
37. Yao J, Kez, Wang X, Peng F, Li B, Wu R (2014) Epithelial-mesenchymal transition and apoptosis of renal tubular epithelial cells are associated with disease progression in patients with IgA nephropathy. Mol Med Rep 10: 39-44.
38. Monestier M, Fasy TM, Novick KE, Losman MJ, Rigal D, Wong GY, Terzidis-Trabelsi H, Pilatte Y, Rostoker G. (1994) Histone-reactive IgA antibodies in adult IgA nephropathy and other primary glomerulonephritis. Nephron 68:25-31.
39. Kumar SV, Kulkarni OP, Mulay SR et al (2015) Neutrophil extracellular trap-related extracellular histones cause vascular necrosis in severe GN. J Am Soc Nephrol 26:2399-2413.

40. Van Dam LS, Rabelink TJ, van Kooten C, Teng YKO (2018) Clinical Implications of Excessive Neutrophil Extracellular Trap Formation in Renal Autoimmune Diseases. Kidney Int Rep 19:196-211.
41. Malek V, Sharma N, Gaikwad AB (2019) Histone Acetylation Regulates Natriuretic Peptides and Neprilysin Gene Expressions in Diabetic Cardiomyopathy and Nephropathy. Cur Mol Pharmacol 12:61-71.
42. Hadden MJ, Advani A (2019) Histone Deacetylase Inhibitors and Diabetic Kidney Disease. Int J Mol Sci 19. doi: 10.3390/ijms19092630
43. Feng Z, Tang L, Wu L, Cui S, Hong Q, Cai G, Wu D, Fu B, Wei R, Chen X (2014) Na+/H+ exchanger-1 reduces podocyte injury caused by endoplasmic reticulum stress via autophagy activation. Lab Invest 94:439-54.
44. Wilson PC, Kashgarian M, Moeckel G (2018) Interstitial inflammation and interstitial fibrosis and tubular atrophy predict renal survival in lupus nephritis. Clin Kidney J 11:207-218.
45. Bruchfeld A, Wendt M, Miller EJ (2016) Macrophage migration inhibitory factor in clinical kidney disease. Front Immunol 7:8 doi: 10.3389/fimmu.2016.00008.
46. Boor P (2018) MIF in kidney diseases. Der Pathologe. doi:10.1007/s00292-018-0548-1
47. Djudjaj S, Lue H, Rong S, Papasotiriou M, Klinkhammer BM, Zok S, Klaener O, Braun GS, Lindenmeyer MT, Cohen

CD, Bucala R, Tittel AP, Kurts C, Moeller MJ, Floege J, Ostendorf T, Bernhagen J, Boor P (2016) Macrophage migration inhibitory factor mediates proliferative GN via CD74. J Am Soc Nephrol 27:1650-64

48. Smith A, Piga I, Galli M, Stella M, Denti V, Del Puppo M, Magni F (2017) Matrix-Assisted Laser Desorption/Ionisation Mass Spectrometry Imaging in the study of gastric cancer: a mini review. Int J Mol Sci 18:2588. https://doi.org/10.3390/ijms18122588
49. Galli M, Pagni F, De Sio G, Smith A, Chinello C, Stella M, L'imperio V, Manzoni M, Garancini M, Massimini D, Mosele N, Mauri G, Zoppis I, Magni F (2017) Proteomic profiles of thyroid tumors by mass spectrometry-imaging on tissue microarrays. Biochim Biophys Acta Proteins Proteom 1865:817-827.

CHAPTER III

Detecting proteomic indicators to distinguish Diabetic Nephropathy from Hypertensive Nephrosclerosis by integrating MALDI-MSI with high mass accuracy MS

Andrew Smith[a], Vadim Iablokov[b], Mariafrancesca Mazza[a], Sonia Guarnerio[a], Vanna Denti[a], Mariia Ivanova[a], Martina Stella[a], Isabella Piga[a], Clizia Chinello[a], Bram Heijs[c], Peter A. van Veelen[c], Hallgrimur Benediktsson[d], Daniel A. Muruve[b] and Fulvio Magni[a]

a) Department of Medicine and Surgery, Clinical Proteomics and Metabolomics Unit,
University of Milano-Bicocca, Vedano al Lambro, Italy
b) Department of Medicine, Cumming School of Medicine, University of Calgary, Calgary,
Canada
c) Center for Proteomics and Metabolomics, Leiden University Medical Center, Leiden, The
Netherlands
d) Department of Pathology and Laboratory Medicine, Cumming School of Medicine, University of Calgary, Calgary, Canada

Submitted

KEY WORDS: diabetic nephropathy, hypertensive nephrosclerosis, chronic kidney disease, MALDI-MSI, mass spectrometry, proteomics

ABBREVIATIONS:

AGE: Advanced glycation end-product

ANX5: Annexin A5

BMCKD: Biobank for the Molecular Classification of Kidney Disease

CKD: Chronic Kidney Disease

CO3: Complement 3

ESRD: End-stage renal disease

DN: Diabetic nephropathy

eGFR: Estimated glomerular filtration rate

FFPE: Formalin-fixed paraffin-embedded

FTICR: Fourier-transform ion cyclotron resonance

HN: Hypertensive nephrosclerosis

IHC: Immunohistochemistry

LDHB: Lactate Dehydrogenase B

MALDI: Matrix-assisted laser desorption/ionisation

MSI: Mass spectrometry imaging

nLC-ESI: Nano-liquid chromatography electrospray ionisation

PAS: Periodic acid–Schiff

PGRMC1: Progesterone receptor membrane component 1

SGLT2: Sodium-glucose cotransporter-2

ABSTRACT

Introduction

Diabetic nephropathy (DN) and hypertensive nephrosclerosis (HN) represent the most common causes of chronic kidney disease (CKD) and many patients progress to end-stage renal disease. Patients are treated primarily through the management of cardiovascular risk factors and hypertension, however patients with HN have a more favourable outcome. A non-invasive clinical approach to separate these two entities, especially in hypertensive patients who also have diabetes, would allow for targeted treatment and more appropriate resource allocation to those patients at highest risk of CKD progression.

Methods

In this preliminary study, high spatial resolution MALDI-MSI was integrated with high mass accuracy MALDI-FTICR-MS and nLC-ESI-MS/MS analysis in order to detect tissue proteins within kidney biopsies to discriminate cases of DN (n=9) from cases of HN (n=9).

Results

Differences in the tryptic peptide profiles of the two groups could clearly be detected, with these becoming even more evident in the more severe histological classes, even if this was not evident with routine histology. In particular, four putative proteins were detected and had a higher signal intensity within regions of DN tissue with extensive sclerosis or fibrosis. Among these, two proteins (PGRMC1 and CO3) had a signal intensity that increased at the latter stages of the disease and may be associated with progression.

Discussion/Conclusion

This preliminary study represents a valuable starting point for a future study employing a larger cohort of patients to develop sensitive and specific protein biomarkers that could reliably differentiate between diabetic and hypertensive causes of CKD to allow for improved diagnosis, fewer biopsy procedures and refined treatment approaches for clinicians.

1 INTRODUCTION

Individuals with chronic kidney disease (CKD) are at risk of progression to end-stage renal disease (ESRD), which requires life-saving dialysis or renal transplant. The most common causes of CKD in developed countries are diabetes mellitus and hypertension (1). Diabetic kidney disease, or diabetic nephropathy (DN), accounts for approximately 44% of individuals requiring dialysis in western countries (2). Hyperglycemia in diabetic patients damages glomerular blood vessels, decreases the glomerular filtration rate (GFR) and increases macromolecule filtration. Injured glomeruli result in albuminuria, which is associated with a more rapid decrease in GFR and progression of CKD. Poorly controlled hypertension, on the other hand, can cause a subtype of kidney disease known as hypertensive nephrosclerosis (HN), which can also lead to ESRD. In these cases, hypertension is thought to primarily damage the arteries and arterioles of the kidney, which leads to glomerulosclerosis. Both CKD subtypes lead to ESRD over time, however, DN is associated with a yearly decline in the GFR that is roughly four times that of HN (3). Clinicians may have difficulty confirming the cause of CKD in patients presenting with albuminuria who have both hypertension and diabetes, and cannot reliably predict who will rapidly progress to ESRD. Differentiating between DN and HN is becoming especially important with the advent of SGLT2 inhibitors which have recently been proven to effectively reduce CKD progression in type 2 diabetics, but not in patients with hypertensive nephrosclerosis (4). The inability to differentiate between DN and HN stems from lack of safe, cost-effective, sensitive and

specific clinical biomarkers. Clinically, CKD is staged by estimated GFR (eGFR) and albuminuria. Lower eGFR and greater albuminuria are both indicative of progressive kidney dysfunction and are synergistic (5). Whilst proteinuria and other clinical signs can offer clues, diabetic nephropathy and HN are indistinguishable based on eGFR and albuminuria alone, especially in HN patients who have a component of secondary focal segmental glomerulosclerosis. As a result, most patients are simply treated the same or referred early to nephrologists, which may result in excessive diagnostic testing and unnecessary specialist follow-up especially for patients with non-diabetic HN and lower risk of progression (6). Alternatively, a kidney biopsy can be performed to confirm, or refute either diagnosis, but this procedure is associated with a 6-8% risk of major bleeding complications and not an ideal solution (7) .

Biomarkers that distinguish DN from HN would result in more precise patient care and better resource utilisation, especially as it pertains to SGLT2 inhibition. A biomarker that can correctly differentiate between these two causes of CKD would lead to targeted therapy and focused monitoring for clinicians. Furthermore, if detectable in blood or urine, biomarkers would allow for early disease identification and intervention, thus improving health care.

The discovery of urinary biomarkers for diabetic subtypes of CKD is a growing field of clinical research and fragments of collagen type I (COL I) have been reported to be excreted more in the urine of patients with DN (8). However, whilst urine samples are convenient for clinical screening, they can often be difficult to process and can contain many

proteins which are not produced by the kidney itself (9). Matrix-assisted laser desorption/ionisation (MALDI) mass spectrometry imaging (MSI) represents an ideal tool for the discovery of biomarkers that originate in renal tissues given that it combines the chemical specificity of MS with the imaging characteristics of traditional histology (10), generating thousands of ion images per single experiment and offering a molecular dimension to routine histopathology in complex renal tissue (11). In fact, MALDI-MSI has already been shown to be capable of playing a key role in the identification of diagnostic and prognostic markers in kidney disease (12)(13)(14). Such protein signatures can then be translated to clinically useful biomarkers present in blood or urine.

In this pilot study, we aimed to use high spatial resolution MALDI-TOF-MSI, and integrating it with high mass accuracy MALDI-FTICR-MS and nLC-ESI-MS/MS analysis, to discover tissue proteins capable of differentiating diabetic nephropathy from hypertensive nephrosclerosis.

2 MATERIALS AND METHODS

2.1 Patient Selection

Patients with a histological diagnosis of diabetic nephropathy (DN) or hypertensive nephrosclerosis (HN) were randomly selected from the Biobank for the Molecular Classification of Kidney Disease (BMCKD) at the University of Calgary, Alberta, Canada (15). Tissue samples in the BMCKD database represent the secondary use of specimens collected for clinical care under a protocol approved by the Conjoint Health Research Ethics Board at the University of Calgary. Samples are coded and do not contain any patient-identifying data, thus patient consent was not required. Available clinical patient data was obtained retrospectively from Calgary Lab Services using an anonymous coding system and existing data sources. De-identified patient data was requested at the time of biopsy and included age, sex, pathologic diagnosis, date of biopsy, eGFR, random urine albumin:creatinine ratios (ACR), urinalysis dip positivity for protein (UDP) and red blood cells (UDR). These clinical parameters were then used to characterise and compare 9 matched samples from the DN and HN group (Table 1). Samples were further classified into mild, moderate and severe DN or HN by a renal pathologist. Some clinical data was not completely available for all subjects however (see below). Patient characteristics were compared using T-tests for continuous variables such as age, ACR, creatinine, and eGFR, and Mann-Whitney test for ordinal data such as UDP and UDR. The study protocol was approved by the Conjoint Health Research Ethics Board at the University of Calgary.

Characteristic	DN	HN
Age (SEM, n)	68 (4.8, 9)	57 (5.2, 9)
Male Gender	44%	44%
ACR (SEM, n)	249.7 mg/mmol (118.2, 6)	39.8 mg/mmol (31.8, 4)
Cr (SEM, n)	235.7 µmol/L (53.8, 9)	219.6 µmol/L (40.94, 8)
eGFR (SEM, n)	33.2 ml/min/1.73 m^2 (7.4, 9)	32.3 ml/min/1.73 m^2 (6.7, 8)
UDP (n)	2 (9)	3 (6)
UDR (n)	1 (9)	1 (4)

Table 1. Patient characteristics of the sample cohort analysed by MALDI-TOF- MSI. *ACR, albumin to creatinine ration; Cr, creatinine; DN, diabetic nephropathy; eGFR, estimated glomerular filtration rate; HN, hypertensive nephrosclerosis; SEM, standard error of the mean; UDP, urine dip protein; UDR, urine dip red blood cells*.

2.2 Sample preparation for MALDI-TOF-MSI

For this analysis, fixation time was set at 12 hours following the biopsy procedure, as previously described (16). Five-micron-thick sections were cut and mounted onto conductive indium tin oxide glasses. Paraffin removal and antigen retrieval was performed as previously described (17). Then, trypsin deposition (Sigma-Aldrich, 20 ng/µl) was performed using the iMatrixSpray (Tardo Gmbh, Subingen, Switzerland) automated spraying system and then left in a humid chamber overnight at 40ºC. Finally, matrix deposition for MALDI-MSI analysis was performed by spraying six layers of α-cyano-4-hydroxycinnamic acid (10 mg/ml in 50:50 acetonitrile:water w/0.4%

trifluoroacetic acid) using the iMatrixSpray (Tardo Gmbh, Subingen, Switzerland) with an optimised method and an incorporated heat bed set at 40^{o}C (14).

2.3 MALDI-TOF-MSI analysis

For each tissue section, mass spectra were acquired in reflectron positive mode, within the *m/z* 700 to 3000 mass range, using a rapifleX MALDI Tissuetyper™ (Bruker Daltonik GmbH, Bremen, Germany) MALDI-TOF/TOF MS equipped with a Smartbeam 3D laser operating at 5kHz frequency. A mixture of standard peptides within the mass range of m/z 750 to 3150 (PepMix I, Bruker Daltonik) was used for external calibration. MALDI-MS images were acquired with a single spot laser setting of 18 µm and a raster sampling of 20 µm in both *x* and *y* dimensions.

2.4 MALDI-TOF-MSI data analysis

Data files containing the individual spectra of each entire measurement region (115,068 for DN and 96,539 for HN, respectively) were then imported into SCiLS Lab 2016b software (Bruker Daltonics GmbH) to perform pre-processing: baseline subtraction (Convolution algorithm), normalisation (Total Ion Current algorithm) and spatial denoising. Average (avg) spectra, representative of the whole measurement regions, were generated to display differences in the protein profiles. Peak picking and alignment were performed as feature extraction for statistical analysis and this resulted in the detection of 281 *m/z* features within the dataset. Unsupervised Principal Component Analysis (PCA)

was also performed to reduce the high complexity of the data. Finally, Receiver Operative Characteristic (ROC) analysis was performed, with an AUC (Area Under the Curve) of ≥ 0.80 and a p-value of ≤ 0.05 being required for a peak to be considered as statistically significant. These signals were curated to only include *m/z* values representative of the monoisotopic mass of a tryptic peptide.

2.5 Sample preparation for MALDI-FTICR-MS and nLC-ESI-MS/MS analysis

For MALDI-FTICR-MS and nLC-ESI MS/MS analysis, replicate tissue sections of all the specimens previously analysed by MALDI-MSI were prepared as previously described in Section 2.2. The matrix was removed from the tissue by washing with a solution containing 50:50 acetonitrile:water w/ 0.4% trifluoroacetic acid and subsequently collected. All the material obtained from the DN and HN specimens were pooled together, respectively. The resulting solutions were concentrated using an HETO vacuum concentrator until a final elution volume of approximately 20 µL was reached. This concentrated solution was brought to a final volume of 120 µL by resuspending in phase A (98 / 2 / 0.1; water/acetonitrile/trifluoroacetic acid). The solution was then stocked at -20 °C prior to the MALDI-FTICR-MS and nLC-ESI-MS/MS analyses.

2.6 MALDI-FTICR MS analysis

A volume of 0.4 µL taken each pooled sample was spotted onto an MTP Ground Steel MALDI Target Plate. MALDI-FTICR-MS profiling was performed on a 12 T SolariX XR mass spectrometer (Bruker Daltonics GmbH, Bremen, Germany) operating in positive-ion mode, using 150 laser shots per spot and a 100 µm laser spot size. Spectra were recorded in the *m/z* range of 700–3500 with a 512k data point transient (1.1 s duration), corresponding to an estimated resolution of 200 000 at *m/z* 400. Data acquisition was performed using ftmsControl (Bruker Daltonics GmbH).

2.7 MALDI-FTICR MS data analysis

Raw data files were uploaded into Compass DataAnalysis 4.1. Individual spectra were then exported in ASCII format, transformed into tab delimited files, and individually imported into mMass version 5.5.0 (freely available at www.mmass.org). Peak picking for each spectrum was performed by setting a relative intensity threshold (base peak) of 2.5%. The peak lists were treated with a deisotoping algorithm set to remove isotope peaks with a maximal charge of 2^+ and an isotope mass tolerance of 0.02 Da. The resulting peak list was then used to assign an accurate mass to those *m/z* signals previously detected by MALDI-TOF-MSI analysis.

2.8 nLC-ESI-MS/MS analysis

Each of the tryptic peptide extracts (DN and HN) were analysed using an Easy nLC1000 coupled to a Orbitrap Fusion™ Lumos™ mass spectrometer. Firstly, 5 µL of each sample was diluted in 15 µL of 0.1% formic acid and 7 µL of each fraction was injected onto an in-house-prepared precolumn (100 µm × 15 mm; Reprosil-Pur C18-AQ 3 µm) and eluted via a homemade analytical column (25 cm × 75 µm; Reprosil-Pur C18-AQ 3 µm). The gradient went from 98% to 64% of Phase A (0.1% formic acid) over the course of 120 minutes. Phase B was 0.01% formic acid:acetonitrile (80:20). The analytical column was drawn to a tip of ~5 µm and acted as the electrospray needle of the MS source. The Lumos mass spectrometer was operated in top n mode for 3 seconds. Parameters were as follows: full scan, resolution of 120 000, AGC target of 4 000 000, maximal fill time of 50 ms; MS/MS, resolution of 30 000, AGC target of500 000, maximal fill time of 60 ms, and intensity threshold of 25 000., The allowed charges were 1–4 and excluded after n=1 for 60 seconds. The Thermo.RAW files were converted to MGF files using the MSconvert software (64-bit for Windows, http://proteowizard.sourceforge.net).

2.9 nLC-ESI-MS/MS data analysis

Proteins were identified by performing a database search using in-house Mascot software (version 2.4.1) and Swissprot database (accessed June 2018, 557,491 sequences; 198,3112,666 residues), employing a peptide tolerance of 10 ppm and an MS/MS tolerance of 20 mmu. Trypsin was set as the digestive enzyme, with no fixed

modifications, and one missed cleavage was allowed. Variable modifications were selected: methionine oxidation and two modifications following FFPE treatment (+12 Da and +30 Da). Automatic decoy database search and a built-in Percolator algorithm were applied. Only peptide sequences matched with a p-value of ≤ 0.05 were considered as positive identifications. The protein identification lists for DN and HN were exported in CSV format, respectively and data was filtered in order to obtain a list of proteins specific for each disease class.

2.10 Integration of MALDI-TOF-MSI data with nLC-ESI-MS/MS protein identification

These accurate mass measurements for the MSI signals of interest were then aligned with the mass values belonging to the positively identified peptide sequences obtained using nLC-ESI-MS/MS. A protein identification was putatively assigned to a signal if an error of less than ±10 ppm was observed between the *m/z* value observed in MALDI-FTICR MS and the *m/z* of the related amino acidic sequence determined by nLC-ESI-MS/MS.

2.11 PGRMC1 and C3 Immunohistochemistry

Formalin fixed and paraffin-embedded kidney biopsies were obtained from the BMCKD. Tissue sections were cut at 7 μm onto Superfrost Plus microscope slides (ThermoFisher, Waltham, WA). Tissue sections were then deparaffinised and washed in distilled water. Antigen retrieval was accomplished by incubating sections in a

solution containing 10 mM tris base and 1 mM EDTA with a pH of 9.0 in a steamer for 15 minutes. Slides were then allowed to cool in a heated solution for an additional 35 minutes and washed in tris-buffered saline (TBS). Endogenous peroxidase activity was blocked with Bloxall solution (Vector Laboratories, Burlingame, CA; SP-6000) according to manufacturer's instructions. Sections were incubated with ImmPRESS blocking serum (Vector; MP7401) for 60 minutes, followed by a 60-minute incubation with 1:1000 rabbit anti-human PGRMC-1 (Sigma-Aldrich, Oakville, ON; HPA002877). Sections were then washed in TBS and incubated with ImmPRESS anti-rabbit IgG (Vector; MP-7401) following the manufactures instructions. Following a wash in TBS the sections were developed with ImmPACT Dab substrate for 80 seconds (Vector; SK-4105) and washed in distilled water. Finally, sections were counterstained with hematoxylyn, dehydrated, and mounted with permount. Staining for C3 was performed on frozen sections cut at 7 μm using the Omnis IHC slide stainer (Dako, Mississauga, ON) using manufacturer's instructions and a pre-diluted FITC anti-C3 primary antibody (Roche, Basil, Switzerland; 760-2686). PGRMC1 staining intensity was quantified by the Aperio Positive Pixel Count Algorithm (Leica Biosystems, Concord, ON).

3 RESULTS

The primary aim of this pilot study was to evaluate the possibility to integrate the capabilities of high spatial resolution MALDI-MSI with complementary, high mass accuracy MS techniques, in order to detect *in situ* proteomic alterations that could distinguish diabetic nephropathy from hypertensive nephrosclerosis.

3.1. Patient characteristics

Nine patients with DN and 9 patients with HN were randomly selected from the BMCKD database (Table 1). Males accounted for 44% of individuals in both groups. There were no significant differences in age, serum creatinine, eGFR, urinalysis dip positive protein or blood. Although patients with HN generally had lower ACR's, the differences were not statistically significant due to the small numbers. ACR values were not available for 3 DN and 5 HN subjects. Urinalysis dip protein (UDP) and red blood cells (UDR) was not available for 3 and 5 HN subjects respectively. The histological characteristics of this case series are represented in Figure 1 using Periodic acid–Schiff (PAS) staining.

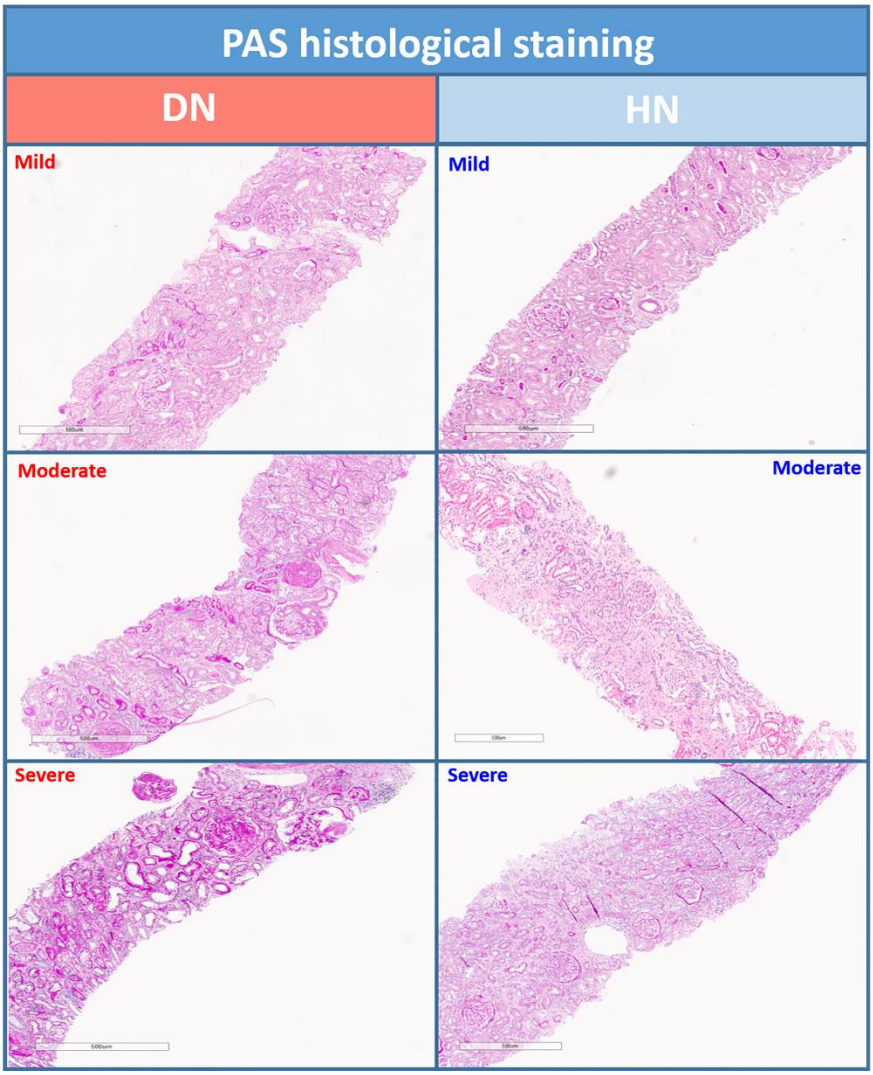

Figure 1: Representative Periodic acid–Schiff (PAS) stained renal biopsies of our diabetic nephropathy (left, red) and hypetensive nephrosclerosis (right, blue) case series. Scale bars are provided.

3.1 Proteomic signatures of diabetic nephropathy and hypertensive nephrosclerosis

Initially, unsupervised principal component analysis (PCA) was performed on the entire MALDI-TOF-MSI dataset (DN and HN, n=18) in order to highlight any proteomic differences between the two disease groups. As shown in Figure 2 (A), the majority of the spectra from the two disease groups were distributed in the same region of the PCA score chart (green circle) and thus can be considered to have similar proteomic profiles. However, the spectra from the DN group (red dots) displayed a more heterogeneous distribution with respect to the HN group (blue dots) and, in fact, there was a region of the PCA score chart where spectra deriving primarily from DN tissue were clustered (black circle), thus suggesting additional alterations of the proteome in this disease.

ROC analysis was then performed, comparing the entire DN dataset with the entire HN dataset. A total of six *m/z* signals, from among the 281 detected *m/z* features, were observed with an AUC ≥ 0.8 and a p-value ≤ 0.05. These are reported in Table 2 and denoted by asterisks in the average tryptic peptide profiles presented in Figure 2 (B).

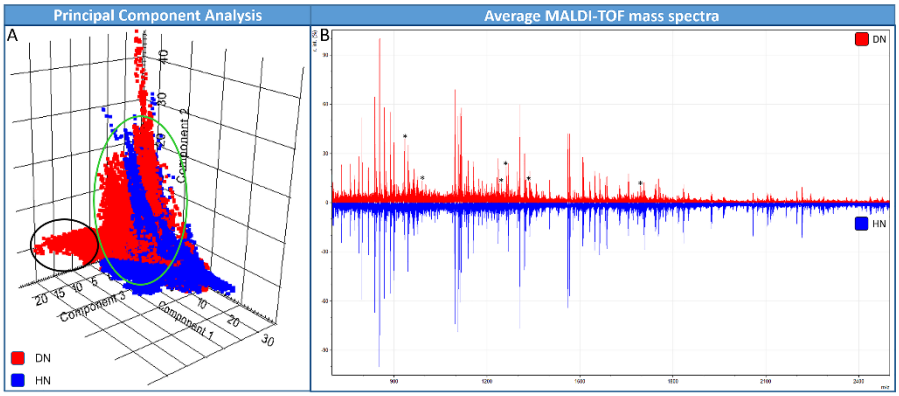

Figure 2: (A) Three-dimensional Principal Component Analysis score chart containing spectra obtained from cases of diabetic nephropathy (red dots) and hypertensive nephrosclerosis (blue dots). All PCA score charts are presenting the variation present within the first three components. (B) Average tryptic peptide profiles representative of diabetic nephropathy (top, red) and hypertensive nephrosclerosis (bottom, blue) in the *m/z* 700 to 2500 mass range. Relative intensity (r. int.) is expressed as a percentage. Signals highlighted by ROC analysis are denoted by asterisks.

m/z in MALDI-TOF-MSI	AUC Value
933.53	0.87
1001.56	0.85
1245.72	0.82
1261.75	0.83
1357.76	0.82
1694.95	0.80

Table 2: The six *m/z* signals (AUC ≥0.80) detected by ROC analysis when comparing the DN and HN groups.

3.2 Proteomic signatures associated with the progression of diabetic nephropathy

In order to evaluate the possibility to detect proteins associated with the more rapid advancement of diabetic nephropathy, each disease group were separated into mild, moderate and severe classes following pathological evaluation.

Initially, PCA was performed comparing only those cases that were histologically evaluated as mild from within the DN and HN groups. As presented in Figure 3A, there were clusters of spectra from the mild DN group (yellow dots) that shared the same distribution as the spectra from the mild HN group (blue dots) and are indicated by a black circle. Conversely, there were further clusters of spectra from the mild DN group with a distinctly different distribution (red circle), suggestive of additional proteomic alterations that are not observed within the mild HN group. Furthermore, when those cases of HN that were histologically evaluated as moderate were added to the PCA analysis, the spectra from the mild DN group (yellow dots) were clustered

closely with the moderate HN group (fuchsia dots), indicating similar protein profile (Figure 3B, black circle).

A similar trend was also observed when the moderate and advanced stages of the disease were compared using PCA. As represented in Figure 3C, the spectra obtained from moderate DN (green dots) were shown to be more similar to those obtained from severe HN (red dots) with a region of overlap observed in the first two components of the PCA score chart (black circle). Conversely, the spectra deriving from the moderate class of HN (fuchsia dots), whilst having a distribution more similar to severe HN than moderate DN, were distributed in a slightly different region of the PCA score chart. Finally, when the severe cases of both diseases were evaluated (Figure 3D), the corresponding spectra (DN; violet dots, HN; pink dots) were well separated, indicating significant differences between their respective tissue proteomes.

The signal intensity of those six discriminatory *m/z* features previously detected (Table 2) was also evaluated at each of the disease stages (Figure 4). In particular, the average signal intensity of *m/z* 933.53 and 1261.75 displayed a similar trend that was represented by a large increase between the mild/moderate stages and the severe stage of DN. This was also further supported by an increased AUC value when comparing the corresponding mild and severe cases of the two diseases (*m/z* 933.5 – AUCs of 0.84 and 0.97, respectively*; m/z* 1261.75 – AUCs of 0.80 and 0.93, respectively).

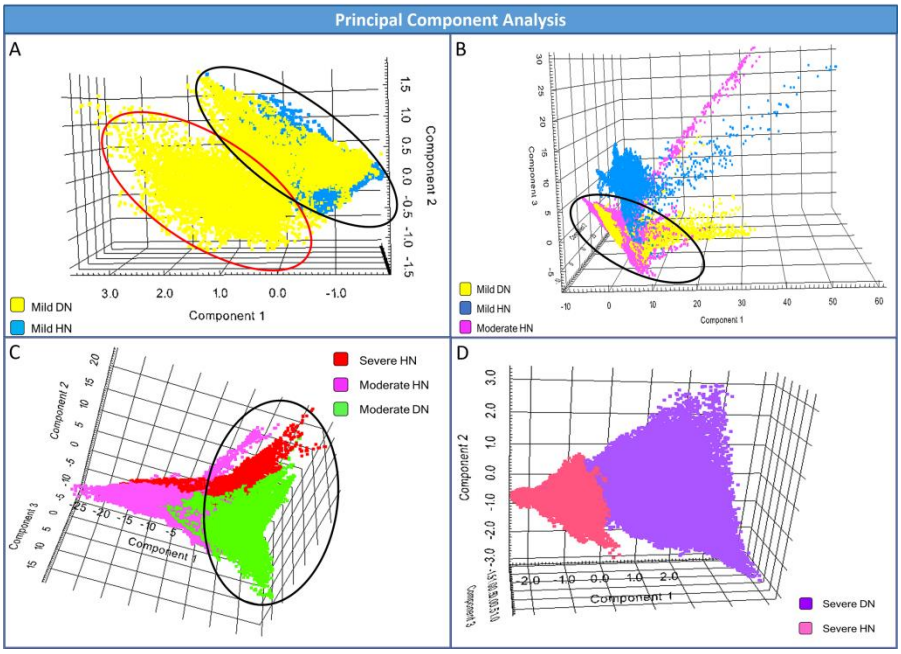

Figure 3: (A-D) Three-dimensional Principal Component Analysis score charts containing spectra obtained from the different histological stages of diabetic nephropathy and hypertensive nephrosclerosis. All PCA score charts are presenting the variation present within the first three components.

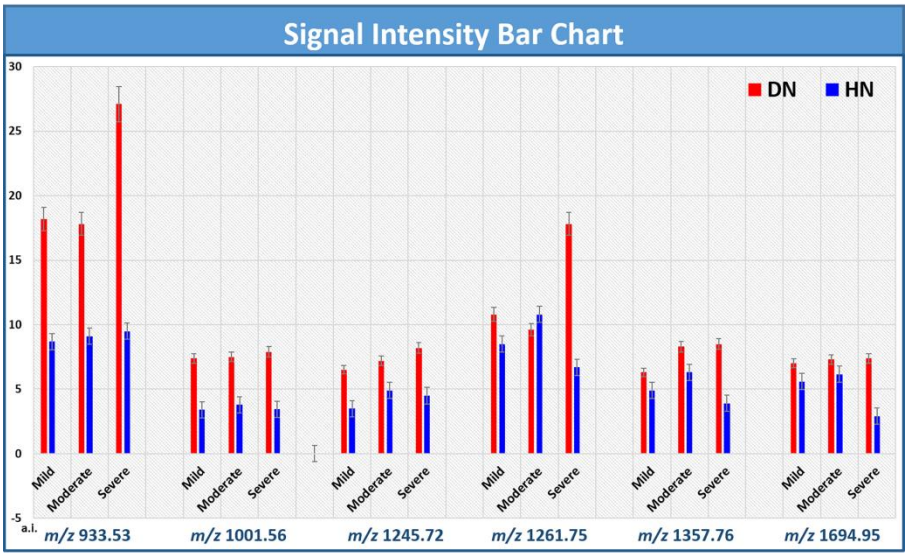

Figure 4: Intensity bar chart of the six *m/z* signals that could discriminate between diabetic nephropathy (red bars) and hypertensive nephrosclerosis (blue bars) at the different histological stages, respectively. Absolute intensity (a.i.) is expressed as arbitrary units. Standard error bars are included.

3.3 Putative protein identification using MALDI-FTICR MS and nLC-ESI-MS/MS

A total of 633 and 630 proteins were identified in the pooled DN and HN samples, respectively (data not provided). The obtained accurate masses of the discriminatory *m/z* signals were then correlated with the obtained protein identification list and this led to the putative identification of four proteins: PGRMC1, Progesterone receptor membrane component 1 (Peptide sequence: FDGVQDPR), ANXA5, Annexin A5 (Peptide sequence: VLTEIIASR), CO3, Complement Component C3 (Peptide sequence: QELSEAEQATR), and LDHB, Lactate Dehydrogenase B (Peptide sequence: LIAPVAEEEATVPNNK). This is summarised in Table 3.

m/z **MALDI-TOF-MSI**	***m/z*** **MALDI-FTICR MS**	**Putative Identity**	**Error (ppm)**
933.53	933.43960	PGRMC1_HUMAN	3.75
1001.56	1001.58776	ANXA5_HUMAN	4.23
1245.72	1245.62079	---	---
1261.75	1261.6060	CO3_HUMAN	9.51
1357.76	1357.67142	---	---
1694.95	1694.8830	LDHB_HUMAN	4.78

Table 3: Putative identification for four of the six signals detected by ROC analysis following integration of the accurate mass values obtained by MALDI-FTICR MS and nLC-ESI-MS/MS. Error values are presented in ppm.

3.4 Co-registration of MALDI-TOF-MS images with histology

The tissue localisation of those putatively identified *m/z* signals was evaluated. Co-registration of the proteomic MALDI-TOF-MSI information with the PAS-stained histological image highlighted that, within DN renal tissue, the highest signal intensities were observed in tubulointerstitial regions with extensive sclerosis or with a significant accumulation of connective tissue or fibrosis. (Figure 5). Whilst these signals were also present in HN tissue, within tubulointerstitial regions (data not shown), they were of much lower signal intensity with respect to DN and supportive of the data provided in Figure 4 and Table 1.

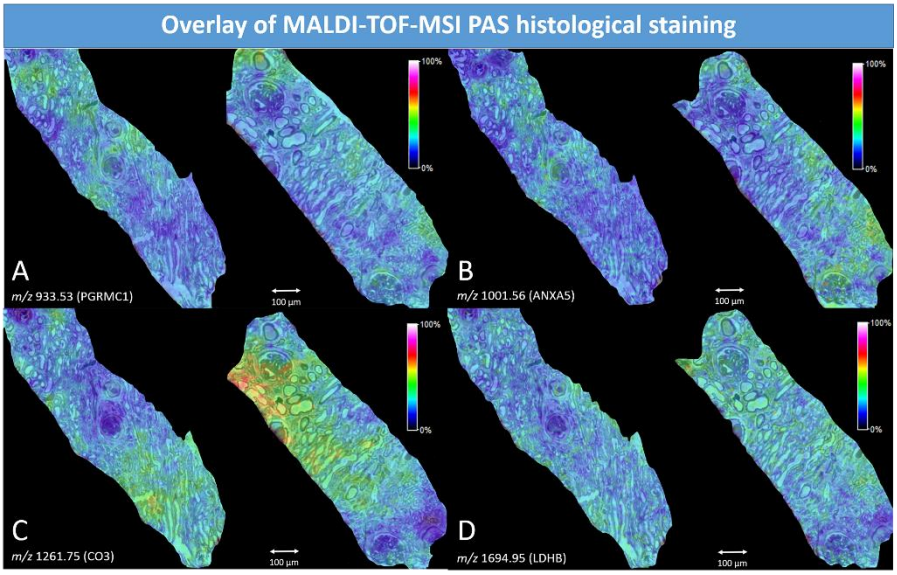

Figure 5: Exemplary MALDI-TOF-MS images, overlaid with the Periodic acid–Schiff (PAS) stained counterpart, highlighting the spatial distribution of (A) *m/z* 933.53 (PGRMC1); (B) *m/z* 1001.56 (ANXA5); (C) *m/z* 1261.75 (CO3); (D) *m/z* 1694.95 (LDHB) in diabetic nephropathy renal tissue. The highest signal intensities were observed

in regions with extensive sclerosis or with a significant accumulation of connective tissue or fibrosis. Intensity colour scale is provided.

3.5 Immunohistochemistry validation of PGRMC1 and CO3

Quantitative IHC staining for PGRMC1 and CO3 was performed on all the cases analysed by MALDI-TOF-MSI (n=18). Regarding PGRMC1, the MALDI-TOF-MSI findings were supported and the same localisation within the tubulointerstitium was observed. Specifically, there was increased cytoplasmic activity in the tubular cells of the DN cases with respect to HN cases, in particular at the moderate and severe stages, with an increased number of moderate and strong positive pixels being observed (Figure 6). This difference was not statistically significant and could be attributable to the low patient numbers.

Regarding CO3, tissue expression was barely detectable by immunofluorescence probably due to the limitations and sensitivity of antibody-based probes and detection. However, the localisation within the tissue compartments was again comparable to that observed in MALDI-TOF-MSI (data not shown).

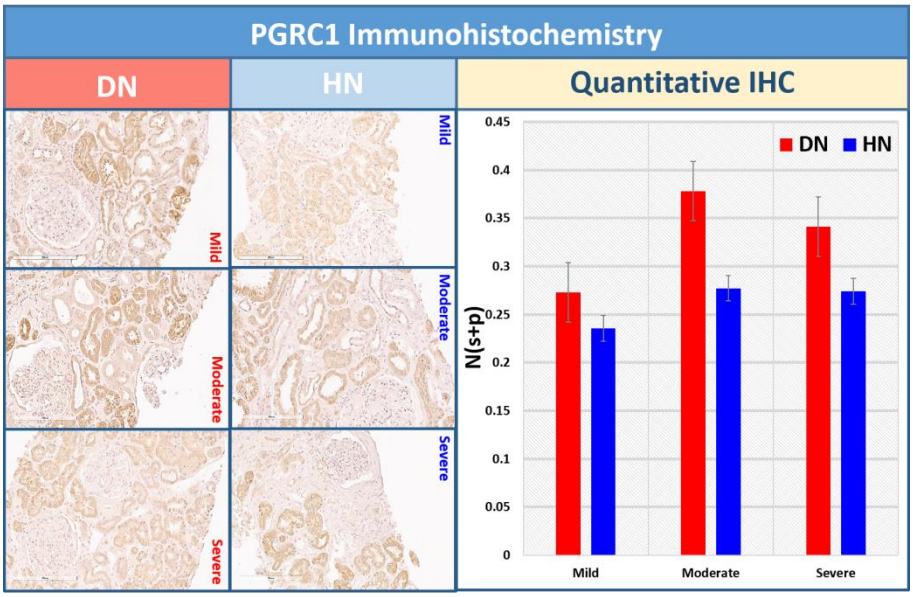

Figure 6: PGRMC1 immunohistochemistry in diabetic nephropathy and hypertensive nephrosclerosis: (Left) Increased cytoplasmic activity could be observed in the tubular cells of the DN cases (Right) Intensity bar chart depicting the output of the quantitative IHC with an increased number of moderate and strong positive pixels (N(s+p)) being observed in the different histological classes of diabetic nephropathy (red bars) and hypertensive nephrosclerosis (blue bars), in particular at the moderate and severe stages. Standard deviation error bars are included.

4 DISCUSSION

The prevalence of CKD worldwide is estimated to be 7.2% in people aged 30 or older and the most common causes of CKD in developed countries are diabetes mellitus and hypertension, clinical conditions which often co-exist. The inability to differentiate between diabetic nephropathy and hypertensive nephrosclerosis in patients with both hypertension and diabetes stems from the lack of safe, cost-effective, sensitive and specific clinical biomarkers. Thus, only clinical parameters are used to make treatment and patient care decisions. Therefore, a biomarker that can correctly differentiate between these two causes of CKD would lead to targeted therapy and focused monitoring for clinicians. In fact, such a biomarker is highly relevant in the current climate given the success of sodium-glucose cotransporter-2 (SGLT2) inhibitors, such as canagliflozin, in significantly slowing down the progression of kidney disease in patients with diabetes (4)(18). However, a large proportion of participants in the CREDENCE study had hypertension in addition to diabetes, and thus the exact nature of their kidney disease was not confirmed. Identifying patients with diabetic nephropathy using a biomarker would allow future studies and clinicians to better select patients in whom SGLT2 inhibitors may be most effective.

After defining the inclusion criteria in base of clinical parameters, high spatial resolution MALDI-TOF-MSI was applied in the present series that contained groups of DN and HN. Initially, unsupervised PCA indicated the presence of proteomic differences between the subsets of cells present in the two groups (Figure 2A). These differences were

further underlined by performing supervised ROC analysis, highlighting those signals with discriminatory capability (Table 2 and Figure 2B). Further supporting this, these discriminatory signals were also among the key factors considered in the loadings plot of the PCA. When the two groups were separated in base of their severity following histological evaluation, even greater differences could be observed between the tissue proteome of the two diseases (Figure 3). In particular, the proteomic profiles of mild and moderate DN were more similar to those from the more advanced histological classes of HN (Figure 3B and C). Together, this data suggests that early stages of DN contain pathophysiologic derangements that are seen in more severe stages of HN. This observation is consistent with increased clinical disease severity of DN compared to HN and the propensity for more rapid progression to kidney failure. Furthermore, given that these alterations may also be detected at an earlier stage with respect to routine renal histology, this may enable earlier, and more correct clinical patient management (19).

Following integration of the MALDI-TOF-MSI data with that of MALDI-FTICR MS and nLC-ESI-MS/MS, four signals that could discriminate between DN and HN were putatively identified: PGRMC1 (*m/z* 933.53), ANXA5 (*m/z* 1001.56), CO3 (*m/z* 1261.75) and LDHB (*m/z* 1694.95). When the tissue localisation of these signals was evaluated, all were found to be of higher intensity in areas of tissue with large amounts of glomerulosclerosis or an accumulation of connective tissue and fibrosis within the tubulointerstitium (Figure 5), histological features which commonly correspond with the more severe

stage of the disease development. This may be particularly relevant in DN given that there is already prior evidence to suggest that renal fibrosis, as a result of the accumulation of connective tissue, is induced by the production and deposition of advanced glycation end-products (AGEs) (20) and can be associated with poorer renal outcomes (21). When the signal intensity of these proteins were evaluated within the different histological groups of DN, PGRMC1 and CO3 showed a marked increase in signal intensity in the severe class with respect to the mild and moderate classes (Figure 4), where the presence of fibrotic and sclerotic tissue is more prevalent (22), providing a tentative suggestion that the increased detection of these proteins may be associated with poorer renal outcome.

The finding of increased CO3 is not surprising since complement activation is increasingly recognised as an effector mechanism during tissue injury in various forms of CKD including DN (23). Whilst DN has historically been considered as a non immune-mediated renal disease, there is emerging data to suggest that the activation of the complement cascade may contribute to the development of diabetic nephropathy and may also explain the rapid progression of DN with respect to HN (24)(25). In particular, an overexpression of C3 has been detected in renal tissue of DN with respect to controls in multiple animal models, with an even larger overexpression in those animals with induced ischemia (26). Notwithstanding that CO3 was not clearly detected in this DN patient cohort using standard immunofluorescence, primarily due to the limited sensitivity of antibody based probes and detection. Nevertheless, this data provides further insight as to the

mechanisms that may underlie DN versus HN progression in humans. In light of this, the role of C3 in human DN could be further investigated, especially in tubulointerstial compartments, in order to verify its utility in the distinction between diabetic and hypertensive causes of CKD.

Upon quantitative IHC validation, PGRMC1 was observed to be localised to the tubulointerstitium, as observed by MALDI-TOF-MSI. Furthermore, there was increased cytoplasmic activity in the tubular cells of the DN cases. Whilst the same marked increase in tissue positivity was not observed in the severe group, this is not to be unexpected given the differing levels of sensitivity and specificity between MALDI-MS based techniques and IHC (27) (28). Irrespective of this, the detection of increased levels of PGRMC1 in DN, using both techniques, still heralds promise in this clinical context. PGRMC1 (progesterone receptor membrane component 1) is implicated in diverse cellular processes, including proliferation and resistance to apoptosis (29). Furthermore, it is commonly overexpressed in many cancers including ovarian, breast and kidney (30)(31)(32) and its expression in human tumours may be triggered by hypoxia (33).

Focusing on the expression of PGRMC1 in the kidney, our results confirm previous findings localizing PGRMC1 to the cytoplasm of tubular epithelial cells in the kidney (32). Zhang and colleagues showed that renal cell carcinomas highly expressed PGRMC1. Furthermore, increased levels of PGRMC1 were found in the sera of renal cell carcinoma patients and was associated with worse survival (32). Whilst the authors did not speculate on the driving force behind

its expression, PGRMC1 is likely induced by the hypoxic tumour milieu in renal cell carcinoma. Interestingly, tubulointerstitial damage seen in diabetic nephropathy is thought to be, in part, due to tissue hypoxia. Chronic ischemia is the primary cause of tissue hypoxia in diabetic nephropathy and is thought to arise in two ways (34). First, intrarenal vasoconstriction due to RAS activation or decreased NO activity can limit blood flow and decrease oxygen delivery. Second, blood flow may be limited structurally by the presence of interstitial fibrosis surrounding the peritubular capillaries. Thus, increased PGMC1 expression may represent worsening hypoxia in diabetic nephropathy and its increased intensity in regions with interstitial fibrosis is supportive of this hypothesis.

If the tissue findings related to these two proteins (CO3 and PGRMC1) is confirmed in a larger cohort of patients, it may then be relevant to follow their expression in the urine of patients with DN and HN. Complement component C3 has already been detected in the urine of patients with DN and, in fact, its abundance was negatively correlated with eGFR and associated with poorer renal outcome (35). Furthermore, it has been shown that the urinary excretion of PGRMC1 may be indicative of its direct kidney origin (36) and, in particular, altered levels of PGRMC1 were detected in the urine of patients with type 1 and type 2 diabetes with respect to controls (37). Therefore, given the potential to detect these proteins in urine, they may represent possible targets to distinguish diabetic and hypertensive forms of kidney disease using a non-invasive approach.

On the contrary, whilst a number of studies have also demonstrated the increased excretion of collagen fragments in patients with DN (35)(36), we did not detect differences in collagen expression between DN and HN. However, collagen alpha-1 chains, for example, are expressed as general markers of fibrosis and may not represent a useful marker to distinguish between DN and HN given that renal fibrosis is a common pathway and hallmark of all CKD progression (37). Furthermore, if the spatially resolved analysis of extracellular matrix proteins are to be correctly investigated using this approach, the use of matrix metalloproteinases, such as collagenase type III or elastase, which specifically target collagens would represent the more efficient strategy (38). Unfortunately, this was outside of the scope of this study.

Whilst our case series was defined by using primarily pathological criteria, and can thus reduce possible confounding factors in the analysis, this can often limit the size of the sample cohort and represents the largest shortcoming of this study. This can be overcome by performing a study in a larger cohort to verify and build upon these findings. However, notwithstanding this limitation, this preliminary study highlights the feasibility of integrating high spatial resolution MALDI-MSI with high mass accuracy MS in order to search for novel kidney-derived protein markers of DN. The cluster of putative proteins presented here represents a valuable starting point for a future study employing a larger cohort of patients and, if verified, would allow for the development of clinical biomarkers in blood or urine that would assist the clinician in providing more precise therapy for patients with DN and HN.

ACKNOWLEDGEMENTS

Our special thanks go to Kevin Chapman and Michelle Nelson for their technical and administrative support of the study.

STATEMENT OF ETHICS

The authors confirm that this research complies with the relevant ethics guidelines. Tissue samples in the BMCKD database represent the secondary use of specimens collected for clinical care under a protocol approved by the Conjoint Health Research Ethics Board at the University of Calgary. Samples are coded and do not contain any patient-identifying data, thus patient consent was not required.

DISCLOSURE STATEMENT

The authors state that they have no conflicts of interest

FUNDING SOURCES

The research leading to these results has received funding from MIUR: FIRB 2007 (RBRN07BMCT_11), FAR 2014–2016 and in part by Fondazione Gigi & Pupa Ferrari Onlus.

AUTHOR CONTRIUBTIONS

All authors have contributed to the production of this manuscript in accordance with the ICMJE Criteria for Authorship.

REFERENCES

1. Jha V, Garcia-Garcia G, Iseki K, Li Z, Naicker S, Plattner B, et al. Chronic kidney disease: Global dimension and perspectives. Lancet [Internet]. 2013;382(9888):260–72. Available from: http://dx.doi.org/10.1016/S0140-6736(13)60687-X
2. Woroniecka KI, Park ASD, Mohtat D, Thomas DB, Pullman JM, Susztak K. Transcriptome analysis of human diabetic kidney disease. Diabetes. 2011;60(9):2354–69.
3. Furuichi K, Shimizu M, Okada H, Narita I, Wada T. Clinico-pathological features of kidney disease in diabetic cases. Clin Exp Nephrol [Internet]. 2018;0(0):1–6. Available from: http://dx.doi.org/10.1007/s10157-018-1556-4
4. Perkovic V, Jardine MJ, Neal B, Bompoint S, Heerspink HJL, Charytan DM, et al. Canagliflozin and Renal Outcomes in Type 2 Diabetes and Nephropathy. N Engl J Med [Internet]. 2019;NEJMoa1811744. Available from: http://www.nejm.org/doi/10.1056/NEJMoa1811744
5. Adler AI, Stevens RJ, Manley SE, Bilous RW, Cull CA, Holman RR. Development and progression of nephropathy in type 2 diabetes: The United Kingdom Prospective Diabetes Study (UKPDS 64). Kidney Int. 2003;63(1):225–32.
6. Vanholder R, Annemans L, Brown E, Gansevoort R, Gout-Zwart JJ, Lameire N, et al. Reducing the costs of chronic kidney disease while delivering quality health care: A call to action. Nat Rev Nephrol [Internet]. 2017;13(7):393–409. Available from: http://dx.doi.org/10.1038/nrneph.2017.63

7. Korbet SM, Volpini KC, Whittier WL. Percutaneous renal biopsy of native kidneys: A single-center experience of 1,055 biopsies. Am J Nephrol. 2014;39(2):153–62.
8. Rossing K, Mischak H, Dakna M, Zürbig P, Novak J, Julian BA, et al. Urinary Proteomics in Diabetes and CKD. J Am Soc Nephrol. 2008;19(7):1283–90.
9. Thongboonkerd V. Practical points in urinary proteomics. J Proteome Res. 2007;6(10):3881–90.
10. Smith A, Piga I, Galli M, Stella M, Denti V, del Puppo M, et al. Matrix-assisted laser desorption/ionisation mass spectrometry imaging in the study of gastric cancer: A mini review. Int J Mol Sci. 2017;18(12).
11. L'Imperio V, Smith A, Chinello C, Pagni F, Magni F. Proteomics and glomerulonephritis: A complementary approach in renal pathology for the identification of chronic kidney disease related markers. Proteomics - Clin Appl. 2016;10(4):371–83.
12. Smith A, L'Imperio V, De Sio G, Ferrario F, Scalia C, Dell'Antonio G, et al. α-1-Antitrypsin detected by MALDI imaging in the study of glomerulonephritis: Its relevance in chronic kidney disease progression. Proteomics. 2016;16(11–12):1759–66.
13. Smith A, L'Imperio V, Ajello E, Ferrario F, Mosele N, Stella M, et al. The putative role of MALDI-MSI in the study of Membranous Nephropathy. Biochim Biophys Acta [Internet]. 2017;1865(7):865–74. Available from:

http://www.ncbi.nlm.nih.gov/pubmed/27890680

14. Smith A, L'Imperio V, Denti V, Mazza M, Ivanova M, Stella M, et al. High Spatial Resolution MALDI-MS Imaging in the Study of Membranous Nephropathy. Proteomics - Clin Appl. 2019;13(1):1–10.
15. Muruve DA, Mann MC, Chapman K, Wong JF, Ravani P, Page SA, et al. The biobank for the molecular classification of kidney disease: Research translation and precision medicine in nephrology. BMC Nephrol. 2017;18(1):1–11.
16. De Sio G, Smith AJ, Galli M, Garancini M, Chinello C, Bono F, et al. A MALDI-Mass Spectrometry Imaging method applicable to different formalin-fixed paraffin-embedded human tissues. Mol Biosyst. 2015;11(6):1507–14.
17. De Sio G, Smith AJ, Galli M, Garancini M, Chinello C, Bono F, et al. A MALDI-Mass Spectrometry Imaging method applicable to different formalin-fixed paraffin-embedded human tissues. Mol Biosyst [Internet]. 2015 Jun;11(6):1507–14. Available from: http://www.ncbi.nlm.nih.gov/pubmed/25592401
18. Guthrie R. Canagliflozin and cardiovascular and renal events in type 2 diabetes. Postgrad Med. 2018;130(2):149–53.
19. L'Imperio V, Smith A, Ajello E, Piga I, Stella M, Denti V, et al. MALDI-MSI Pilot Study Highlights Glomerular Deposits of Macrophage Migration Inhibitory Factor (MIF) as a Possible Indicator of Response to Therapy in Membranous Nephropathy. Proteomics Clin Appl [Internet]. 2018 Oct 25;e1800019. Available from:

http://www.ncbi.nlm.nih.gov/pubmed/30358918

20. Sugimoto K, Yasujima M, Yagihashi S. Role of advanced glycation end products in diabetic neuropathy. Curr Pharm Des [Internet]. 2008;14(10):953–61. Available from: http://www.ncbi.nlm.nih.gov/pubmed/18473845
21. Yamagishi S, Matsui T. Advanced Glycation end Products, Oxidative Stress and Diabetic Nephropathy. Oxid Med Cell Longev. 2010;3(2):101–8.
22. Tervaert TWC, Mooyaart AL, Amann K, Cohen AH, Cook HT, Drachenberg CB, et al. Pathologic Classification of Diabetic Nephropathy. J Am Soc Nephrol [Internet]. 2010;21(4):556–63. Available from: http://www.jasn.org/lookup/doi/10.1681/ASN.2010010010
23. Sun ZJ, Li XQ, Chang DY, Wang SX, Liu G, Chen M, et al. Complement deposition on renal histopathology of patients with diabetic nephropathy. Diabetes Metab. 2018;6–11.
24. Flyvbjerg A. The role of the complement system in diabetic nephropathy. Nat Rev Nephrol [Internet]. 2017;13(5):311–8. Available from: http://dx.doi.org/10.1038/nrneph.2017.31
25. Zhang J, Wang Y, Zhang R, Li H, Han Q, Guo R, et al. Implication of decreased serum complement 3 in patients with diabetic nephropathy. Acta Diabetol. 2018;55(1):31–9.
26. Kelly KJ, Liu Y, Zhang J, Dominguez JH. Renal C3 complement component: Feed forward to diabetic kidney disease. Am J Nephrol. 2015;41(1):48–56.
27. KRIEGSMANN J, KRIEGSMANN M, CASADONTE R.

MALDI TOF imaging mass spectrometry in clinical pathology: A valuable tool for cancer diagnostics (Review). Int J Oncol [Internet]. 2015 Mar;46(3):893–906. Available from: https://www.spandidos-publications.com/10.3892/ijo.2014.2788

28. Winter M, Tholey A, Kristen A, Röcken C. MALDI Mass Spectrometry Imaging: A Novel Tool for the Identification and Classification of Amyloidosis. Proteomics. 2017;17(22):1–9.
29. Ahmed IS, Rohe HJ, Twist KE, Craven RJ. Pgrmc1 (progesterone receptor membrane component 1) associates with epidermal growth factor receptor and regulates erlotinib sensitivity. J Biol Chem. 2010;285(32):24775–82.
30. Peluso JJ, Liu X, Saunders MM, Claffey KP, Phoenix K. Regulation of ovarian cancer cell viability and sensitivity to cisplatin by progesterone receptor membrane component-1. J Clin Endocrinol Metab. 2008;93(5):1592–9.
31. Crudden G, Loesel R, Craven RJ. Overexpression of the cytochrome P450 activator HprG (heme-1 domain protein/human progesterone receptor) in tumors. Tumor Biol. 2005;26(3):142–6.
32. Zhang D, Xia X, Wang X, Zhang P, Lu W, Yu Y, et al. PGRMC1 is a novel potential tumor biomarker of human renal cell carcinoma based on quantitative proteomic and integrative biological assessments. PLoS One. 2017;12(1):1–15.
33. Dressman HK, Hans C, Bild A, Olson JA, Eric Rosen P, Marcom K, et al. Gene expression profiles of multiple breast

cancer phenotypes and response to neoadjuvant chemotherapy. Clin Cancer Res. 2006;12(3 I):819–26.

34. Kanwar Y, Sun L, Xie P, Chen S. A Glimpse of Various Pathogenic Mechanisms of Diabetic Nephropahty. Annu REv Pathol. 2011;(7):395–423.

35. Maahs DM, Siwy J, Argilés À, Cerna M, Delles C, Dominiczak AF, et al. Urinary collagen fragments are significantly altered in diabetes: A link to pathophysiology. PLoS One. 2010;5(9).

36. Alkhalaff A, Zürbig P, Bakker SJL, Bilo HJG, Cerna M, Fischer C, et al. Multicentric validation of proteomic biomarkers in urine specific for diabetic Nephropathy. PLoS One. 2010;5(10).

37. Liu Y. Cellular and molecular mechanisms of renal fibrosis. Nat Rev Nephrol [Internet]. 2011 Oct 18;7(12):684–96. Available from: http://www.ncbi.nlm.nih.gov/pubmed/22009250

38. Angel PM, Comte-Walters S, Ball LE, Talbot K, Mehta A, Brockbank KGM, et al. Mapping Extracellular Matrix Proteins in Formalin-Fixed, Paraffin-Embedded Tissues by MALDI Imaging Mass Spectrometry. J Proteome Res. 2018;17(1):635–46.

CHAPTER IV

High spatial resolution MALDI-MS Imaging in the study of Membranous Nephropathy

Andrew Smith PhD[a#], Vincenzo L'Imperio MD[b#], Vanna Denti MSc[a], Mariafrancesca Mazza BSc[a], Mariia Ivanova MD[a], Martina Stella MSc[a], Isabella Piga PhD[a], Clizia Chinello PhD[a], Elena Ajello MD[c], Federico Pieruzzi MD[c], Fabio Pagni MD[b], and Fulvio Magni PhD[a]

[#] Equally contributing authors

[a] University of Milano-Bicocca, Department of Medicine and Surgery, Clinical Proteomics and Metabolomics Unit, Vedano al Lambro, Italy

[b] University of Milano-Bicocca, San Gerardo Hospital, Department of Medicine and Surgery, Pathology, Monza, Italy

[c] University of Milano-Bicocca, Department of Medicine and Surgery, Nephrology Unit, Monza, Italy

Published in Proteomics - Clin Appl. 2019;13(1):1–10.

ABBREVIATIONS

α-SMA - α-Smooth muscle actin

CKD – Chronic kidney disease

ESRD – End-stage renal disease

FFPE – Formalin-fixed paraffin-embedded

GBM - Glomerular basement membrane

LID - Laser induced dissociation

MN – Membranous nephropathy

MIF - Macrophage migration inhibitory factor

NR – Treatment non-responder

PAS – Periodic acid-Schiff

PLA2R - Phospholipase A2 receptor

R – Treatment responder

ROI – Region of interest

SHH - Sonic hedgehog

THSD7A - Thrombospondin type 1 containing 7A domain

KEY WORDS: high spatial resolution, high-throughput, MALDI-MSI, membranous nephropathy, proteomics

STATEMENT OF CLINICAL RELEVANCE

Membranous Nephropathy is the most frequent cause of nephrotic syndrome in adults. The natural course of the disease is characterised by the "rule of third", with one third of patients experiencing complete remission, with the remaining experiencing continuous relapses or progression of the disease. Additionally, the therapeutic approach to the disease is not standardised and this leads to further heterogeneity in terms of response. Therefore, a biomarker able to predict the likelihood of a patient responding favourably to the treatment seems mandatory.

Here we demonstrate how high spatial resolution MALDI-MSI can assist in the search for proteins able to predict a patient's response to treatment *a priori*, going beyond what was previously possible by visualising the spatial localisation of proteins within the sub-compartments of the glomeruli and tubulointerstitium. To highlight the plausibility of this, we present two proteins, Sonic Hedgehog (SHH) and α-smooth muscle actin (α-SMA), whose signal intensity and spatial localisation differed between responders and non-responders to therapeutic treatment (Ponticelli Regimen).

By taking advantage of high-spatial resolution MALDI-MSI, protein signatures can be generated from specific regions, and cell subtypes, from within the kidney and this may assist in the search for novel proteins implicated in Membranous Nephropathy and other glomerular diseases.

ABSTRACT

MALDI-MSI technology has advanced rapidly during recent years with the development of instruments equipped with low-diameter lasers that are suitable for high spatial resolution imaging. This may provide significant advantages in certain fields of molecular pathology where more specific protein fingerprints of individual cell types are required, such as renal pathology.

Here we performed MALDI-MSI analysis of a cohort of MN patients among which patients either responded favourably (R; n=6), or unfavourably (NR; n=4), to immunosuppressive treatment (Ponticelli Regimen), employing a 10µm laser spot diameter.

Specific tryptic peptide profiles of the different cellular regions within the glomerulus could be generated, similarly for the epithelial cells belonging to the proximal and distal tubules. Conversely, specific glomerular and sub-glomerular profiles could not be obtained whilst using the pixel size performed in previous studies (50µm). Furthermore, we highlight two proteins, Sonic Hedgehog (SHH) and α-smooth muscle actin (α-SMA), whose signal intensity and spatial localisation within the sub-glomerular and tubulointerstitial compartments differed between treatment responders and non-responders.

The current study exemplifies the advantage of using high spatial resolution MALDI-MSI for the study of MN and highlights that such

findings have the potential to provide complimentary support in the routine prognostic assessment of MN patients.

1 INTRODUCTION

Matrix-assisted laser desorption/ionisation mass spectrometry imaging (MALDI-MSI) has developed into a highly powerful analytical tool for the visualisation of biomolecules directly *in situ* [1].The technique combines the chemical specificity of MS with the imaging characteristics of traditional histology, generating thousands of ion images per single experiment and offering a molecular dimension to routine histopathology in complex biological tissues. The technique has already been applied to a wide range of analyte classes [2–7] with the detection of tissue proteins representing one of the most stimulating aspects of MSI in pathology given their significant role in defective cell signalling. Therefore, the ability to resolve the spatial localisation of multiple proteins within a single section of pathological tissue can enable the detection of disease candidates and improve our understanding of disease pathogenesis [8].

Recent advancements in matrix deposition techniques [9] and MALDI-TOF-MSI instrumentation [10] have made the concept of resolving the spatial localisation of proteins in individual cells a distinct possibility [9]. The routine introduction of MALDI-TOF-MSI instruments that simultaneously move a small diameter laser beam and sample carrier whilst maintaining the pixel fidelity, along with laser repetition rates of 10kHZ, means that high spatial resolution imaging may be performed all within a practical time frame [11]. However, accompanying this potential are the significant amounts of data that can be generated within a short period, resulting in high data loads and computational

challenges [12]. Therefore, it is important to ascertain whether working at high spatial resolution provides additional diagnostic, or prognostic, information that cannot be obtained when using larger pixel sizes.

One branch of pathology that may benefit most from the application of high spatial resolution MALDI-MSI is renal pathology given the high complexity and heterogeneity associated with glomerular diseases [13]. Membranous nephropathy (MN) represents one of the most pressing fields of application [14] given that this glomerulopathy represents the most frequent cause of nephrotic syndrome in adults and approximately one third of patients progress to end stage renal disease (ESRD) [15]. Furthermore, there still remains a fair degree of heterogeneity in terms of patient response and outcomes following the administration of immunosuppressive treatment [16] and a marker that can reliably predict the response of a patient to this therapeutic treatment *a priori* is lacking.

Most recently, our group applied MALDI-MSI in order to assess the feasibility of this technique to detect potential markers of differential treatment response in MN [17]. Macrophage migration inhibitory factor (MIF) was detected, along with a further two unidentified signals (*m/z* 1111 and *m/z* 1198), as being able to distinguish between those patients who responded (R) and whose who did not respond (NR) to immunosuppressive treatment (Ponticelli Regimen) [17]. However, given the complexity of the disease, high spatial resolution MALDI-MSI of the sub-glomerular and tubular structures may provide further insights into the pathology of this disease that would not be otherwise possible when using larger pixel sizes.

Here we report a high spatial resolution MALDI-MSI study focused on membranous nephropathy and the differential response of patients to immunosuppressive treatment. Initially, we highlight the additional cellular specificity that can be obtained when employing a 10µm pixel when compared with 50µm, spatially resolving signals deriving from different cells of the glomeruli. The spatial localisation of those signals previously detected (*m/z* 1111 and *m/z* 1198) was visualised within the glomerular and tubular structures. These signals were also putatively identified using on-tissue MALDI-MS/MS in order to hypothesise their potential biological role on the basis of their cellular location.

2 MATERIALS AND METHODS

2.1 Patient selection

Patients with a histological diagnosis of MN on renal biopsy, taken between January 2008 to November 2016 at the University of Milano-Bicocca, San Gerardo Hospital, Monza, Italy, were collected. The appropriate Ethical Committee approved the collection of these specimens and informed consent was obtained from all participants. The primary MN patients to be included in the study were selected as previously described [14,17]. Finally, these cases were further divided in the Responder (n=6) and Non-Responder (n=4) groups with at least twelve months of follow-up, as indicated by KDIGO-GN response criteria [18]. Patient characteristics are reported in Supplementary Table 1.

Supplementary Table 1: Clinical data of the analysed patients

Age *	70	±	15
Gender (M/F) *	6	/	1
Proteinuria (g/24h) *	9	±	5
Serum creatinine (mg/dl) *	2	±	1
Response to therapy (R/NR)	5	/	2
Systolic hypertension **	7		
First 6 months therapy with iACE	7		
eGFR (CKD-EPI formula, mL/min/1.73m²) *	52, 9	±	27
eGFR, estimated glomerular filtration rate; iACE, inhibitor of angiotensin converting enzyme; CKD-EPI, Chronic Kidney Disease Epidemiology Collaboration			
* Values are expressed in the form "average ± standard deviation"			
** Those patients with at least one value above 140/90 mmHg were considered to be affected by systemic hypertension			

2.2 Sample preparation for MALDI-MSI

For this analysis, fixation time was set at 12 hours following the biopsy procedure, as previously described [19]. Five-micron-thick sections were cut and mounted onto conductive indium tin oxide glasses. Paraffin removal and antigen retrieval was performed as previously described [19]. Then, trypsin deposition (Sigma-Aldrich, 100 ng/µl) was performed using the iMatrixSpray (Tardo Gmbh, Subingen, Switzerland) automated spraying system and then left in a humid chamber overnight at 40^{o}C. Finally, matrix deposition for MALDI-MSI analysis was performed by spraying six layers of α-cyano-4-hydroxycinnamic acid (10 mg/ml in 50:50 acetonitrile:water w/0.4% trifluoroacetic acid) using the iMatrixSpray (Tardo Gmbh, Subingen, Switzerland) with an optimised method [14] and an incorporated heat bed set at 40^{o}C.

2.3 MALDI-MSI analysis

For each MN tissue section, mass spectra were acquired in reflectron positive mode, within the *m/z* 700 to 3000 mass range, using a rapifleX MALDI Tissuetyper™ (Bruker Daltonik GmbH, Bremen, Germany) MALDI-TOF/TOF MS equipped with a Smartbeam 3D laser operating at 2.5 kHz frequency. A mixture of standard peptides within the mass range of *m/z* 750 to 3150 (PepMix I, Bruker Daltonik) was used for external calibration. For every case, MALDI-MS images were acquired with a single spot laser setting of 10 µm and a raster sampling of 10 µm in both *x* and *y* dimensions. Consecutive tissue sections were also

obtained from three of these cases and MALDI-MS images were acquired with a single spot laser setting of 50 μm and a raster sampling of 50 μm in both *x* and *y* dimensions.

Following MALDI-MSI analysis, the matrix was removed with increasing concentrations of ethanol (70% and 100%) and the slides were stained using PAS stain. The slides were converted to digital format using a ScanScope CS digital scanner (Aperio, Park Center Dr., Vista, CA, USA), thus allowing for the direct overlap of images and the integration of proteomic and morphological data. Regions of interest (ROIs) were annotated by the pathologist and included 103 glomeruli and 18 regions of tubules that were affected by the disease.

2.4 On-tissue MALDI-MS/MS analysis

In order to obtain the optimal mass value to be selected for dissociation during on-tissue MALDI-MS/MS, representative MALDI mass spectra were acquired from the desired ROIs in the same modality and mass range employed for the MSI analysis. A single precursor ion was isolated by using the smallest precursor ion selector (PCIS) window possible and dissociated using laser-induced dissociation (LID) and LIFT™ technology, with the laser energy being set within a range of 40-70%. This process was performed until a final MS/MS spectrum was obtained from the accumulation of ~90,000 laser shots.

2.5 MALDI-MSI data analysis

For the comparison of individual pixel spectra, raw peak lists were exported from flexImaging 5.0 (Bruker Daltonik, Bremen, Germany) in CSV format and imported into mMass version 5.5.0 (freely available at www. mmass.org). Baseline correction and spectrum smoothing (Gaussian method, 0.1 *m/z* window size and 2 cycles) were performed prior to peak picking with a S/N threshold of 5. Finally, the peak lists generated from each spectrum were compared using a tolerance of 0.50 Da.

FlexImaging 5.0 was employed to co-register the corresponding histological images and define the virtual ROIs that were previously annotated by the pathologist. Data files containing the individual spectra from each of the annotated glomerular (33, 263 spectra) and tubular (97, 621 spectra) ROIs were then imported into SCiLS Lab 2016b software (http://scils.de/; Bremen, Germany) to perform pre-processing: baseline subtraction (TopHat algorithm), normalisation (Total Ion Current algorithm) and spatial denoising. Average (avg) spectra, representative of the whole measurement regions, were generated to display differences in the tryptic peptide profiles. Peak picking and alignment were performed as feature extraction for statistical analysis and this resulted in the detection of 327 *m/z* features within the dataset. These signals were curated to only include *m/z* values representative of the monoisotopic mass of a tryptic peptide. Finally, Receiver Operative Characteristic (ROC) analysis and the Wilcoxon Rank-Sum Test were performed, with an AUC (Area Under

the Curve) of ≥0.70 and a *p*-value of <0.05 being required for a peak to be considered as statistically significant.

For MALDI-MS/MS spectra, baseline subtraction (TopHat algorithm) and smoothing (Savitzky-Golay algorithm) were performed using FlexAnalysis 3.4 (Bruker Daltonik, Bremen, Germany). All MS/MS spectra were searched against the Swiss-Prot database (accessed January 2018, 556,568 sequences; 199, 530,821 residues) with the Mascot 2.4.1 search engine (Matrix Science, London, UK). Mass tolerances were set at 0.20 Da for MS and 0.40 Da for MS/MS. Trypsin was set as the enzyme, allowing for one partial cleavage. No fixed post-translational modifications were set in the search parameters.

3 RESULTS

The primary aim of this study was to evaluate the additional pathological information that could be obtained when using 10µm pixel sizes for the MALDI-MSI analysis of renal biopsies taken from patients with membranous nephropathy.

3.1 Tryptic peptide profiles of whole glomeruli: 10µm vs 50µm pixel size

Initially, consecutive tissue sections of three cases were analysed using 10µm and 50µm pixel sizes, respectively. As presented in Figure 1, the glomeruli can be spatially resolved from the tubular background when using a 10µm pixel size. For example, the signal intensity of *m/z* 1429

was associated with the presence of glomeruli and, in particular, enabled two closely positioned glomeruli and connecting region of fibrosis to be distinguished from the tubulointerstitium (Left). Conversely, when using a 50μm pixel size, the same glomeruli could quite clearly not be spatially resolved (Right), signifying that pixels obtained from glomerular regions will contain confounding signals from the tubules and intersitium.

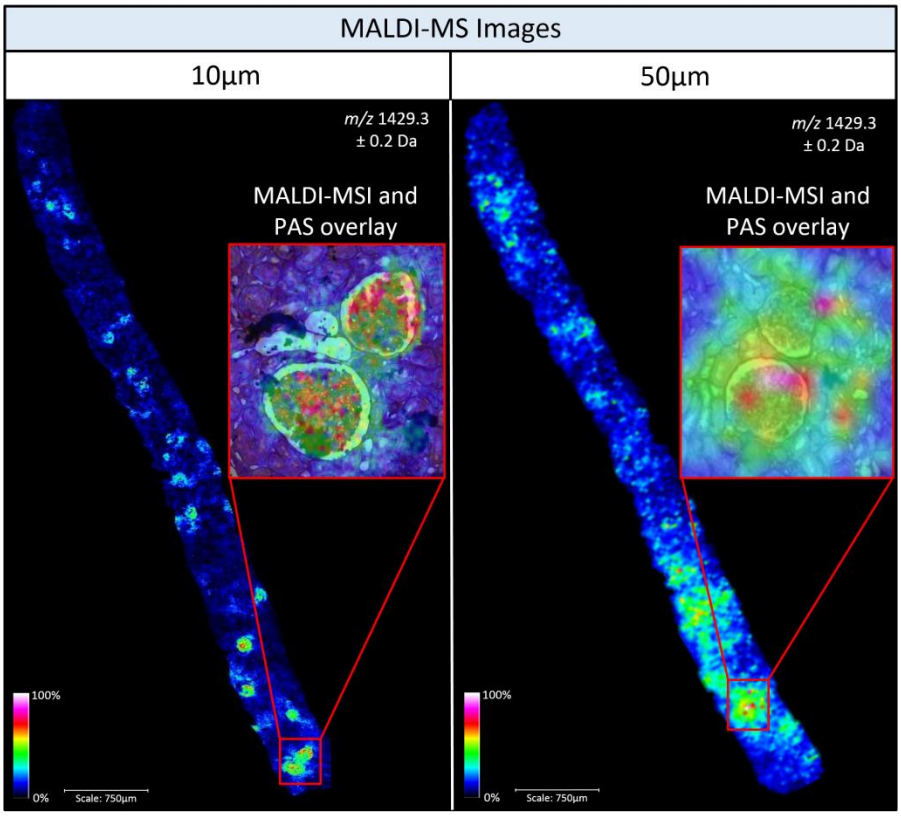

Figure 1: The spatial distribution of *m/z* 1429 in consecutive tissue sections obtained from a patient with Membranous Nephropathy when analysed using a 10µm and 50µm pixel size, respectively. The overlay of the MALDI-MS and PAS-stained images from the same two glomeruli, in both analyses, are highlighted by red boxes.

Subsequently, the average glomerular profiles for each case, using both 10µm vs 50µm pixel sizes, were generated (Figure 2). In particular, the intensity of the previously presented glomerular signal (*m/z* 1429) was more consistent when a 10µm pixel size was employed, whilst it varied greatly among patients when the 50µm pixel size was used, further indicating that pure glomerular profiles may not always be obtained when using a lower spatial resolution.

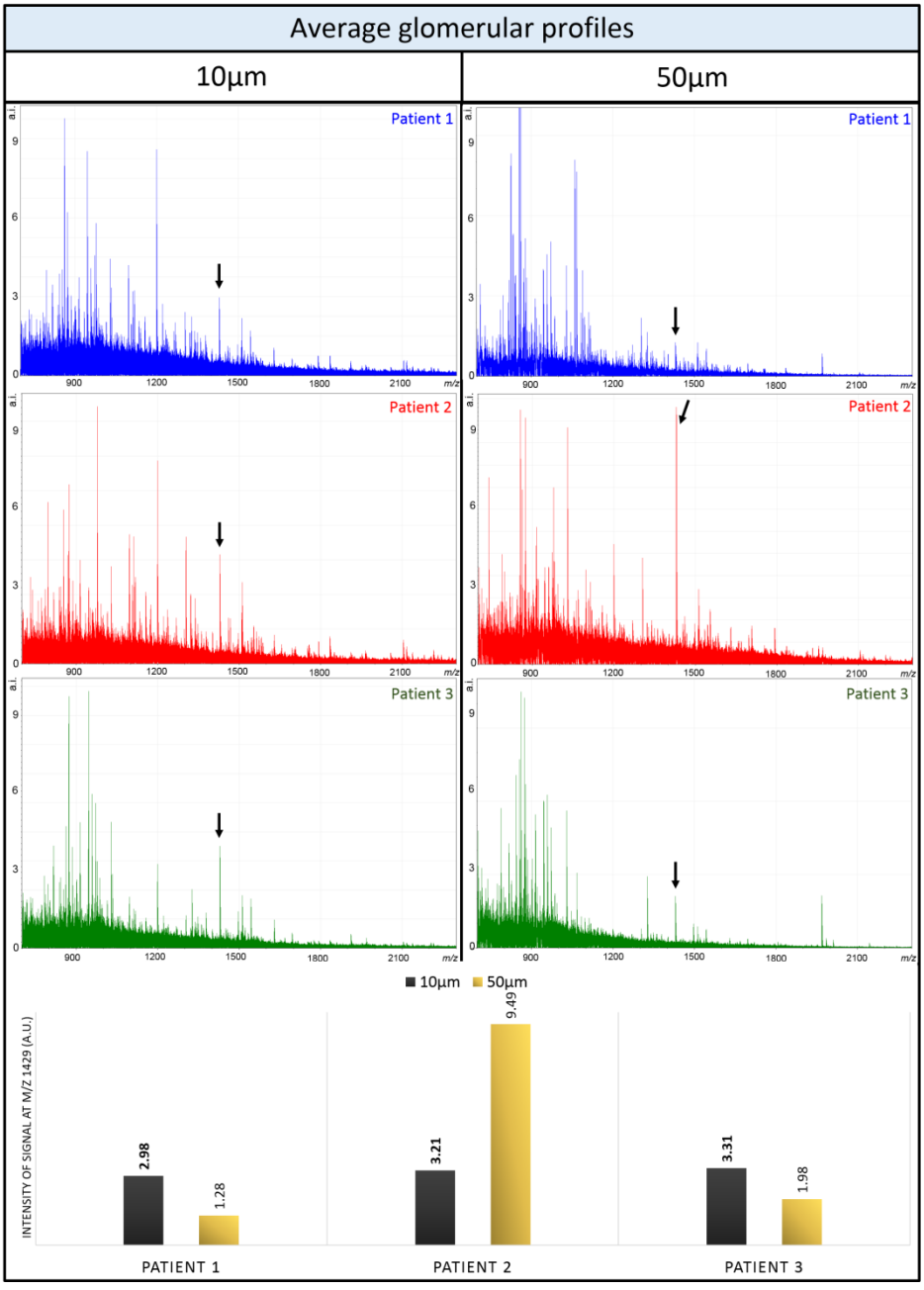
Average glomerular profiles
10µm
50µm
Patient 1
Patient 2
Patient 3
a.i.
m/z
900
1200
1500
1800
2100
10µm
50µm
INTENSITY OF SIGNAL AT M/Z 1429 (A.U.)
2.98
1.28
3.21
9.49
3.31
1.98
PATIENT 1
PATIENT 2
PATIENT 3

Figure 2: Average tryptic peptide profiles of the glomeruli from three patients with Membranous Nephropathy when MALDI-MSI was performed using a 10µm (left) and 50µm (right) pixel size. Black arrows indicate the location of *m/z* 1429. Mass spectra are presented in the in the *m/z* 700 to 2300 mass range. Absolute intensity (a.i.) is expressed as arbitrary units.

Finally, differences in the tryptic peptide profiles obtained from the glomerular and tubular (in close proximity to the glomeruli) structures were then assessed using ROC analysis and the Wilcoxon Rank-Sum Test. Considering the analyses performed with a 10µm pixel size, four *m/z* signals were determined to be discriminative (AUC≥0.7 and *p*-value<0.01, respectively). Conversely, there were no statistically significant signals detected when considering the analyses performed with a 50µm pixel size. This information is provided in Table 1.

Table 1: Discriminative *m/z* signals (AUC of ≥0.70 and a *p*-value of <0.01, respectively) between glomerular and tubular structures

m/z value (± 0.2 Da)	AUC value		*p*-Value	
	10µm	50µm	10µm	50µm
872.8	0.73	0.55	<0.001	>0.05
914.9	0.72	0.57	<0.001	>0.05
1429.2	0.88	0.56	<0.001	>0.05
1512.2	0.72	0.58	<0.001	>0.05

3.2 Tryptic peptide profiles of glomerular cells: 10µm vs 50µm pixel size

Following this, the feasibility of obtaining tryptic peptide profiles that are more specific for the different cell types within the glomerulus was assessed. Data was compared from consecutive tissue sections of the same renal biopsy that had been analysed with the 10µm and 50µm single spot laser setting, respectively. As highlighted in Figure 3 (A), analysis with a 10µm pixel enabled signals, as exemplified by *m/z*

1198, to be spatially resolved from within the sub-structures of the glomerulus. Conversely, this was not possible when a 50µm pixel was employed and the localisation of the tryptic peptides did not correspond with the histological structures of the glomeruli. Subsequently, individual spectra were exported from pixels corresponding with individual mesangial cells and the podocytes, both in the 10µm and 50µm pixel analysis. When employing a 10µm pixel size, the tryptic peptide profiles corresponding with mesangial cells and podocytes showed distinct differences. In fact, when the peak lists obtained from the two spectra were compared, 78 peaks were found to be present only in the profile of the mesangial cells whilst 101 were present only in the profile of podocytes. There were a further 316 peaks (63.80%) that were common to both profiles. However, when the process was performed using spectra obtained with a 50µm pixel size, from within the corresponding glomeruli, only 45 peaks were specific for the mesangial cells whilst only 61 were specific for the podocytes. A further 356 peaks (77.06%) were common to both profiles, indicating a far less specific profile for the mesangial and epithelial cells. Additionally, working with a 10µm pixel size enabled multiple spectra to be obtained specifically from the mesangial cells and podocytes of the glomeruli. As presented in Supplementary figure 1, the average of five single pixel spectrum for each cell type (Supplementary figure 1B) maintained the information and specificity observed in the single pixel spectrum (Supplementary figure 1A). In contrast, only 2 pixels could be obtained when using a 50µm pixel size, with each of them again

presenting a profile that was indicative of both mesangial cells and podocytes mixed together (Supplementary figure 2).

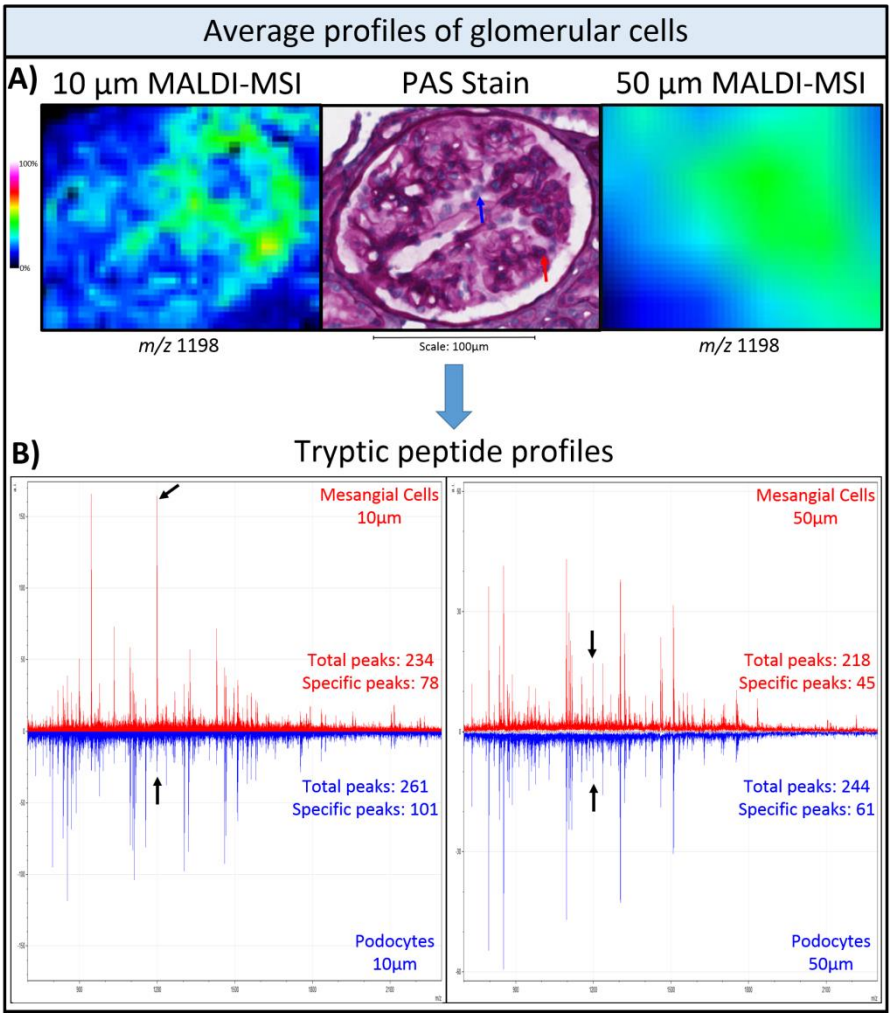

Figure 3: (A) The spatial localisation of *m/z* 1198 within the same glomerulus when using a 10µm pixel (Left) and 50µm pixel (Right). The corresponding PAS stained image is presented in the centre. (B) Single pixel tryptic peptide profiles obtained from mesangial cells (PAS stained image; red arrows) and podocytes (PAS Stained image; blue arrows) using a 10µm pixel (Left) and 50µm pixel (Right). Mass spectra are presented in the *m/z* 700 to 2300 mass range. Absolute intensity (a.i.) is expressed as arbitrary units. The black arrows indicate the peak corresponding with *m/z* 1198.

3.3 Tryptic peptide profiles of tubular epithelial cells

Attention was then focused towards the possibility of also obtaining more specific tryptic peptide profiles from the epithelial cells of the renal tubules whilst using a 10µm pixel size. As performed with the glomeruli, five single spectra were taken from pixels corresponding with the epithelial cells of the proximal and distal tubules, respectively, and average spectra were generated. As shown in Figure 4, the tryptic peptide profiles of epithelial cells belonging to the proximal or distal tubules show a fair degree of similarity. However, only 249 of the 333 picked peaks (74.77%) were present both of the profiles, indicating that there may also the possibility to generate specific profiles of the epithelial cells belonging to the different compartments of renal tubules. Furthermore, the tryptic peptide profiles of the tubular epithelial cells shared distinct similarities with the tryptic peptide profile generated from the podocytes of the glomeruli (Figures 3 and 4), which are themselves specialised forms of epithelial cells.

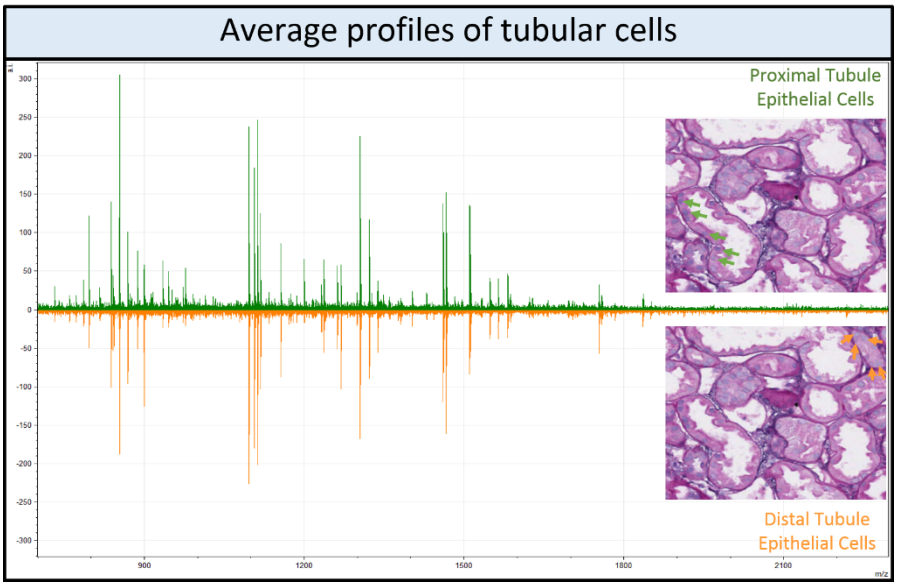

Figure 4: Tryptic peptide profiles of epithelial cells of the proximal tubule (Green) and distal tubule (Orange) generated from the average of five pixels. Mass spectra are presented in the in the *m/z* 700 to 2300 mass range. Absolute intensity (a.i.) is expressed as arbitrary units.

3.4 On-tissue identification of Sonic Hedgehog (SHH) and α-Smooth muscle actin (α-SMA)

On-tissue MALDI-MS/MS, using LID-LIFT™, was then performed in order to identify the signals previously detected to have an altered signal intensity in MN patients who differentially responded to immunosuppressive treatment [17]. Additionally, these signals also appeared to have a differential signal intensity between the mesangial and the epithelial cells (Figures 3 and 4). The signal at *m/z* 1111 was putatively identified as a tryptic peptide (LVKDLSPGDR) of Sonic Hedgehog (SHH) with a Mascot Score of 36.5. The annotated MS/MS

spectrum is provided in Supplementary figure 3. The signal at *m/z* 1198 was then putatively identified as a tryptic peptide (AVFPSIVGRPR) of α-Smooth muscle actin (α-SMA) with a Mascot Score of 39.5. The annotated MS/MS spectrum is provided in Supplementary figure 4.

3.5 Glomerular and tubular localisation of Sonic Hedgehog (SHH) and α-Smooth muscle actin (α-SMA) in treatment responders (R) and non-responders (NR)

The signal intensity and tissue localisation of *m/z* 1111 (SHH) and *m/z* 1198 (α-SMA) were then evaluated within the R and NR groups. Regarding *m/z* 1111 (SHH), the signal was of higher intensity (*p*-value<0.005) in the tubules with respect to the glomeruli when considering the R group (Figure 5a; Column E), being primarily localised to the tubular epithelial cells and the interstitium (Figure 5a, Columns C and D). However, in the NR group, the signal intensity not only increased within the tubular epithelial cells/interstitium (Figure 5a, Columns C and D and E) but also increased within the glomeruli relative to the tubules, showing a similar signal intensity (*p*-value>0.005) to that observed within the tubular epithelial cells (Figure 5a; Column E). Within the glomeruli, the signal displayed a stronger intensity within the glomerular capillary tufts and the podocytes with respect to the mesangial cells (Figure 5a; Columns A and B).

Regarding *m/z* 1198 (α-SMA), the signal intensity within the glomeruli was higher with respect to the tubules (*p*-value<0.005) when considering the R group (Figure 5b; Column E) and was localised

primarily to the mesangial cells of the glomeruli and the epithelial cells of the proximal tubules. Considering the NR group, however, there tubular signal intensity was increased and more similar (*p*-value >0.005) to that observed in the glomeruli (Figure 5b; Column E).

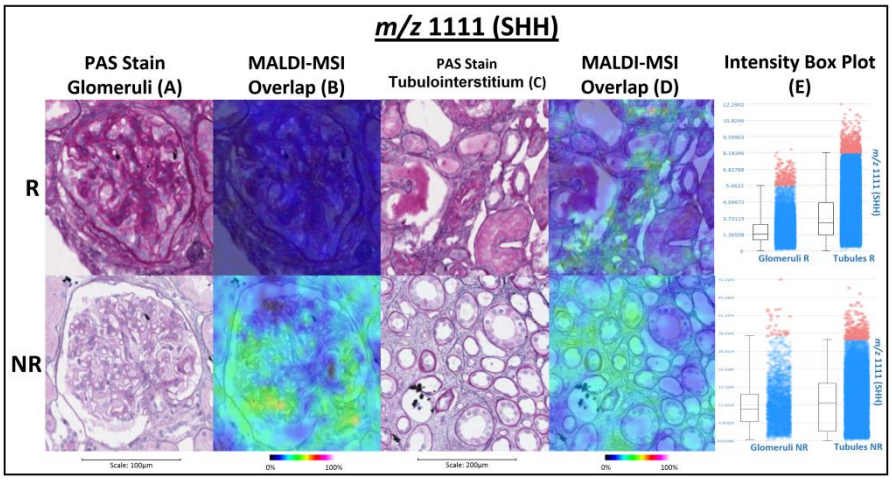

Figure 5a: The signal intensity and spatial localisation of *m/z* 1111 (SHH) in the glomeruli and tubulointerstitium of treatment responders (R; Top row) and non-responders (NR; Bottom Row). Dimension and intensity scales are provided below.

(A) PAS stained image of the glomerulus

(B) MALDI-MS image overlapped with the PAS stained image of the glomerulus shown in column A

(C) PAS stained image of the tubulointerstitium

(D) MALDI-MS image overlapped with the PAS stained image of the tubulointerstitium shown in column C

(E) Box plot of the signal intensity in glomeruli and tubules

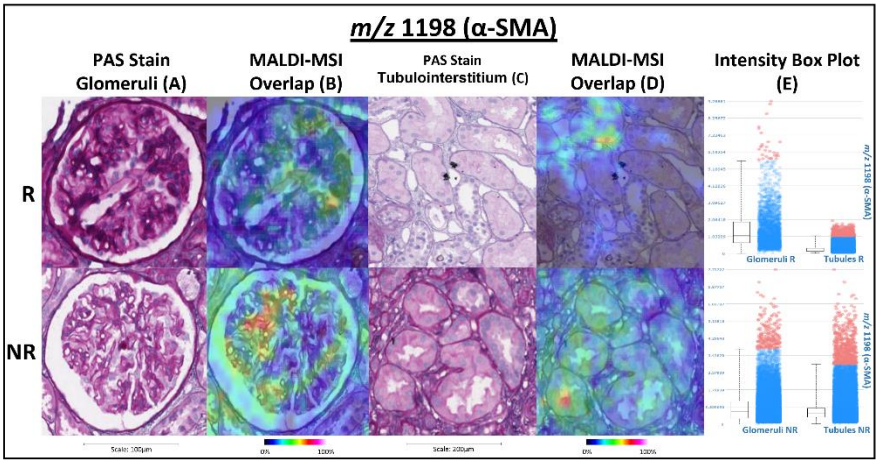

Figure 5b: The signal intensity and spatial localisation of *m/z* 1198 (α-SMA) in the glomeruli and tubulointerstitium of treatment responders (R; Top row) and non-responders (NR; Bottom Row). Dimension and intensity scales are provided below.

(A) PAS stained image of the glomerulus

(B) MALDI-MS image overlapped with the PAS stained image of the glomerulus shown in column A

(C) PAS stained image of the tubulointerstitium

(D) MALDI-MS image overlapped with the PAS stained image of the tubulointerstitium shown in column C

(E) Box plot of the signal intensity in glomeruli and tubules

4 DISCUSSION

Matrix assisted laser desorption/ionisation mass spectrometry imaging is now an established and robust tool for the spatially resolved analysis of biomolecules directly *in situ* [21] [23]. The technological advancements associated with matrix deposition and TOF-MS instrumentation are continually driving clinical applications forward, especially in the area of pathology [20]. In this vein, one of the most important advancements in MALDI-MSI technology during recent years is the development of instruments equipped with low-diameter lasers that are suitable for high spatial resolution, high-throughput molecular imaging [11]. This high spatial resolution MALDI-MS imaging may open the door in certain fields of molecular pathology where protein fingerprints of small clusters, or even individual, cells are required. One particular field that may benefit greatly from the employment of this modern MS instrumentation is renal pathology, especially considering that the individual cells of the glomeruli (endothelial, epithelial, mesangial and podocytes) can be affected in a heterogeneous manner during the development of glomerular diseases and this may have an impact on the disease course [22]. However, accompanying the potential of high spatial resolution analysis is the significant amounts of data that can be generated within a short time frame, resulting in high data loads and computational challenges when performing statistical analysis of large patient cohorts [12]. Therefore, it is important to ascertain whether working at high spatial resolution

provides additional pathological information that cannot be obtained when using larger pixel sizes

Here we performed MALDI-MSI analysis, employing a laser spot diameter and raster setting of 10µm, respectively, of a further cohort of membranous nephropathy patients that included responders (R) and non-responders (NR) to immunosuppressive treatment (Ponticelli Regimen). It is also important to note that the analysis of even this small cohort generated approximately 600GB of raw data, which equated to approximately one million individual spectra, and this required significantly more computational power in order to open and analyse the data.

Initially, data obtained using a 10µm single spot laser setting was compared with that obtained from consecutive tissue sections of the same renal biopsy that had been analysed with a 50µm single spot laser setting. Glomeruli could be spatially resolved with from the tubulointerstitium and pure glomerular profiles could be obtained whilst using a 10µm pixel size, whilst this was not possible when a 50µm setting was employed (Figures 1 and 2). This was further highlighted when differences in the tryptic peptide profiles of the glomeruli and tubules were assessed. Individual *m/z* features to distinguish between these two renal structures could only be detected when considering the analyses performed with a 10µm pixel size (Table 1). Consequently, if working at a lower spatial resolution (ie.50µm), the accurate detection of potential glomerular disease markers could be hampered due to the presence of confounding signals

from the tubulointerstitium as well as bias being introduced due to the varying positions from which the spectra are acquired during the imaging run. If working at a high spatial resolution (ie.10µm), the potential to obtain specific glomerular profiles using MALDI-MSI would offer a powerful alternative to laser capture microdissection, which, as of today, has been the strategy of choice for the isolation of glomeruli prior to proteomic analysis [27] [28]. The inherent advantages of MALDI-MSI mean that proteomic information could be integrated with routine histology, or immunohistochemistry, on the same tissue section and lead to the detection of specific glomerular markers of renal diseases.

Using a 10µm pixel size also enabled more specific tryptic peptide profiles of podocytes and mesangial cells to be generated, whilst the profiles generated with a 50µm pixel size presumably contained a mixture of cell types, and thus pathologically significant information may have been diluted (Figure 3). This was observed in both the single pixel spectra and the spectra generated from an average of five pixels (Supplementary figure 1).The ability to visualise the proteins present in each of the single cell types from within the glomeruli may have direct pathological relevance to MN in particular. In this disease, for example, podocytes are the target of circulating autoantibodies, such as Phospholipase A2 receptor and Thrombospondin type 1 containing 7A domain [24], and, whilst immune deposits at the mesangial cells are variable in MN, there is evidence to suggest that they may be implicated in inflammatory processes [25].

When comparing the tryptic peptide profiles of epithelial cells of the proximal and distal tubules (Figure 4), only 74.77% of the detected peaks were present in both. Whilst it should be expected that there is a strong overlap in the number of signals common to both profiles, given their origin within epithelia, it is encouraging to see that differences still remained. This is in part due to the fact that the epithelial cells of the proximal tubules have been shown to produce possible antigens implicated in the disease whilst using the Heymann Nephritis model [26] and the potential to characterise their specific proteome may help to better clarify the pathogenesis of the disease.

Following the on-tissue identification of Sonic Hedgehog (SHH) and α-Smooth muscle actin (α-SMA), we then proceeded to evaluate their signal intensity and localisation within the glomeruli and tubular regions of treatment responders (R) and non-responders (NR). The findings related to SHH reflected those previously observed [17], with a much stronger signal intensity in the NR group. However, we could now also observe an increase in the glomerular signal intensity relative to that observed in tubular regions. In the NR group, this finding could reflect early modifications in the renal tissue of these patients that precede the development of chronic lesions such as sclerosis of the glomerular tuft, which can be triggered by the activation of SHH pathway as previously demonstrated [29]. Moreover, recent evidence suggests that this protein can be implicated in the epithelial-to-mesenchymal transition of glomerular and tubular cells which can lead to the development of renal fibrosis following kidney injury [30–32]. These phenomena could correlate with a poor prognosis of patients in

the NR group and the detection of these early modifications could help in discriminating cases with a worse outcome.

Regarding α-SMA, we noted that the signal was localised to the mesangial cells of the glomeruli in both patient groups, whilst there was a marked increase in the signal intensity corresponding with the epithelial cells of the proximal tubules within the NR group. This data confirms the findings of previous studies that described a correlation between the increase of α-SMA expression in the tubulointerstitial compartment and the development of interstitial fibrosis with consequent progression of renal disease in MN [33–35]. On this basis, the lower signal intensity observed in the tubulointerstitium of the R group could reflect a lower likelihood of progression to ESRD in these patients. The overexpression of this protein in mesangial cells during the development of many kinds of glomerulonephritis has also been extensively studied. Whilst there is some evidence to suggest that this may be a non-specific finding with a low predictive role in the outcome of glomerulonephritis [36,37], and thus we should approach these findings with caution, some author have also noted a negative correlation between α-SMA expression in the mesangial cells and the levels of serum creatinine at the time of biopsy [38]. They hypothesised that mesangial cells expressing α-SMA are capable of higher contractile activity, thus leading to glomerular hyperfiltration as an early adaptive mechanism to glomerular damage. As previously touched upon, α-SMA is expressed in many tissues, thus we should approach this protein cautiously when considering its possible clinical value. Furthermore, given the very limited number of samples used in

this study it is important to note that no definitive conclusion regarding the potential markers found here can be drawn. However, it is again encouraging that we could spatially resolve these proteins within the same cellular locations as observed with routine immunohistochemistry [38]. This further stresses that the detection of cell specific markers of disease progression and response to therapy in MN may be possible by taking the route of high spatial resolution MALDI-MSI.

CONCLUDING REMARKS

Notwithstanding the large amount of data that can be generated, and the significant strain that this places on computer resources, the ability to spatially resolve the glomerular and tubular structures present within a renal biopsy can provide additional diagnostic and prognostic information that would not be possible using larger pixel sizes. The usual caveats of employing a small sample cohort apply to this study, thus future work will involve analysis on a larger cohort of patients with the aim of verifying the predictive role of those proteins presented in this paper. The final aim would be to generate a larger panel of markers that can assist the renal pathologist during the prognostic assessment of MN cases and whilst deciding the therapeutic treatment.

ACKNOWLEDGEMENTS

Our special thanks go to Riccardo Tagliabue, Loredana Tusa and Lorella Riva for their technical support and to the nephrological team of San Gerardo Hospital for the routine execution of the renal biopsies.

FUNDING

The research leading to these results has received funding from MIUR: FIRB 2007 (RBRN07BMCT_11), FAR 2014–2016 and in part by Fondazione Gigi & Pupa Ferrari Onlus.

CONFLICT OF INTEREST STATEMENT

The authors state that they have no conflicts of interest.

REFERENCES

[1] Caprioli, R.M., Farmer, T.B., Gile, J., Molecular imaging of biological samples: localization of peptides and proteins using MALDI-TOF MS. *Anal. Chem.* 1997, 69, 4751–60.

[2] Kriegsmann, J., Kriegsmann, M., Casadonte, R., MALDI TOF imaging mass spectrometry in clinical pathology: A valuable tool for cancer diagnostics (Review). *Int. J. Oncol.* 2015, 46, 893–906.

[3] Meding, S., Nitsche, U., Balluff, B., Elsner, M., Rauser S., Schöne C., Nipp M., Maak M., Feith M., Ebert M.P., Friess H., Langer R., Höfler H., Zitzelsberger H., Rosenberg R., Walch A., Tumor classification of six common cancer types based on proteomic profiling by MALDI imaging. *J. Proteome Res.* 2012, 11, 1996–2003.

[4] Nipp, M., Elsner, M., Balluff, B., Meding, S., Meding S., Sarioglu H., Ueffing M., Rauser S., Unger K., Höfler H., Walch A., Zitzelsberger H., S100-A10, thioredoxin, and S100-A6 as biomarkers of papillary thyroid carcinoma with lymph node metastasis identified by MALDI imaging. *J. Mol. Med. (Berl).* 2012, 90, 163–74.

[5] Horn, P.J., Chapman, K.D., Lipidomics in situ: insights into plant lipid metabolism from high resolution spatial maps of metabolites. *Prog. Lipid Res.* 2014, 54, 32–52.

[6] Römpp, A., Guenther, S., Takats, Z., Spengler, B., Mass spectrometry imaging with high resolution in mass and space (HR(2) MSI) for reliable investigation of drug compound

distributions on the cellular level. *Anal. Bioanal. Chem.* 2011, 401, 65–73.

[7] Holst, S., Heijs, B., de Haan, N., van Zeijl, R.J.M., Briaire-de Bruijn I.H., van Pelt G.W., Mehta A.S., Angel P.M., Mesker W.E., Tollenaar R.A., Drake R.R., Bovée J.V., McDonnell L.A., Wuhrer M., Linkage-Specific in Situ Sialic Acid Derivatization for N-Glycan Mass Spectrometry Imaging of Formalin-Fixed Paraffin-Embedded Tissues. *Anal. Chem.* 2016, 88, 5904–13.

[8] Smith, A., Mosele, N., L'Imperio, V., Pagni, F., Magni, F., in:, *Integr. Omi. Approaches Syst. Biol. Clin. Appl.*, John Wiley & Sons, Inc., Hoboken, NJ, USA 2018, pp. 156–172.

[9] Baker, T.C., Han, J., Borchers, C.H., Recent advancements in matrix-assisted laser desorption/ionization mass spectrometry imaging. *Curr. Opin. Biotechnol.* 2017, 43, 62–69.

[10] Zavalin, A., Yang, J., Caprioli, R., Laser beam filtration for high spatial resolution MALDI imaging mass spectrometry. *J. Am. Soc. Mass Spectrom.* 2013, 24, 1153–6.

[11] Ogrinc Potočnik, N., Porta, T., Becker, M., Heeren, R.M.A., Ellis, S.R., Use of advantageous, volatile matrices enabled by next-generation high-speed matrix-assisted laser desorption/ionization time-of-flight imaging employing a scanning laser beam. *Rapid Commun. Mass Spectrom.* 2015, 29, 2195–203.

[12] Heijs, B., Abdelmoula, W.M., Lou, S., Briaire-de Bruijn, I.H., Dijkstra J., Bovée J.V., McDonnell L.A., Histology-Guided High-Resolution Matrix-Assisted Laser Desorption Ionization

Mass Spectrometry Imaging. *Anal. Chem.* 2015, 87, 11978–83.

[13] L'Imperio, V., Smith, A., Chinello, C., Pagni, F., Magni, F., Proteomics and glomerulonephritis: A complementary approach in renal pathology for the identification of chronic kidney disease-related markers. *Proteomics Clin Appl* 2015, 371–383.

[14] Smith, A., L'Imperio, V., Ajello, E., Ferrario, F. Mosele N., Stella M., Galli M., Chinello C., Pieruzzi F., Spasovski G., Pagni F., Magni F., The putative role of MALDI-MSI in the study of Membranous Nephropathy. *Biochim. Biophys. Acta* 2017, 1865, 865–874.

[15] Ponticelli, C., Membranous nephropathy. *J. Nephrol.* 2007, 20, 268–87.

[16] Ponticelli, C., Glassock, R.J., Glomerular diseases: membranous nephropathy--a modern view. *Clin. J. Am. Soc. Nephrol.* 2014, 9, 609–16.

[17] L'Imperio, V., Smith, A., Ajello, E., Piga, I., Denti, V., Tettamanti, S., Sinico, R.A., Pieruzzi, F., Garozzo, M.,Vischini, G., Nebuloni, M., Pagni, F., Magni, F., MALDI-MSI pilot study highlights glomerular deposits of macrophage migration inhibitory factor (MIF) as a possible indicator of response to therapy in Membranous Nephropathy. *PROTEOMICS – Clin. Appl.* 2018, doi: 10.1002/prca.201800019. [Epub ahead of print].

[18] Chapter 7: Idiopathic membranous nephropathy. *Kidney Int. Suppl.* 2012, 2, 186–197.

[19] De Sio, G., Smith, A.J., Galli, M., Garancini, M., Chinello C.,

Bono F., Pagni F., Magni F., A MALDI-Mass Spectrometry Imaging method applicable to different formalin-fixed paraffin-embedded human tissues. *Mol. Biosyst.* 2015, 11, 1507–14.

[20] Cole, L.M., Clench, M.R., Mass spectrometry imaging for the proteomic study of clinical tissue. *Proteomics. Clin. Appl.* 2015, 9, 335–41.

[21] Pagni, F., L'imperio, V., Bono, F., Garancini, M., Roversi G., De Sio G., Galli M., Smith A.J., Chinello C., Magni F., Proteome analysis in thyroid pathology. *Expert Rev Proteomics* 2015, 12, 375–390.

[22] Yoshimoto, K., Yokoyama, H., Wada, T., Furuichi, K., Sakai N., Iwata Y., Goshima S., Kida H. , Pathologic findings of initial biopsies reflect the outcomes of membranous nephropathy. *Kidney Int.* 2004, 65, 148–53.

[23] Pagni, F., De Sio, G., Garancini, M., Scardilli, M., Chinello C., Smith A.J., Bono F., Leni D., Magni F., Proteomics in thyroid cytopathology: Relevance of MALDI-imaging in distinguishing malignant from benign lesions. *Proteomics* 2016, 16, 1775–1784.

[24] Ronco, P., Debiec, H., A podocyte view of membranous nephropathy: from Heymann nephritis to the childhood human disease. *Pflugers Arch.* 2017, 469, 997–1005.

[25] Savić, V., Vlahović, P., Stefanović, V., Increased expression of glomerular mesangial cell 5'-nucleotidase in membranous nephropathy. *Nephron* 2002, 92, 219–21.

[26] Farquhar, M.G., Saito, A., Kerjaschki, D., Orlando, R.A., The

Heymann nephritis antigenic complex: megalin (gp330) and RAP. *J. Am. Soc. Nephrol.* 1995, 6, 35–47.

[27] Jain, D., Green, J.A., Bastacky, S., Theis, J.D., Sethi, S., Membranoproliferative glomerulonephritis: the role for laser microdissection and mass spectrometry. *Am. J. Kidney Dis.* 2014, 63, 324–8.

[28] Andeen, N.K., Yang, H.Y., Dai, D.F., MacCoss, M.J., Smith, K.D., DnaJ Homolog Subfamily B Member 9 Is a Putative Autoantigen in Fibrillary GN. *J. Am. Soc. Nephrol.* 2018, 29, 231–239.

[29] Huang, T.-H., Shui, H.A., Ka, S.-M., Tang, B.L., Chao T.K., Chen J.S., Lin Y.F., Chen A., Rab 23 is expressed in the glomerulus and plays a role in the development of focal segmental glomerulosclerosis. *Nephrol. Dial. Transplant* 2009, 24, 743–54.

[30] Ding, H., Zhou, D., Hao, S., Zhou, L., He W., Nie J., Hou F.F., Liu Y., Sonic hedgehog signaling mediates epithelial-mesenchymal communication and promotes renal fibrosis. *J. Am. Soc. Nephrol.* 2012, 23, 801–13.

[31] Zhou, D., Li, Y., Zhou, L., Tan, R.J., Xiao L., Liang M., Hou F.F., Liu Y., Sonic hedgehog is a novel tubule-derived growth factor for interstitial fibroblasts after kidney injury. *J. Am. Soc. Nephrol.* 2014, 25, 2187–200.

[32] Fabian, S.L., Penchev, R.R., St-Jacques, B., Rao, A.N., Sipilä P., West K.A., McMahon A.P., Humphreys B.D., Hedgehog-Gli pathway activation during kidney fibrosis. *Am. J. Pathol.* 2012,

180, 1441–53.

[33] Roberts, I.S., Burrows, C., Shanks, J.H., Venning, M., McWilliam, L.J., Interstitial myofibroblasts: predictors of progression in membranous nephropathy. *J. Clin. Pathol.* 1997, 50, 123–7.

[34] Badid, C., Desmoulière, A., McGregor, B., Costa, A.M., Fouque D., Hadj Aïssa A., Laville M., Interstitial alpha-smooth muscle actin: a prognostic marker in membranous nephropathy. *Clin. Nephrol.* 1999, 52, 210–7.

[35] Mezzano, S.A., Aros, C.A., Droguett, A., Burgos, M.E., Ardiles L.G., Flores C.A., Carpio D., Vío C.P., Ruiz-Ortega M., Egido J., Renal angiotensin II up-regulation and myofibroblast activation in human membranous nephropathy. *Kidney Int. Suppl.* 2003, S39-45.

[36] MacPherson, B.R., Leslie, K.O., Lizaso, K. V, Schwarz, J.E., Contractile cells of the kidney in primary glomerular disorders: an immunohistochemical study using an anti-alpha-smooth muscle actin monoclonal antibody. *Hum. Pathol.* 1993, 24, 710–6.

[37] Groma, V., Marcussen, N., Olsen, S., A quantitative immunohistochemical study of the expression of mesangial alpha-smooth muscle actin and the proliferation marker Ki-67 in glomerulonephritis in man. *Virchows Arch.* 1997, 431, 345–50.

[38] Saratlija Novakovic, Z., Glavina Durdov, M., Puljak, L., Saraga, M., Saraga M., Ljutic D., Filipovic T., Pastar Z., Bendic A., Vukojevic K., The interstitial expression of alpha-smooth

muscle actin in glomerulonephritis is associated with renal function. *Med. Sci. Monit.* 2012, 18, CR235-40.

CHAPTER V

5.1 Summary

Chronic glomerulonephritis (GN) is a vast group of immune-mediated inflammatory kidney diseases, which are the leading cause of chronic kidney disaease (CKD) wordwide, which is of the major health and socioeconomic burdens and one of the main reasons of end-stage renal disease (ESRD).

CKD nowadays accounts for approximately 11%–13% of the wold's population, having a serious impact on the quality of life and overall social cost in case of ESRD. As prognosed, the number of patients with CKD will significantly increase in the next years due to the aging of population and increase in concomitant diseases as hypertension, cardiovascular diseases and diabetes. [1-3]

Effective early identification and management of CKD is utterly important to prevent its progression and its complications.

Among the most common GN, IgA nephropathy, membranous nephropathy and diabetic nephropathy take leading positions so far. [3]

There are number of guidelines of CKD and GN managemnent, where kidney biopsy plays key role in the glomerular disease evaluation. [2,3]

The main aim of the biopsy is descriptive reflection of actual kidney kidney state with emphasis on available damage, its extension and level of acivity or chronicity. [3,4]

Nevertheless, the kidney biopsy gives us an important insight, the actual state of the disease oftenly does not add any significant

prognostical information and does not permit an individual approach, which should be applied in every case. [4, 5]

Given that there as still many concerns about various GN triggers and incomplete pathogenesis understanding, there is an urging need of reliable biomarkers discovery to improve stratification of patients with higher risk of ESRD development and improving CKD the management of CKD patients overall. [6-8]

The development of proteomic techniques is a new promising starting point, where matrix-assisted laser desorption/ionization imaging mass spectrometry (MALDI-MSI) represents a potential technique employed in biomarker discovery with an advantage of performing direct, on-tissue analysis, which enables the spatial distribution and relative intensity of proteins to be correlated with morphological information. The method has already shown its feasibility in many studies including those on GN kidney biopsies. [9-17] and understanding the molecular nature of GN might open new horizons in its diagnosis management strategies with a potential transfer into new era of less invasive diagnostic tools.

In our work, we aimed to study several most diffuse forms of chronic glomerulonephritis using MALDI-MSI, attemting to detect possible molecular alterations significant of these diseases' progression.

We performed all the analysis on formalin fixed paraffin embedded (FFPE) renal tissue biopsies with high spatial resolution MALDI-MSI which enabled the localization of protein signals in the various tissue compartments of the kidney. The comparison of molecular profiles of various GN forms were performed, which resulted in distinguishing

specific tryptic peptides profiles of differeren cell regions within the kidney. We also were able to detect the proteins with an altered intensity, implicated in inflammatory and healing pathways. These findings give us an idea that numerous proteins uncovered may have a possible role in diagnosis, prognosis or different response to therapy. All identified signals have to be potentially investigated, representing possible future targets to be assigned as diagnostic or prognostic markers of varius forms of GN. Furthermore, the possiblity to spatially resolve individual glomeruli and the individual cell-types within the kidney is pushing the boundaries of MALDI-MSI technology, especially at the protein level, and represents a promising line of future development in this area of study.

5.2 Conclusions

Whilst the result presented in this thesis should be verified in a larger cohort of patients, these findings represent a promising starting part in the search for novel protein signatures implicated in the development and progression of these GN.

All of the signals that were detected by MALDI-MSI and and putatively identified using complementary MS-based techniques correspond with proteins that are linked to inflammatory or healing pathways and were localised to the corresponding histological regions of inflammatory infiltrates or fibrosis and could be proposed as possible protein markers of progression. While some of these proteins have already been reported in literature, one of the primary advantages of MALDI-MSI, with respect to routine immunohistochemistry based

techniques, is that the multiple proteins can be monitored within a single analysis. Thus, using MALDI-MSI may help us to improve our understanding of the complex molecular events that are associated with CKD progression. In turn, this can facilitate the more comprehensive stratifications of patients, ear-makring those who would progress to end-stage renal disease more rapidly or respond negatively to therepautic treatment. Generating a collective panel of markers may fulfil our understanding of disease pathogensis and assist in the clinical assessment and management of these cases. Furthermore, the ability of high spatial resolution of MALDI-MSI to spatially resolve the intra-glomerular and -tubular structures present within a renal biopsy may be valuable source of additional diagnostic and prognostic information and, alterantviely, help us to better understand how these possible protien markers may be implicated in the development of these diseases.

5.3 Future perspectives

The future prospectives of our study is to confirm, and build upon, these findings in a larger cohort of patients. Once these findings have been verified, and the identity of these proteins confirmed using complementary MS-based techniques, the aim is to generate a collective panel of markers which could assist the pathologist in the diagnostic/prognostic assessment of these cases and help guide the clinician in the management of CKD patients. Clearer guidelines for the clinical management of such CKD patients would enable more precise treatment strategies to be employed, which would improve

patient outlook and having positive impact on the ecnomoic burden associated with CKD.

5.4 References

1. KDIGO Clinical Practice Guidelines for Glomerulonephritis. Chapter 1: Introduction, Kidney International Supplements,Volume 2, Issue 2, 2012, 156-162, http://www.kdigo.org/clinical_practice_guidelines/pdf/KDIGO-GN-Guideline.pdf
2. NICE Chronic kidney disease in adults: assessment and management. Clinical guideline, 2015, https://www.nice.org.uk/guidance/cg182#
3. KDIGO Clinical Practice Guidelines for Glomerulonephritis. Chapter 2: General principles in the management of glomerular disease, Kidney International Supplements,Volume 2, Issue 2, 2012, 156-162, http://www.kdigo.org/clinical_practice_guidelines/pdf/KDIGO-GN-Guideline.pdf
4. Cook TH (2007) Interpretation of Renal Biopsies in IgA Nephropathy. In: Tomino Y (ed): IgA Nephropathy Today. Contrib Nephrol. Karger, Basel. Vol. 157, pp 44-49.
5. Tomino Y. (2016) Pathogenesis And Treatment in IgA Nephropathy. Springer, Tokyo
6. Coppo R (2016) Biomarkers and targeted new therapies for IgA nephropathy. Pediatr Nephrol 32:725-731.

7. Floege J, Sharon G et al. (2019) Management and treatment of glomerular diseases (part 1): conclusions from a Kidney Disease: Improving Global Outcomes (KDIGO). Kidney Int 95:268-280
8. Yeo SC, Cheung CK., Barratt J (2018) New insights into the pathogenesis of IgA nephropathy. Pediatr Nephrol 33:763-777.
9. Smith A, L'Imperio V, De Sio G, et al. (2016) Alpha-1-Antitrypsin detected by MALDI imaging in the study of glomerulonephritis: Its relevance in chronic kidney disease progression. Proteomics 16:1759- 66.
10. Smith A, L'Imperio V, Ajello E, Ferrario F, Mosele N, Stella M, Galli M, Chinello C, Pieruzzi F, Spasovski G, Pagni F, Magni F (2017) The putative role of MALDI-MSI in the study of Membranous Nephropathy. Biochim Biophys Acta Proteins Proteom 1865:865-874.
11. De Sio G et al. (2015) A MALDI-Mass Spectrometry Imaging method applicable to different formalin-fixed paraffin-embedded human tissues. Mol Biosyst 11:1507-14. doi: 10.1039/c4mb00716f.
12. Sun L, Zou LZ, Chen MJ (2016) Make precision medicine work for chronic kidney disease. Free supplementary material doi: 10.1159/000455101.
13. Addie RD et al. (2015) Current State and Future Challenges of Mass Spectrometry Imaging for Clinical Research.Anal Chem 87:6426-33

14. Baluff B et al. (2014) De novo discovery of phenotypic intratumor heterogeneity using imaging mass spectrometry. J Pathol 235:3-13
15. Ucal Y et al. (2017) Clinical applications of MALDI imaging technologies in cancer and neurodegenerative diseases. Biochim Biophys Acta. pii: S1570-9639(17)30005-5. doi: 10.1016/j.bbapap.2017.01.005. [Epub ahead of print]
16. Kasap M, Akpinar G, Kanali A (2017) Proteomic studies associated with Parkinson's disease. Expert Rev Proteomics 14:193-209
17. Mainini V et al. (2014) MALDI imaging mass spectrometry in glomerulonephritis: feasibility study. Histopathology 64:901–906.

LIST OF PUBLICATIONS DURING THE PHD PERIOD

1. Dyayk O, Ivanova M (2016) Pathomorphological characteristic of IgG4-related diseases. Patologia 2:58-62 DOI: 10.14739/2310-1237.2016.2.81051
2. Ivanova M, Dyadyk O, Smith A, Santorelli L, Stella M, Galli M, Chinello C, Magni F (2017) Proteomics and Matrix-Assisted Laser Desorption/ Ionization Mass Spectrometry Imaging as a Modern Diagnostic Tool in Kidney Diseases. Pochki 6:25-30.
3. Ivanova M, Magni F, Dyadyk O, Smith A, Stella M, galli M, Chinello C, Denti V (2017) E-PS-13-004. Matrix-associated laser desorption/ionisation (MALDI) mass- spectrometry imaging in a study of IgA nephropathy linked to IgG4-sclerosing diseases. Virchows Arch 471 (Suppl 1): S336
4. Dyadyk O, Ivanova M (2018) Proteomics in clinic and kidney diseases investigation. Regional Innovations Medical Science 3:24-26
5. Ivanov D, Ivanova M, Bevzenko T (2018) Febuxostat improves GFR and BP in non-diabetic adults with CKD 2-3: 6 years treatment and follow-up. Neph Dial Transplant 33:626
6. Smith A, L'Imperio V, Denti V, Mazza M, Ivanova M, Stella M, Piga I Chinello C, Ajello E, Pierizzi F, Pagni F, Magni F (2018) High spatial resolution MALDI-MS Imaging in the Study of Membranous Nephropathy. Proteomics Clin Appl. https://onlinelibrary.wiley.com/doi/full/10.1002/prca.201800016

7. Chinello C, Stella M, Piga I, Smith A, Bovo G, varallo M, Ivanova M, Denti V, Grasso M, Grasso A, Del Puppo M, Magni F (2019) Proteomics of liquid biopsies: depicting RCC infiltration into the renal vein bu MS analysis of urine and plasma. J Proteomics 191:29-37.
8. Ivanova M, Dyaydyk O, Smith A, Magni F (2919) PS-04-020 Discovering triggers of IgA nephropathy progression by Matrix assisted laser desorption/ionisation mass spectrometry imaging. Virchows Archiv Abstracts 31st European Congress of Pathology. https://doi.org/10.1007/s00428-019-02631-8
9. Ivanov D, Bevzenko T, Kushnirenko S, Ivanova M, Rotova S, taran O (2019) SP Use of sodium-glucose co-transporter 2 (SGLT2) inhibitor in patients with diabetes mellitus free of chronic kidney disease 2-3a stages: 1 year of experience. Neph Dial Transplant 34(s1) doi: 10.1093/ndt/gfz103.SP085
10. Ivanov D, Ivanova T, Fedorenko O, Kushnirenko S, Ivanova M (2019) Options of modern anti-relapse therapy for urinary tract infections in children: CRUTIL trial. Pochki 2:80-86 DOI: https://doi.org/10.22141/2307-1257.8.2.2019.166663
11. Smith A, Iablokov V, Mazza M, Guarniero, Denti V, Ivanova M, Stella M, Piga I, Chinello C, Heijs B, van Veelen P, Benediktsson H, Muruve D, Magni F (2019) Detecting proteomic indicators to distinguish Diabetic Nephropathy from Hypertensive Nephrosclerosis by integrating MALDI-MSI with high mass accuracy MS. Kidney and blood pressure research (under review).

12. Ivanova M, Dyadyk O, Ivanov D, Clerici F, Smith A, Magni F (2019) Matrix-assisted laser desorption/ionization mass spectrometry imaging to uncover protein alterations associated with the progression of IgA nephropathy. Virchows archive (under review).

AKNOWLEDGEMENTS

I would like to express my deep gratitude to my family, for all the support and love during this period and all my life.

I am very grateful to Universty Milano-Bicocca and personally to Professor Magni for the opportunities given and wisdom shared.

My special thanks to Professor Dyadyk for helping me reach what I am professionally and personally, for endless supervision and patronage.

My great appreciation to all laboratory team for help, advices, assistance, encouragements and friendship.

Thank You for this precious time.